MICROCOPY RESOLUTION TEST CHART

NATIONAL BUREAU OF STANDARDS-1963-A

AD-A140 520

COLLEGE OF ENGINEERING

THERMO-MECHANICAL AND THERMAL

BEHAVIOR OF HIGH-TEMPERATURE STRUCTURAL MATERIALS

Interim Report to
Office of Naval Research

Contract No.: N00014-78-C-0431

January 1, 1982 - December 31, 1982

by

D. P. H. Hasselman
Virginia Polytechnic Institute and State University
Blacksburg, Virginia 24061

VIRGINIA POLYTECHNIC INSTITUTE STATE UNIVERSITY

THERMO-MECHANICAL AND THERMAL

BEHAVIOR OF HIGH-TEMPERATURE STRUCTURAL MATERIALS

Interim Report to
Office of Naval Research
NR 032588
Contract No.: N00014-78-C-0431

January 1, 1983 - December 31, 1983

by

D. P. H. Hasselman
Virginia Polytechnic Institute and State University
Blacksburg, Virginia 24061

and

L. D. Bentsen, J. J. Brennan, H. Hencke, T. D. Nguyen
R. Ruh, J. P. Singh, H. Tawil, J. R. Thomas, Jr.
T. -Y. Tien, G. Ziegler

SECURITY CLASSIFICATION OF THIS PAGE *(When Data Entered)*

REPORT DOCUMENTATION PAGE		READ INSTRUCTIONS BEFORE COMPLETING FORM
1. REPORT NUMBER	2. GOVT ACCESSION NO. AD-A140520	3. RECIPIENT'S CATALOG NUMBER
4. TITLE *(and Subtitle)* Thermo-Mechanical and Thermal Behavior of High-Temperature Structural Materials		5. TYPE OF REPORT & PERIOD COVERED Jan. 1, 1983 - Dec. 31, 1983
		6. PERFORMING ORG. REPORT NUMBER
7. AUTHOR(*s*) D. P. H. Hasselman and co-authors		8. CONTRACT OR GRANT NUMBER(*s*) N00014-78-C-0431
9. PERFORMING ORGANIZATION NAME AND ADDRESS Virginia Polytechnic Institute and State University, Blacksburg, Virginia 24061		10. PROGRAM ELEMENT, PROJECT, TASK AREA & WORK UNIT NUMBERS
11. CONTROLLING OFFICE NAME AND ADDRESS Office of Naval Research, Code 471 Arlington, VA 22217		12. REPORT DATE Dec. 31, 1983
		13. NUMBER OF PAGES 102
14. MONITORING AGENCY NAME & ADDRESS*(if different from Controlling Office)*		15. SECURITY CLASS. *(of this report)* unclassified
		15a. DECLASSIFICATION/DOWNGRADING SCHEDULE

16. DISTRIBUTION STATEMENT *(of this Report)*
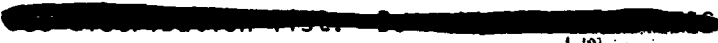
This document has been approved
for public release and sale; its
distribution is unlimited.

17. DISTRIBUTION STATEMENT *(of the abstract entered in Block 20, if different from Report)*

18. SUPPLEMENTARY NOTES

19. KEY WORDS *(Continue on reverse side if necessary and identify by block number)*

Thermal shock, thermal stress, thermal diffusivity, thermal conductivity; composites, radiation heat transfer, cyclic heating, optical thickness, crack stability, micro-cracking, porosity.

20. ABSTRACT *(Continue on reverse side if necessary and identify by block number)*

This report contains preprints of studies completed during the reporting period on the thermo-mechanical and thermal behavior of high-temperature structural materials, as follows:

DD _{1 JAN 73} **1473** EDITION OF 1 NOV 65 IS OBSOLETE
S/N 0102-LF-014-6601

SECURITY CLASSIFICATION OF THIS PAGE *(When Data Entered)*

Technical Publications

I   H. Tawil, L. D. Bentsen, D. P. H. Hasselman, "Effect of Heat Treatment on the Thermal Diffusivity of an Aluminosilicate Fiber-Reinforced Carbon Matrix."

II   L. D. Bentsen, D. P. H. Hasselman, "Role of Porosity in the Effect of Microcracking on the Thermal Conductivity of Brittle Ceramic Composites."

III   L. D. Bentsen, D. P. H. Hasselman, J. J. Brennan, "Radiative Contribution to the Thermal Diffusivity and Conductivity of a Silicon Carbide Fiber Reinforced Glass-Ceramic."

IV   R. Ruh, L. D. Bentsen, D. P. H. Hasselman, "Thermal Diffusivity Anisotropy of SiC-BN Composites."

V   L. D. Bentsen, T. -Y. Tien and D. P. H. Hasselman, "Effect of Crystallization of the Grain Boundary Phase on the Thermal Diffusivity of a Sialon Ceramic."

VI   J. P. Singh, G. Ziegler, D. P. H. Hasselman, "Effect of Drop-Height on the Critical Temperature Difference (ΔT_c) for Brittle Ceramics Subjected to Thermal Shock by Quenching into Water."

VII   T. D. Nguyen, J. R. Thomas, Jr., D. P. H. Hasselman, "Effect of Thermal Diffusivity on Magnitude of Thermal Stress in a Brittle Ceramic Subjected to Rapid Thermal Cycling."

VIII   H. Hencke, J. R. Thomas, Jr., D. P. H. Hasselman, "Role of Material Properties in the Thermal Stress Fracture of Brittle Ceramics Subjected to Conductive Heat Transfer."

IX   D. P. H. Hasselman and J. P. Singh, "Criteria for the Thermal Stress Failure of Brittle Structural Materials."

Accession For

NTIS GRA&I

DTIC TAB

Unannounced

Justification

Distribution/

Availability Codes

Avail and/or

Dist Special

A-1

THERMO-MECHANICAL AND THERMAL
BEHAVIOR OF HIGH-TEMPERATURE STRUCTURAL MATERIALS

PREFACE

Technical ceramics because of their chemical inertness, high melting
point, good wear resistance, excellent mechanical stability at high temp-
erature and other unique properties, represent a class of materials eminently
suited for many critical engineering applications. Unfortunately, because
of their brittleness and unfavorable combination of pertinent material
properties, technical ceramics generally are highly susceptible to catas-
trophic failure in non-uniform thermal environments, which give rise to
thermal stresses of high magnitude.

Thermal stress failure analysis of structural materials represents
a multi-disciplinary problem which involves the principles of heat trans-
fer, mechanics and materials engineering. Over the last few decades much
general understanding of the nature of thermal stress failure of brittle
materials has been generated. However, due to the multi-disciplinary
nature of the problem, the ability to predict thermal stress failure quan-
titatively for design or other purposes has lagged behind the progress made
in other engineering fields. The objective of the present program is to
improve the qualitative and quantitative understanding of the nature of
thermal stress failure of brittle structural materials, including the ex-
perimental as well as theoretical variables. In order to achieve this
objective, the participating investigators and scope of the program are
organized such that full advantage is taken of the combined inputs from a
number of engineering disciplines. In a similar spirit, a number of studies
were conducted in cooperation with investigators at other institutions.

The effort of this program consists of four main themes, including:
experimental thermal shock testing with supporting analyses, measurement
of thermophysical properties relevant to thermal stress failure, the
analysis of mechanisms of thermal stress failure and the dissemination
of information on thermal stresses in the form of review articles, con-
ferences, etc.

A total of sixty-four (64) published, accepted or submitted technical
publications have resulted from this research program since its initiation.
The status of these publications is summarized in Table 1.

Studies completed within the period covered by this report are pre-
sented as individual chapters in the main body of this report. The title
of these chapters with a brief comment are as follows:

Chapter I: H. Tawil, L. D. Bentsen and D. P. H. Hasselman, "Effect of Heat Treatment on the Thermal Diffusivity of an Alumino-silicate Fiber-Reinforced Carbon Matrix"

This study showed that composites of a carbon matrix reinforced by alu-minosilicate fibers exhibited an irreversible increase in thermal diffusivity when thermally cycled to temperatures in excess of 600° C. X-ray analysis showed that this observation is attributable to crystallization of both the carbon matrix and the aluminosilicate fibers.

Chapter II: L. D. Bentsen, D. P. H. Hasselman, "Role of Porosity in the Effect of Microcracking on the Thermal Conductivity of Brittle Ceramic Composites"

This study revealed that the formation of microcracks and their effect on thermal conductivity is a very sensitive function of the pore content. This effect arises because for pore sizes below a minimum value, the stress intensity factor due to internal stresses resulting from thermal expansion mismatches is too low to result in microcrack formation.

Chapter III: L. D. Bentsen, D. P. H. Hasselman, J. J. Brennan, "Radia-tive Contribution to the Thermal Diffusivity and Conducti-vity of a Silicon Carbide Fiber Reinforced Glass-Ceramic"

It was found experimentally that the thermal diffusivity and conductivity of a lithium aluminosilicate glass-ceramic with or without SiC-fiber rein-forcements increased with increasing specimen thickness. These observations indicate the existence of a radiative contribution to the total heat transfer.

Chapter IV: R. Ruh, L. D. Bentsen, D. P. H. Hasselmen, "Thermal Diffu-sivity of SiC-BN Composites"

Composites of hot-pressed SiC with a dispersed phase of BN showed signi-ficant anisotropy in thermal diffusivity relative to the hot-pressing direc-tion. This effect is due to the preferred orientation of the BN particles promoted during hot-pressing. The anisotropy in thermal diffusivity was maintained to temperatures as high as 1400° C.

Chapter V: L. D. Bentsen, T.-Y. Tien, D. P. H. Hasselmen, "Effect of Crystallization of the Grain Boundary Phase on the Thermal Diffusivity of a Sialon Ceramic"

The results of this study showed that the degree of crystallinity of the grain boundary phase has a significatn effect on the thermal diffusivity of a sialon ceramic.

Chapter VI: J. P. Singh, G. Ziegler, D. P. H. Hasselman, "Effect of
              Drop-Height on the Critical Temperature Difference (ΔT_c)
              for Brittle Ceramics Subjected to Thermal Shock by Quench-
              ing into Water"

The critical temperature difference (ΔT_c) required to initiate thermal
stress fracture in a number of brittle ceramics subjected to thermal shock
by quenching into water was found to be independent of drop-height. These
findings were interpreted in terms of the relative contributions to the heat
transfer during the quench.

Chapter VII: T. D. Nguyen, J. R. Thomas, Jr., D. P. H. Hasselman,
               "Effect of Thermal Diffusivity on Magnitude of Thermal
               Stress in a Brittle Ceramic Subjected to Rapid Thermal
               Cycling"

An analysis was conducted of the magnitude of thermal stresses in a
ceramic component subjected to thermal cycling of such high frequency that
thermal equilibrium between thermal cycles is not achieved. It was found
that under such conditions the magnitude of thermal stress, in addition to
the usual properties such as coefficient of thermal expansion, Young's modu-
lus and Poisson's ratio, also depends simultaneously on the magnitude of
the thermal diffusivity and thermal conductivity. It was also found that
the magnitude of the thermal stresses decreased as the frequency increased.

Chapter VIII: H. Hencke, J. R. Thomas, Jr., D. P. H. Hasselmen, "Role
                of Material Properties in the Thermal Stress Fracture of
                Brittle Ceramics Subjected to Conductive Heat Transfer"

The magnitude of thermal stresses in a ceramic component subjected to
heating or cooling by direct thermal contact, in addition to being a function
of the coefficient of thermal expansion, Young's modulus and Poisson's ratio,
also was found to be a function of the thermal conductivity, thermal diffu-
sivity and specific heat of both the component as well as the surrounding
medium. Sample calculations indicated that thermal stress fracture of cer-
amic specimens subjected to thermal shock by quenching in a fluid is the
result more of conductive rather than convective heat transfer.

Chapter IX: D. P. H. Hasselman, J. P. Singh, "Criteria for the Thermal
              Stress Failure of Brittle Structural Materials"

This review article presents all known information on the material
variables which affect the thermal stress fracture of brittle ceramics.
Appropriate experimental data were presented.

Table 1. Technical Publications To Date (4/1/78 - 12/31/83)

1. D. P. H. Hasselman and W. A. Zdaniewski, "Thermal Stress Resistance Parameters for Brittle Materials Subjected to Thermal Stress Fatigue," J. Am. Ceram. Soc., 61 (7-8) 375 (1978).

2. D. P. H. Hasselman, "Effect of Cracks on Thermal Conductivity," J. Comp. Mat., 12, 403-07 (1978).

3. K. Chyung, G. E. Youngblood and D. P. H. Hasselman, "Effect of Crystallization on the Thermal Diffusivity of a Cordierite Glass-Ceramic," J. Amer. Ceram. Soc., 61, 530 (1978).

4. W. Zdaniewski, H. Knoch, J. Heinrich and D. P. H. Hasselman, "Effect of Oxidation on Thermal Diffusivity of Reaction-Sintered Silicon Nitride," Ceram. Bull., 58, 539 (1979).

5. G. Ziegler and D. P. H. Hasselman, "Effect of Data Scatter on Apparent Thermal Stress Failure Mode of Brittle Ceramics," Ceramurgia, 5, 126 (1979).

6. D. P. H. Hasselman, "Role of Physical Properties in the Resistance of Brittle Ceramics to Fracture in Thermal Buckling," J. Amer. Ceram. Soc., 62, 125 (1979).

7. K. Satyamurthy, J. P. Singh, M. P. Kamat and D. P. H. Hasselman, "Effect of Spatially Varying Porosity on Magnitude of Thermal Stress During Steady State Heat Flow," J. Amer. Ceram. Soc., 62, 432 (1979).

8. D. P. H. Hasselman and J. P. Singh, "Analysis of Thermal Stress Resistance of Micro-cracked Brittle Materials," Ceram. Bull., 58, 856 (1979).

9. G. E. Youngblood, L. Bentsen, J. W. McCauley and D. P. H. Hasselman, "Thermal Diffusivity of Ba-Mica/Alumina Composites," J. Amer. Ceram. Soc., 58, 620 (1979).

10. D. P. H. Hasselman and Y. Tree, "On the Thermal Fracture of Ice," J. Mat. Sc., 14, 1499 (1979).

11. D. P. H. Hasselman, "Figures-of-Merit for the Thermal Stress Resistance of High-Temperature Brittle Materials," Ceramurgia International, 4, 147 (1979).

12. Bob R. Powell, Jr., G. E. Youngblood, D. P. H. Hasselman and Larry D. Bentsen, "Effect of Thermal Expansion Mismatch on the Thermal Diffusivity of Glass-Ni Composites," J. Amer. Ceram. Soc., 63, 581 (1980).

13. D. P. H. Hasselman, J. C. Swearengen, E. K. Beauchamp and W. A. Zdaniewski, "Effect of Alumina Dispersions on the Thermal Conductivity/ Diffusivity and Thermal Stress Resistance of a Borosilicate Glass," J. Mat. Sc., 15, 518-20 (1980).

14. D. P. H. Hasselman, J. R. Thomas, Jr., M. P. Kamat and K. Satyamurthy, "Thermal Stress Analysis of Partially Absorbing Brittle Ceramics Subjected to Radiation Heating," J. Am. Ceram. Soc., 63, 21-25 (1980).

15. J. P. Singh, J. R. Thomas, Jr., and D. P. H. Hasselman, "Analysis of Effect of Heat Transfer Variables on Thermal Stress Resistance of Brittle Ceramics Measured by Quenching Experiments," J. Am. Ceram. Soc., 63, 140-44 (1980).

16. K. Satyamurthy, J. P. Singh, D. P. H. Hasselman and M. P. Kamat, "Effect of Spatially Varying Thermal Conductivity on Magnitude of Thermal Stress in Brittle Ceramics Subjected to Convective Heating", J. Am. Ceram. Soc., 63, 363 (1980).

17. D. P. H. Hasselman, P. F. Becher and K. S. Mazdiyasni, "Analysis of the Resistance of High-E, Low-E Brittle Composites to Failure by Thermal Shock," Materials Technology, 11, 82 (1980).

18. K. Satyamurthy, J. P. Singh, M. P. Kamat and D. P. H. Hasselman, "Thermal Stress Analysis of Brittle Ceramics with Density Gradients Under Conditions of Transient Convective Heat Transfer," Proc. Brit. Ceram. Soc., 80, 10 (1980).

19. N. Claussen and D. P. H. Hasselman, "Improvement of Thermal Shock Resistance of Brittle Structural Ceramics by a Dispersed Phase of Zirconia," Proceedings of Conference on Thermal Stresses in Materials and Structures in Severe Thermal Environments, Plenum Press (1980).

20. J. P. Singh, J. R. Thomas and D. P. H. Hasselman, :Thermal Stresses in Partially Absorbing Flat Plate Symmetrically Heated by Thermal Radiation and Cooled by Convection," J. of Thermal Stresses, 3, 341 (1980).

21. K. Satyamurthy, D. P. H. Hasselman and J. P. Singh, "Effect of Nature of Concavity of Temperature Distribution on Position and Sign of Maximum Thermal Stress," J. Thermal Stresses, 3, 551 (1980).

22. C. Shih, J. P. Singh and D. P. H. Hasselman, "Effect of Crack Interaction on the Fracture Initiation and Crack Propagation in Brittle Ceramics Subjected to Severe Thermal Shock," High Temp-High Pressures, 12, 477 (1980).

23. J. P. Singh, J. R. Thomas, Jr. and D. P. H. Hasselman, "Stresses Due to Thermal Trapping in Semi-Absorbing Materials Subjected to Intense Radiation," Proc. Conf. Thermal Stresses in Materials and Structures in Severe Thermal Environments, Plenum Press (1980).

24. K. Satyamurthy, D. P. H. Hasselman, J. P. Singh, and M. P. Kamat, "Effect of Spatial Variation of Thermal Conductivity on Magnitude of Tensile Thermal Stresses in Brittle Materials Subjected to Convective Heating," Proc. Conf. Thermal Stresses in Materials and Structures in Severe Thermal Environments, Plenum Press, (1980).

25. Proc. Conf. Thermal Stresses in Materials and Structures in Severe Thermal Environments. Co-edited by D. P. H. Hasselman and R. A. Heller, by Plenum Press (1980).

26. K. Satyamurthy, J. P. Singh, D. P. H. Hasselman and M. P. Kamat, "Transient Thermal Stresses in Cylinders with Square Cross-Section Under Conditions of Convective Heat Transfer," J. Amer. Ceram. Soc., 63 (11-12) 694-98 (1980).

27. G. Ziegler, L. D. Bentsen and D. P. H. Hasselman, "Orientation Effects on the Thermal Diffusivity of Hot-Pressed Silicon Nitride," J. Amer. Ceram. Soc., 64, 35 (1981).

28. J. P. Singh, C. Shih and D. P. H. Hasselman, "Analysis of Effect of Crack Interaction on Nature of Strength Loss of Brittle Ceramics Subjected to Thermal Shock," J. Amer. Ceram. Soc., 64 (8)C106-09 (1981).

29. K. Niinara, L. D. Bentsen, K. Mazdiyasni and D. P. H. Hasselman, "Anisotropy Effects in the Thermal Diffusivity of Si_3N_4-BN Composites," J. Amer. Ceram. Soc., 64 (9) C117-118 (1981).

30. J. R. Thomas, Jr., J. P. Singh and D. P. H. Hasselman, "Analysis of Thermal Stress Resistance of Partially Absorbing Ceramic Plate Subjected to Asymmetric Radiation, I: Convective Cooling at Rear Surface," J. Amer. Ceram. Soc., 64, 163 (1981).

31. J. P. Singh, K. Satyamurthy, J. R. Thomas and D. P. H. Hasselman, "Analysis of Thermal Stress Resistance of Partially Absorbing Ceramic Plate Subjected to Asymmetric Radiation II: Convective Cooling at Front Surface," J. Amer. Ceram. Soc., 64, 169 (1981).

32. J. P. Singh, D. P. H. Hasselman, W. M. Su, J. A. Rubin and R. Palicka, "Observations on the Nature of Micro-Cracking in Brittle Composites," J. Mat. Sc., 16, 141 (1981).

33. G. Ziegler and D. P. H. Hasselman, "Effect of Phase Composition and Microstructure on the Thermal Diffusivity of Silicon Nitride," J. Mat. Sc., 16, 495 (1981).

34. J. P. Singh, Y. Tree and D. P. H. Hasselman, "Effect of Bath and Specimen Temperature on the Thermal Stress Resistance of Brittle Ceramics Subjected to Thermal Quenching," J. Mat. Sc., 16 (8) 2109-2118 (1981).

35. K. Niihara, J. P. Singh, L. D. Bentsen and D. P. H. Hasselman, "Observation on the Sub-Critical Growth and Healing of Micro-cracks in Brittle Ceramics," pp. 323-34, Surface and Interfaces in Ceramics and Ceramic-Metal Systems, Plenum Press (1981).

36. L. D. Bentsen, D. P. H. Hasselman, and N. Claussen, "Effect of Micro-cracking on the Conduction of Heat in Brittle Composites," pp. 369-82 in Proc. Conf. Degradation of Engineering Materials, (VPI Press) (1981).

37. J. P. Singh, K. Niihara and D. P. H. Hasselman, "Analysis of Thermal Fatigue Behavior of Brittle Structural Materials," J. Mat. Sc., 16, 2789-97 (1981).

38. J. R. Thomas, Jr., J. P. Singh and D. P. H. Hasselman, "Thermal Stress in Materials Heated Internally by Radiation Absorption," J. of Nuclear Materials, 103-104, 167 (1981).

39. J. R. Thomas, J. P. Singh, and D. P. H. Hasselman, "Role of Thermal Expansion in the Thermal Stress Resistance of Semi-Absorbing Brittle Materials Subjected to Severe Thermal Radiation," pp. 121-30 in Proc. 7th Thermal Expansion Symposium, Plenum Press (1982).

40. Y. Chen, M. M. Abraham, L. D. Bentsen, and D. P. H. Hasselman, "Effect of Ni-Alloying on the Thermal Diffusivity/Conductivity of MgO Single Crystals," Comm. Amer. Ceram. Soc., 65 (7) C104-05 (1982).

41. J. J. Brennan, L. D. Bentsen and D. P. H. Hasselman, "Determination of the Thermal Conductivity and Diffusivity of Thin Fibers by the Composite Technique," J. Mat. Sc., 17, 2337 (1982).

42. K. Niihara, J. P. Singh and D. P. H. Hasselman, "Observations on the Characteristics of a Fluidized Bed for the Thermal Shock Testing of Brittle Ceramics," J. Mat. Sc., 17, 2553-59 (1982).

43. J. R. Thomas, Jr., J. P. Singh and D. P. H. Hasselman, "Thermal Stresses in a Partially Absorbing Flat Plate Asymmetrically Heated by Cyclic Thermal Radiation and Cooled by Convection," J. Thermal Stresses, 5, 247 (1982).

44. D. P. H. Hasselman, "Effect of Micro-cracking on Thermal Conductivity: Analysis and Experiment," pp. 417-31 in Thermal Conductivity 16, ed. by D. C. Larsen, Plenum Press (New York) (1983).

45. T. Ozyener, K. Satyamurthy, C. E. Knight, G. Ziegler, J. P. Singh and D. P. H. Hasselman, "Effect of ΔT- and Spatially Varying Heat Transfer Coefficient on Thermal Stress Resistance of Brittle Ceramics Measured by the Quenching Method," J. Amer. Ceram. Soc., 66, 53 (1983).

46. D. P. H. Hasselman and L. D. Bentsen, "Effect of Microstructural and Compositional Heterogeneity on the Conduction of Heat in Structural Materials for High-Temperature Use," Proc. on Thermomechanical Behavior of High-Temperature Materials, J. of Thermal Insulation, 6, 91 (1983).

47. M. Bucknam, L. D. Bentsen, James Makosey, G. R. Angell, and D. P. H. Hasselman, "The Measurement of the Thermal Conductivity of Refractories by the Laser-Flash Method," Proc. and Trans. Brit. Ceram. Soc., 82, 18-23 (1983).

48. J. P. Singh, J. R. Thomas and D. P. H. Hasselman, "Thermal Stresses in a Partially Absorbing Flat Plate Asymmetrically Heated by Cyclic Thermal Radiation and Cooled by Convection; Addendum," J. Thermal Stresses, 6, 93-95 (1983).

49. J. P. Singh, J. I. Frankel, J. R. Thomas, Jr., and D. P. H. Hasselman, "Thermal Stresses in Partially Absorbing Flat Plate Due to Sudden Interruption of Steady-State Asymmetric Radiation, I: Convective Cooling at Rear Surface," J. Thermal Stresses, 6, 15 (1983).

50. J. I. Frankel, J. P. Singh, J. R. Thomas, Jr., and D. P. H. Hasselman, "Thermal Stresses in Partially Absorbing Flat Plate Due to Sudden Interruption of Steady-State Asymmetric Radiation, II: Convective Cooling at Front Surface," J. Thermal Stresses, 6, 25 (1983).

51. L. D. Bentsen, D. P. H. Hasselman and R. Ruh, "Effect of Hot-Pressing Temperature on the Thermal Diffusivity/Conductivity of SiC-AlN Composites," J. Amer. Ceram. Soc., 66, 40 (1983).

52. W. Chang, C. E. Knight, D. P. H. Hasselman and R. G. Mitchiner, "Analysis of Thermal Stress Failure of Segmented Thick-Walled Refractory Structures," J. Amer. Ceram. Soc. (in press).

53. J. P. Singh, J. R. Thomas, Jr., and D. P. H. Hasselman, "Role of Absorption Coefficient in the Frequency Dependence of the Thermal Stresses in a Partially-Absorbing Plate Subjected to Cyclic Thermal Radiation," J. of Thermal Stresses (in press).

54. J. R. Thomas, J. I. Frankel and D. P. H. Hasselman, "Effect of Interface Reflections and Angle of Incidence of Radiation on Thermal Stresses in Semi-Transparent Materials," J. Thermal Stresses (in press).

55. M. Srinivasen, L. D. Bentsen, and D. P. H. Hasselman, "Thermal Diffusivity of Silicon Carbide-Silicon Composites, pp. 677-87 in Thermal Conductivity 17, ed. by J. G. Hust, Plenum Press (New York) (1983).

56. J. P. Singh, G. Ziegler and D. P. H. Hasselman, "Effect of Drop-Height on the Critical Temperature Difference (ΔT_c) for Brittle Ceramics Subjected to Thermal Shock by Quenching into Water," J. Amer. Ceram. Soc. (in press).

57. D. P. H. Hasselman and J. P. Singh, "Criteria for the Thermal Stress Failure of Brittle Structural Ceramics," in Thermal Stresses, State-of-the-Art, R. B. Hetnarski, Ed. (in press).

58. T. D. Nguyen, J. R. Thomas, Jr. and D. P. H. Hasselman, "Effect of Thermal Diffusivity on Magnitude of Thermal Stress in a Brittle Ceramic Subjected to Rapid Thermal Cycling," J. Amer. Ceram. Soc. (in review).

59. H. Hencke, J. R. Thomas, Jr., and D. P. H. Hasselman, "Role of Material Properties in the Thermal Stress Fracture of Brittle Ceramics Subjected to Conductive Heat Transfer," J. Amer. Ceram. Soc. (in review).

60. H. Tawil, L. D. Bentsen, D. P. H. Hasselman, "Effect of Heat Treatment on the Thermal Diffusivity of an Aluminosilicate Fiber-Reinforced Carbon Matrix," Carbon (in review).

61. L. D. Bentsen, D. P. H. Hasselman, "Role of Porosity in the Effect of Microcracking on the Thermal Conductivity of Brittle Ceramic Composites," Proc. 18th Thermal Conductivity Conference, Plenum Press (in press).

62. L. D. Bentsen, D. P. H. Hasselman, J. J. Brennan, "Radiative Contribution to the Thermal Diffusivity and Conductivity of a Silicon Carbide Fiber Reinforced Glass-Ceramic," Proc. 18th Thermal Conductivity Conference, Plenum Press (in press).

63. R. Ruh, L. D. Bentsen, D. P. H. Hasselman, "Thermal Diffusivity Anisotropy of SiC-BN Composites," J. Amer. Ceram. Soc. (in review).

64. L. D. Bentsen, T. -Y. Tien, D. P. H. Hasselman, "Effect of Crystallization of the Grain Boundary Phase on the Thermal Diffusivity of a Sialon Ceramic," J. Amer. Ceram. Soc. (in review).

Chapter I

Effect of Heat Treatment on the Thermal Diffusivity of an Aluminosilicate Fiber-Reinforced Carbon Matrix

H. Tawil*, L. D. Bentsen, D. P. H. Hasselman

Department of Materials Engineering

Virginia Polytechnic Institute and State University

Blacksburg, Virginia 24061 USA

---

*On sabbatical leave from Societe Europeenne
 de Propulsion, Bordeaux, France.

EFFECT OF HEAT TREATMENT ON THE THERMAL DIFFUSIVITY
OF AN ALUMINOSILICATE FIBER-REINFORCED CARBON MATRIX

H. Tawil*, L. D. Bentsen and D. P. H. Hasselman

Department of Materials Engineering,

Virginia Polytechnic Institute and State University

Blacksburg, Virginia   24061   USA

ABSTRACT

The effect of heat-treatment on the thermal diffusivity of an aluminosilicate fiber-reinforced carbon matrix was measured by the laser-flash method while the specimen was being heat treated. A permanent increase in thermal diffusivity was observed, which was attributed to the combined effects of structural modifications in the carbon at the atomic or molecular level, a change in the morphology of the pore phase within the carbon matrix, and possibly the crystallization of the fibers.

*On leave from Societé Europeènne de Propulsion, Bordeaux, France.

1. INTRODUCTION

Ceramic fiber-reinforced carbon composites are of interest for many industrial and aerospace applications. The ceramic fibers serve to enhance fracture toughness and thermal insulating ability. Heat-treatment of carbon can lead to irreversible changes (increases) in the thermal conductivity and diffusivity due to atomic, molecular or other structural rearrangement (1,2). Such effects should also be present in ceramic fiber-reinforced carbon, as reported in the present paper.

2. EXPERIMENTAL

The fiber-reinforced carbon material used for this study was obtained from a commercial source* in the form of a single block measuring approximately 20 by 20 by 2 cm. The fibers consisted of an aluminosilicate wool+. In the manufacture of the composite the aluminosilicate fibers were first densified with a phenolic resin followed by carbonization which transforms the resin to coke. The composite was then impregnated with a petroleum pitch and once more carbonized at 600 to 900°C for 10 to 20 hours to yield the carbon matrix. In the final composite the volume content of the aluminosilicate fibers was approximately 45%. The absence of x-ray diffraction peaks for the composite indicated that both the carbon matrix as well as the aluminosilicate fibers were primarily amorphous.

---

*CERASEP A102-SEP Industrie, Bordeaux, France.
+Kaowool, Morganite Ceramic Fibers, S.A. Liege, Belgium.

The bulk density, apparent density, and open porosity of disc-shaped samples approximately 12 mm in diameter by 2 mm thick were measured by Archimedes' method using boiling water as the fluid medium. The data obtained for the densities and the porosity indicated the existence of considerable heterogeneity within the block. For eight immediately adjacent samples cut from a single cylinder core-drilled from the block, the bulk density ranged from 1.25 to 1.55 g/cm^3 with a mean value of 1.41 g/cm^3. Similarly, the apparent density ranged from 1.81 to 1.88 g/cm^3 with a mean value of 1.85 g/cm^3. The open porosity ranged from 16 to 33% with a mean value of 24%. However, for all cores drilled from widely different areas of the original block, the densities and porosity showed much greater variation, ranging from 1.05 to 1.55 g/cm^3 for the bulk density, and from 1.46 to 2.16 g/cm^3 for the apparent density. The open porosity ranged from 13.5 to 51%.

Fig. 1 shows a typical scanning electron fractograph of a composite sample. For comparison and interpretation of the data, a few samples of the carbon matrix without the ceramic fibers were included in the study as well.

The effect of heat-treatment on the heat conduction behavior was determined by measurements of the thermal diffusivity by the laser-flash method (3) on the same samples used for the density measurements. In principle, this method consists of subjecting one side of a thin disc-shaped specimen to a single uniformly distributed laser-flash. The time dependence of the temperature

response of the opposite face is then monitored. The thermal diffusivity (κ) is calculated from:

$$\kappa = AL^2/t_{1/2}$$

where L is the specimen thickness and $t_{1/2}$ is the period of time following the laser-flash for the rear surface to reach one-half of the final temperature rise when the heat from the flash is uniformly distributed within the specimen. A is a constant, the value of which is determined by the heat loss from the specimen during the laser-flash as described by Heckman (4).

The laser-flash technique was particularly convenient for the present study as the thermal diffusivity could be measured while the specimens were being heat treated. The heat treatment and measurement of the thermal diffusivity were carried out in a nitrogen atmosphere within a resistively heated carbon furnace*, modified for the laser-flash diffusivity method. Because the changes in specimen thickness could not be monitored during heat treatment, the thermal diffusivity was calculated on the basis of the initial specimen thickness. Two heat-treatment schedules were followed. The first consisted of heating to and cooling from a pre-selected temperature over a total period of some 5 to 6 hours. The second heating schedule consisted of heating at a rate of 80°C/min to the desired temperature followed by holding the specimens under isothermal conditions for periods ranging from 2 to 3 hours.

---

*Model 1000A, Astro Industries, Santa Barbara, CA.

3. RESULTS

The thermal diffusivity at room temperature prior to heat-treatment of adjacent samples cut from a single core showed no significant variation, despite the aforementioned wide variations in bulk and apparent density and porosity. However, at a given value of density and porosity, specimens cut from different areas in the original block showed considerable variation in thermal diffusivity. For instance, at a value of bulk density of 1.4 g/cm^3, the thermal diffusivity ranged from 2.0 x 10^{-3} cm^2/s to 3.3 x 10^{-3} cm^2/s. These variations must be attributable to local variations in composition and microstructure. For this reason, no clear-cut dependence of the thermal diffusivity on density could be established.

Fig. 2 shows the thermal diffusivity for two samples of the fiber-carbon composite cycled to 1000 and 1400°C and for a sample of the carbon matrix without fibers cycled to 1400°C. All three samples show a major increase in the thermal diffusivity on return to room temperature. Such an increase at least in part must be attributed to the permanent structural modification of the carbon matrix, also responsible for the observations of Taylor (1) and Wagner (2) for the effect of heat-treatment on the thermal conductivity of carbons. Of interest to note was that this structural modification of the present samples did not result in a major change in the x-ray diffraction patterns of the carbon matrix following heat-treatment. Comparison of the magnitudes of the thermal diffusivity of the composite and carbon sam-

ples given in Fig. 2 indicates that the effect of the fibers on the thermal insulating ability is retained following thermal cycling.

Fig. 3 shows the time dependence of the thermal diffusivity of fiber-carbon samples held isothermally at 600, 1000 and 1400°C and for a carbon sample held at 1400°C following heating to these temperatures at a rate of 80°C/min. These data show that at any temperature the thermal diffusivity is invariant with time. This suggests that the structural modifications in the carbon phase responsible for the increase in the thermal diffusivity appear to be a function only of the maximum temperature reached. Such structural changes appear not to be the result of a thermally activated process, for which a time dependence of the thermal diffusivity at any given temperature would be expected. In this respect, the findings of this study confirm those of Rappeneau and co-workers (5) that the thermal as well as the mechanical properties are not influenced by the rate of heating during carbonization.

The observed changes in the thermal diffusivity with heat-treatment also were accompanied by weight loss, and by microstructural and dimensional changes. For a number of specimens held at 1000°C for approximately 1 1/2 hours, the weight loss ranged from 3 to 12%. The corresponding weight loss at 1400°C ranged from 9 to 25%. For temperatures below 1400°C, the weight loss of the composite samples can be attributed primarily to the weight loss of the carbon, also observed by Wallouch and Fair (6)

and Markovic and Marinkovic (7). For the composite samples at 1400°C, decomposition of the aluminosilicate fibers probably contributed to the weight loss as well. Evidence for this latter effect is given in Fig. 4 which compares the morphology of fiber surfaces before and after a 2-hour isothermal heat-treatment at 1400°C. For the fibers of Fig. 4, Fig. 5 compares the relative intensities of the Al and Si in the fibers as determined by EDAX analysis before and after heat-treatment at 1400°C for 2 hours. The decrease in the amount of Si relative to the Al suggests that the weight loss of the composite also can be attributed to the evaporation of the silicon in the form of one (or more) of its oxides.

Heat-treatment of the composite samples also caused a significant increase in the open porosity For four samples held at 1000°C for 2 hours, the open porosity increased from a mean value of approximately 24% to about 33% with corresponding changes in the bulk and apparent densities of +7.4% and +19.7%, respectively. For four samples held at 1400°C, the mean value of open porosity increased from 25% to 35%, with corresponding increases in the bulk and apparent densities of 1.9% and 23.9%, respectively. No significance should be attached to the changes in these properties at 1000 and 1400°C in view of the limited number of samples.

A change in open porosity implies a rearrangement of the pore morphology. Such a rearrangement, however, was not readily ascertained by scanning electron fractography possibly because of

the highly heterogeneous nature of the microstructure. As indicated by the theory of the thermal conductivity of composites, the nature of the distribution of second phase inclusions, including pores, has a significant effect on the composite thermal conductivity and diffusivity (8). For this reason, the observed changes in the thermal diffusivity on heat-treatment at least in part also may have been due to changes in the pore structure. A quantitative assessment of this effect, however, is not feasible at this time because of the difficulty in obtaining a quantitative description of the microstructural features of the composite samples, including the pores.

Dimensional changes of the specimens during heat treatment were also observed. At 1000 and 1400°C for 2 hours, the dimensions decreased by an average of about 4 and 5%, respectively. Because the thermal diffusivity was calculated on the basis of the original thickness of the specimens, the data shown in Fig. 2, with the exception of the initial data point at room temperature, represent overestimates by no more than 10%.

The evaporation of the Si (or oxide) from the fibers resulted in a change in their composition. An x-ray analysis of a sample heat-treated at 1400°C for 2 hours revealed diffraction peaks which corresponded to the alumina-silica compound known as mullite. Crystalline materials generally have higher thermal conductivity than the corresponding amorphous phase. The improved thermal conductivity of the fibers is thought to account for the observations as shown in Fig. 2 that the relative perma-

nent increase in the thermal diffusivity following heat treatment at 1400°C is higher for the fiber-carbon composites than for the carbon matrix itself. The absence of a pronounced time dependence of the thermal diffusivity as shown in Fig. 3, suggests that the crystallization of the fibers is essentially complete when the 1400°C temperature is attained.

ACKNOWLEDGEMENT

REFERENCES

1. R. Taylor, High Temperatures - High Pressures, 4, 649 (1972).

2. Paul Wagner, Carbon, 14, 71 (1976).

3. W. J. Parker, R. J. Jenkins, C. P. Butler and G. L. Abbott, J. Appl. Phys., 32, 1679 (1961).

4. R. C. Heckman, J. Appl. Phys., 44, 1455 (1973).

5. J. Rappeneau, M. Yvars, M. Mottet, P. Cornuault, J. Lori and A. Galy, Carbon 10, 471 (1972).

6. R. W. Wallouch and F. V. Fair, Carbon 18, 147 (1980).

7. V. Markovic and S Marinkovic, Carbon 18, 329 (1980).

8. S. C. Cheng and R. I. Vachon,, Int. J. Heat Mass Transfer, 12, 249 (1969).
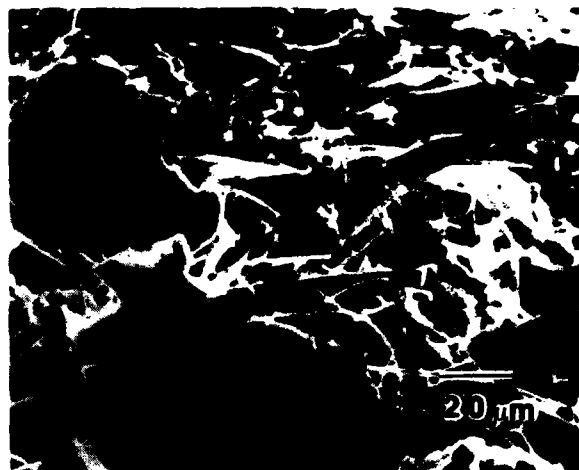
Fig. 1. Scanning electron fractograph of an
aluminosilicate fiber-reinforced carbon
matrix.
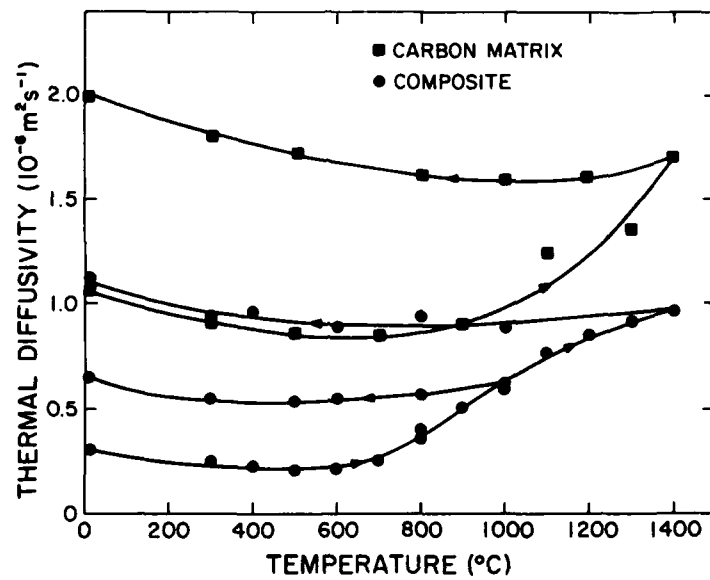
Fig. 2. Effect of thermal cycling on the thermal diffusivity of a carbon matrix and an aluminosilicate-carbon composite.
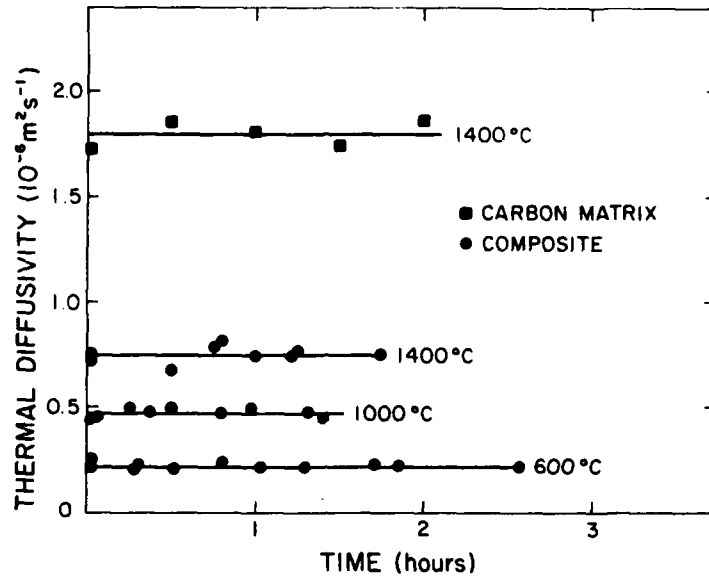
Fig. 3. Effect of isothermal heating on the thermal
diffusivity of a carbon matrix and an
aluminosilicate-carbon composite.
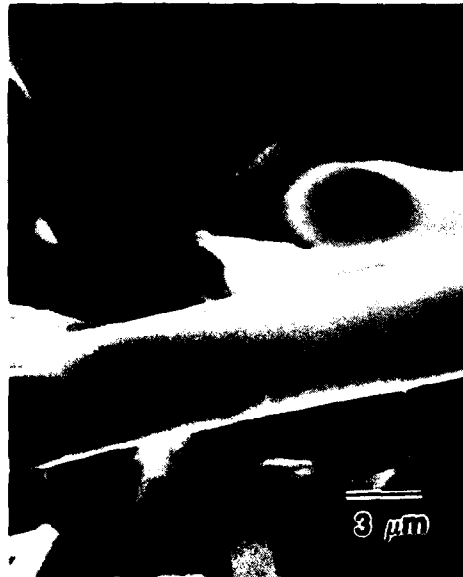
a.   b.

Fig. 4.   Scanning electron fractograph of aluminosilicate fiber
          in fiber-carbon composite prior to (a) and following (b)
          heat treatment at 1400°C for 2 hours.
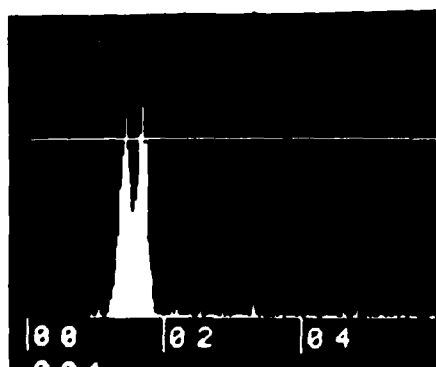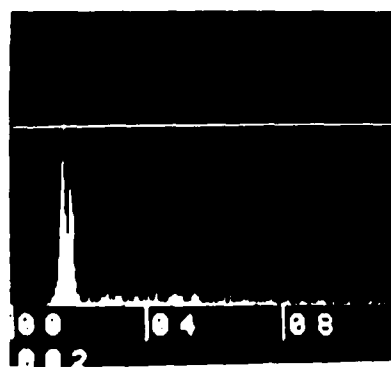
a.   b.

Fig. 5.   Relative content of Al (left peak) and Si (right peak) in aluminosilicate fiber prior to (a) and following (b) heat treatment at 1400°C for 2 hours.

Chapter II

ROLE OF POROSITY IN THE EFFECT OF MICROCRACKING ON THE THERMAL CONDUCTIVITY OF BRITTLE CERAMIC COMPOSITES

L. D. Bentsen and D. P. H. Hasselman
Department of Materials Engineering
Virginia Polytechnic Institute and State University
Blacksburg, Virginia 24061 USA

ROLE OF POROSITY IN THE EFFECT OF MICROCRACKING ON THE THERMAL

CONDUCTIVITY OF BRITTLE CERAMIC COMPOSITES

L. D. Bentsen and D. P. H. Hasselman

Department of Materials Engineering
Virginia Polytechnic Institute and
State University
Blacksburg, Virginia 24061 USA

ABSTRACT

Fracture mechanical principles were used to predict the role of porosity in the formation of microcracks in brittle ceramic composites containing a dispersed phase with a coefficient of thermal expansion less than that of the matrix. It is shown that microcracking will occur only if the amount of porosity lies within a region $P_i<P<P_a$, and that all the microcracks will be of equal size. Using this criterion, the effect of the microcracks and pores on the thermal conductivity is examined. The expected behavior includes a sharp drop in the relative thermal conductivity and diffusivity at P_i, followed by a porosity-independent value between P_i and P_a. These conclusions were confirmed by measurements of the thermal diffusivity of composites containing silicon carbide dispersed in a matrix of magnesium oxide, beryllium oxide, and aluminum oxide, each with a range of compositions and amounts of porosity.

INTRODUCTION

Many brittle materials such as geological formations and structural ceramics for high temperature purposes can undergo extensive microcracking. The principle causes for the formation of microcracks include phase transformations, thermal expansion anisotropy of the grains of polycrystalline aggregates, or mismatches in the thermal expansion of the individual components within a composite. These latter two effects result in the generation of internal stresses upon changes in temperature of the

polycrystal or composite from the manufacturing temperature. The magnitude of these stresses is a function of the range of temperature change, the degree of thermal expansion anisotropy or mismatch, and the elastic properties of the grains or individual components. These internal stresses can be large enough to result in localized fracture and microcrack formation. Such microcracks can have a major effect on the continuum behavior of brittle materials, affecting the elastic moduli, strength, fracture energy, and toughness. Microcracking can also lead to significant improvements in machinability and thermal shock resistance.

Microcracks represent barriers to heat flow by phonon and electron transport and have a significant effect on the thermal conductivity and diffusivity at temperatures low enough that radiative heat transfer across the cracks does not make a major contribution. The continuum heat transport properties of microcracked materials have received much theoretical and experimental attention. Microcracks in structural ceramics of technical interest were found to decrease the thermal conductivity and diffusivity by as much as a factor of three (1-4). A number of theoretical expressions for the effect of cracks on thermal conductivity have appeared in the literature. For a matrix with randomly oriented penny-shaped cracks of radius b, the effective thermal conductivity, K_{eff} is (5)

$$K_{eff} = K_0 (1+8Nb^3/9)^{-1} \qquad (1)$$

where K_0 is thermal conductivity of the crack-free material and N is the number of cracks per unit volume.

Many ceramic materials also contain a pore phase. Porosity of 10 to 30% is desirable for improving the thermal insulating ability and thermal shock resistance of refractory ceramics used in furnace linings and related applications. A residual pore phase of only a few percent in structural ceramics for high performance applications, such as components of high temperature turbine engines, generally results from incomplete densification during sintering or hot-pressing of compacts made by powder metallurgical techniques.

For temperatures at which radiation across the pores is negligible, a porous material represents a special case of a composite consisting of a continuous matrix with a dispersed phase of zero thermal conductivity. Theoretical solutions for the effective thermal conductivity of composites indicate that the pore phase should lead to a decrease in thermal conductivity, with the relative decrease determined by the volume fraction, shape, and orientation of the pores (6-7). Such a decrease in

thermal conductivity or diffusivity was confirmed by experimental data (7-8). For the morphology and orientation of the residual pore phase found in sintered powder compacts, the relative decrease in thermal conductivity generally was found to be of the order of three times the pore volume fraction. Because of the accompanying decrease in the specific heat per unit volume, the corresponding relative decrease in thermal diffusivity is expected to be about two times the fractional porosity. For spherical pores the relative decrease in thermal diffusivity is only one-half the pore volume fraction.

Microcracked brittle materials usually also contain a residual pore phase. For this reason, the thermal transport behavior of ceramics prone to microcracking should be affected by the combined presence of the microcracks and the pore phase. In general, at concentrations sufficiently low that the local temperature fields around second phase inclusions or other thermal discontinuities are not affected by neighboring inclusions or discontinuities, the relative effects of microcracks and porosity on thermal conductivity are additive. At first sight, then, it appears that the combined effects of the cracks and the pore phase on the heat conduction be- havior of microcracked materials could be ascertained from information on the separate effects for the cracks and pores, as determined either from theory or experiment.

For microcracked materials, however, this approach is compli- cated by the very role of the pore phase in the formation of microcracks. For any residual stress distribution, the magnitude of peak stress alone is not sufficient to describe the generation of microcracks. The appropriate criterion for microcrack formation is that the magnitude of the stress intensity factor, which is governed by the magnitude of stress and size of the precursor crack, equals or exceeds the critical stress intensity factor (K_{Ic}) appropriate to the preferred plane of crack propagation, which may be grain boundaries in polycrystalline materials or phase boundaries in compositess. For materials prone to microcracking, pores repre- sent the very source of microcrack precursors, especially the crack- like pores located at the triple points, grain boundaries, and interfaces.

The fracture mechanics of microcrack stability and propagation has received considerable theoretical attention (9-11). Figure 1 illustrates schematically the stability of a circumferential micro- crack (i.e., pore) around a spherical inclusion contained within a brittle matrix. The thermal expansion coefficient of the matrix is greater than that of the inclusion, resulting in tensile tangential stress in the matrix near the inclusion when the composite is cooled from the fabrication temperature, at which the internal

CRACK SIZE/INCLUSION SIZE (C/R)

STRESS INTENSITY FACTOR $K_I/\sigma\sqrt{R}$
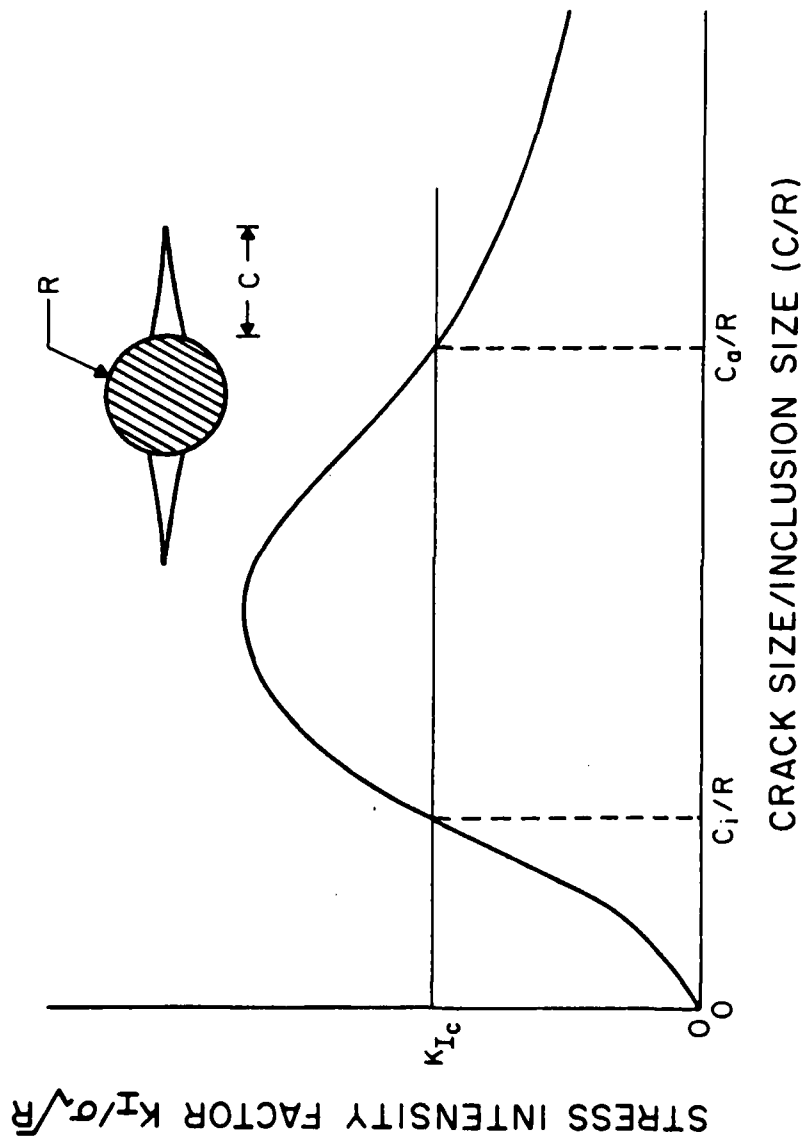
Fig. 1.   Normalized stress intensity factor as a function of relative crack length for a radial crack produced by a spherical inclusion under compression.

stresses are zero. Figure 1 indicates that the stress intensity factor (K_I) is a function of the ratio of the crack size to the inclusion size. Crack instability and propagation will occur only between crack sizes c_i and c_a. For $c<c_i$ no microcracking will occur since the crack size is so small that $K_I<K_{IC}$ for the maximum stress involved. The absence of crack propagation for $c<c_a$, the crack length for crack arrest, is due to the combined effects of the decrease in stress with increasing distance from the inclusion, and the stress relief due to the formation of the crack, which permits accomodation of the mismatch in thermal expansions of the matrix and inclusion. The conclusion obtained from Figure 1 is critical to the objectives of this study and the experimental results to be presented. The figure shows that the crack length for crack arrest, c_a, is independent of the initial crack length $c>c_i$. Furthermore, the value of the initial crack length is included in the value of crack length at crack arrest. It is for this reason that the combined effect of porosity and microcracks are expected to be coupled rather than simply additive.

A direct relationship generally exists between the pore content and the number of pores per unit volume, their geometry and their dimensions. For simplicity, it will be assumed that the dimensions and geometry of all pores are identical. The existence of a minimum crack size, c_i (i.e., pore size), implies that no microcracking will occur below a minimum value of porosity, P_i. Thus for values of porosity $0<P<P_i$, the thermal conductivity will be governed by the effect of the pore phase only. The same effect will prevail for $P>P_a$ for which no microcracks can form either.

For $P_i<P<P_a$, however, microcrack formation will occur, with all cracks being of equal size. Because the size of the microcrack precursor (i.e., the pore) is included within the dimensions of the microcrack at arrest, it is expected that for $P_i<P<P_a$, the thermal conductivity will be governed only by the microcracks and should be independent of pore content.

The implications of the above conclusions with regard to the effect of porosity on the thermal conductivity of brittle materials prone to microcracking is shown schematically in figure 2. For $P<P_i$ and $P>P_a$, the thermal conductivity decreases monotonically with increasing porosity. At P_i, the thermal conductivity decreases discontinuously to a value which remains constant for $P_i<P<P_a$.

Clearly, the dependence of thermal conductivity on pore content shown in figure 2 is valid for the idealized situation of all pores having equal size and geometry. In practice however, the pores will exhibit a range of dimensions and geometries. Depending on the size and shape distributions, the dependence of thermal conductivity on pore content shown in figure 2 will show a more continuous
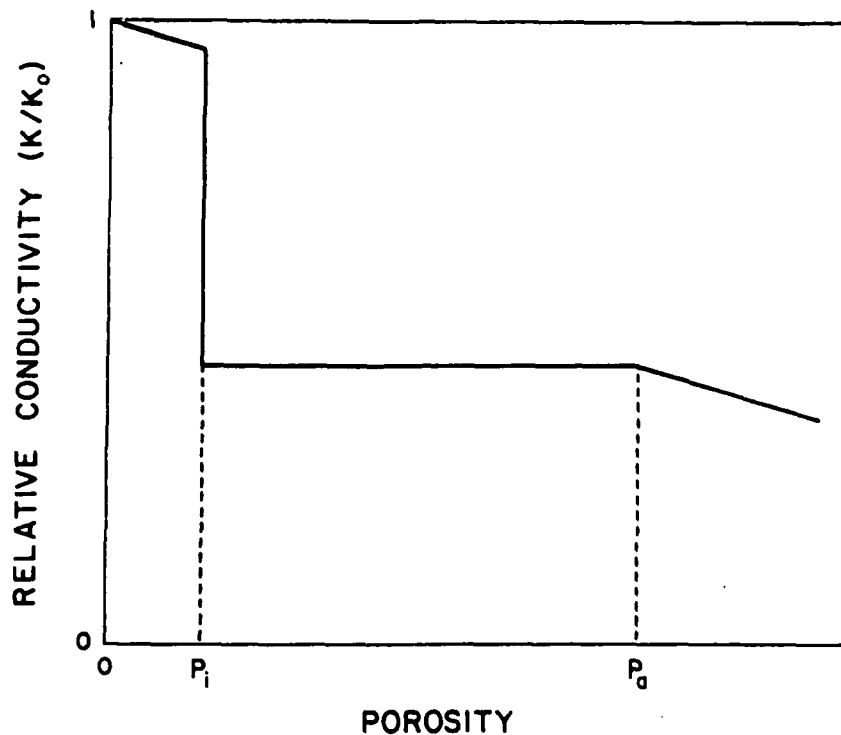
Fig. 2. Predicted effect of porosity on the rela-
tive thermal conductivity of brittle
composites prone to microcracking due to
thermal expansion mismatch.

variation preceeded by an initial rapid decrease in thermal conduc-
tivity at $P \approx P_i$. Furthermore, for $P_i < P < P_a$, a slight decrease in
the thermal conductivity is expected for those small pores which
did not contribute to the formation of microcracks. It should be
noted that microcrack formation itself also contributes to the
creation of porosity. For this reason, the measured pore content
represents the sum of the original pore phase plus the extra
porosity created by microcracks. For two-component composite ma-
terials, an upper bound on the pore content created by the micro-
cracks, (P_{mc}), can be estimated assuming that the total thermal
expansion mismatch between the two components can be accounted for
by the volume of the cracks. This yields:

$$P_{mc} \approx 3\Delta\alpha\Delta T$$

where $\Delta\alpha$ is the mismatch in the coefficients of thermal expansion
of the two components and ΔT represents the temperature range of
cooling from the processing temperature.

The above conclusions regarding the effect of porosity on the thermal conductivity of microcracked materials are supported by experimental data reported herein.

EXPERIMENTAL

The microcracked brittle composites consisted of aluminum oxide, beryllium oxide, or magnesium oxide with a dispersed phase of silicon carbide. Table I lists the coefficients of thermal expansion (12) for the three matrix materials and the silicon carbide, together with the values of thermal conductivity (13), density, specific heat (14), and thermal diffusivity at room temperature. The latter four values are required for the calculation of the composite thermal conductivity without microcracks. Because the coefficients of thermal expansion for the three oxide materials exceed the value for the silicon carbide, microcrack formation will occur in the matrix phase when the composites are cooled from the manufacturing temperature.

The specific process by which these composites were made consisted of pressure sintering mixtures of the appropriate powders in graphite dies. The amount of residual pore phase could not be closely controlled during the pressure sintering operation; therefore, a number of samples were obtained to assure a sufficient range of pore content. Typical microstructures for composites consisting of magnesium oxide with a range of silicon carbide contents are shown in figure 3. The mean grain size of the magnesium oxide matrix was of the order of 1 μm, with similar values for the composites based on aluminum oxide and beryllium oxide. The silicon carbide particles were somewhat disc-shaped with a diameter of about 6 μm and a thickness of about 1-2 μm.

The porosity of the samples was determined from the measured density of the specimens and the theoretical density of the pore-free composites as calculated from the values of density listed in table I. The effect of the pores and microcracks on the heat conduction behavior was determined by measurements of the thermal diffusivity by the flash method (15) using a glass-Nd laser as the flash source. All measurements were made at room temperature using a liquid nitrogen-cooled infrared detector to monitor the transient temperature of the specimen. The specimens were either circular disks about 12 mm in diameter or square plates about 1 cm on a side, each about 2 mm thick.

The specimens for all three series of composites varied in pore content as well as silicon carbide content. To facilitate reporting the data, the actual experimentally determined diffusivity data were multiplied by the density and specific heat to obtain the thermal conductivity. These values of thermal conductivity

Table I. Thermal expansion and room temperature heat transfer properties of
SiC and three oxide matrix materials.

	SiC	Al_2O_3	BeO	MgO
Coefficient of Thermal Expansion* (293-1600 K) ($\times 10^6$/°C)	5.1	8.9	9.8	14.4
Thermal Conductivity (W/m·K)	168.0	36.4	272.0*	48.4*
Density (g/cm^3)	3.21	3.986	3.008	3.576
Specific Heat* (cal/g·C)	.161	.230	.246	.222
Thermal Diffusivity (cm^2/S)	.7770	.0950	.8785	.1457

*Touloukian, et al.
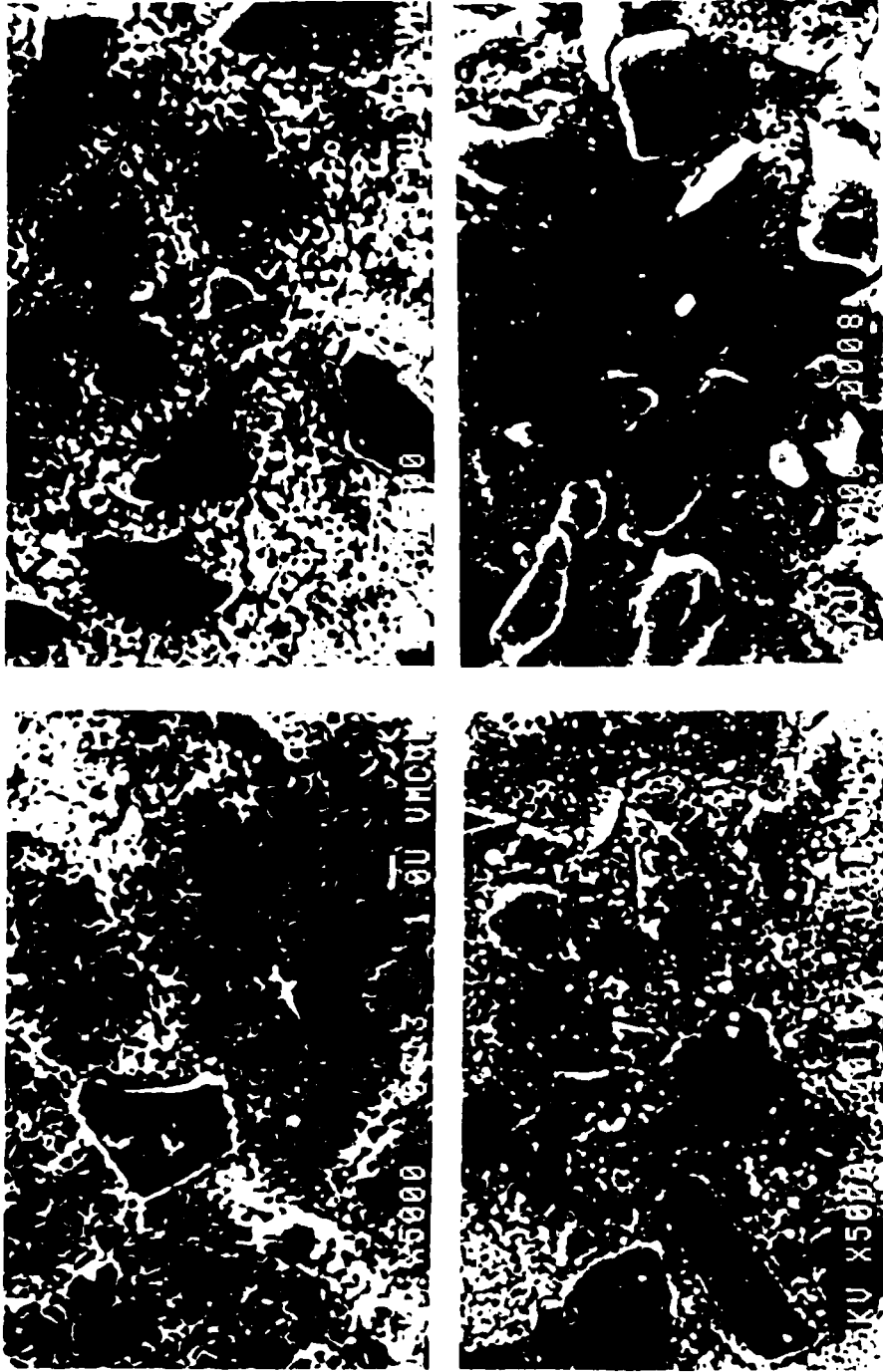
Fig. 3. SEM micrographs of MgO-SiC composites containing, clockwise from upper left, 10, 20, 30, and 40% SiC.

were then dividied by the value of the conductivity without cracks.
This latter value was calculated using the Bruggeman mixture
equation and the appropriate values of the thermal conductivity
of the individual components as listed in table I.

RESULTS AND DISCUSSION

Figure 4 compares typical experimental data for the thermal
diffusivity of the alumina-silicon carbide composites as a function
of silicon carbide content to the values for the crackfree composites
calculated from composite theory. The experimental data clearly fall
far below the calculated values. The difference is attributable to
the formation of the microcracks due to the thermal expansion mis-
match. Dividing the experimental value by the calculated value for
any given silicon carbide content yields the relative thermal
conductivity, which reflects the effect of the microcracks alone,
without the accompanying change in the thermal conductivity due
to the silicon carbide phase. These relative values can then be
plotted as a function of pore content in order to verify the role
of porosity in the heat conduction behavior of microcracked com-
posites.

Figures 5, 6, and 7 show the data for the relative thermal
conductivity of the composites of silicon carbide dispersed in
alumina, beryllia, and magnesia, respectively, as a function of
the pore content. All three sets of data, especially the extensive
set of data for the MgO-SiC system, are in general agreement with
the behavior shown in figure 2, predicted from fracture-mechanical
principles. The very rapid decrease in thermal conductivity with
increasing porosity at the lower values of porosity is clearly evi-
dent. The invariance of the thermal conductivity with porosity at
the higher pore contents is compatible with the conclusion that the
final crack size is independent of the initial pore size (i.e., ini-
tial pore content at a given crack density). The data scatter for
the thermal conductivity at the lowest values of porosity is too
large to make a reliable extrapolation; nevertheless, the general
trend of the data suggests the existence of a minimum value of poro-
sity below which no microcracking occurs.

The amount of porosity created by the formation of the
microcracks cannot be ascertained from the present data. However,
the differences in porosity at a given value of silicon carbide
content must represent the amount of original pore phase prior to
the formation of the microcracks.

Comparison of the data shown in figures 5, 6, and 7 indicates
that the relative thermal diffusivity at the higher pore contents is
lowest for the magnesium oxide matrix, followed by the beryllium
oxide and then the aluminum oxide matrix. This is expected from
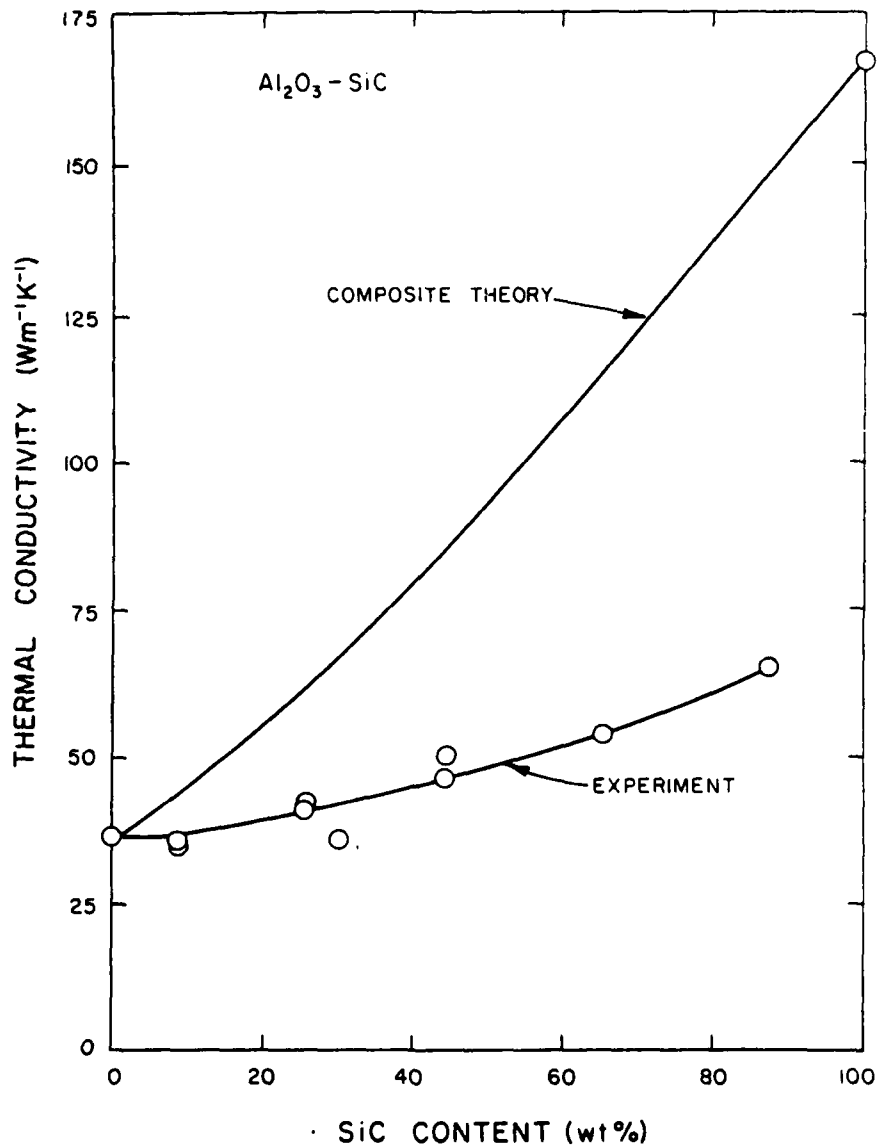
Fig. 4. Room temperature thermal conductivity of
Al_2O_3–SiC composites as compared to values
expected from the theory of mixtures.
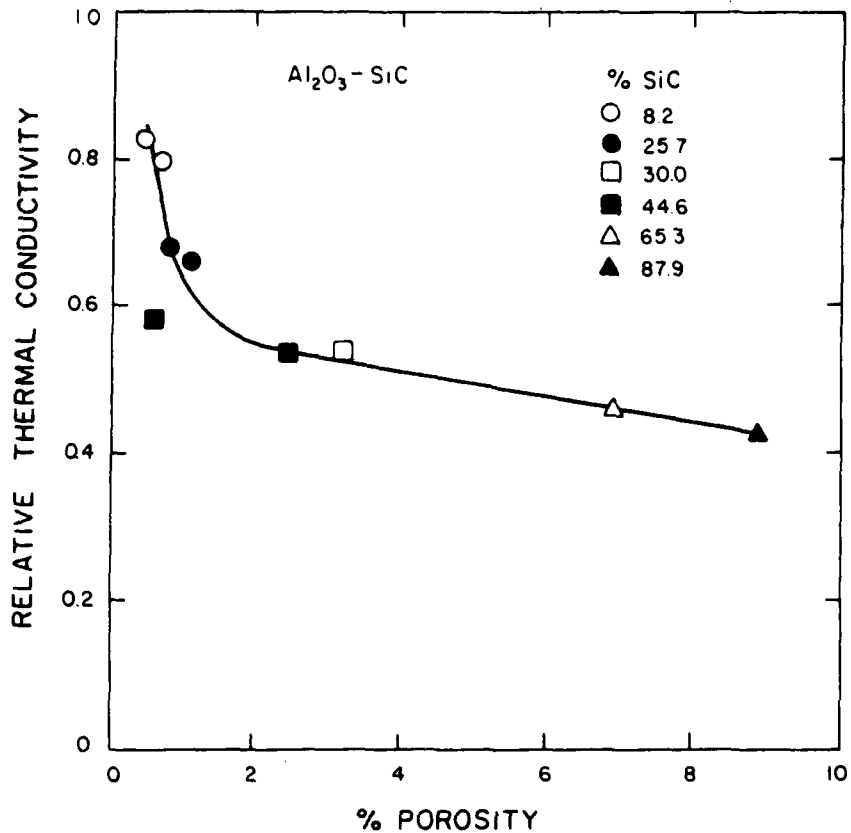
Fig. 5. Effect of pore content on the relative
thermal conductivity of microcracked
Al_2O_3-SiC composites relative to crack-
free values.

the differences in the mismatch in the coefficients of thermal expansion between the silicon carbide and the three matrices. The extent of crack propagation and resulting decrease in thermal diffusivity is expected to increase with increasing thermal expansion mismatch.

In summary, on the basis of the stability of microcracks in internal stress fields produced by thermal expansion heterogeneity, a prediction was made concerning the relative effect of the pore content on the thermal diffusivity and conductivity of brittle materials subject to microcracking and was confirmed by experiment.

ACKNOWLEDGEMENT

This study was conducted as part of a research program on the
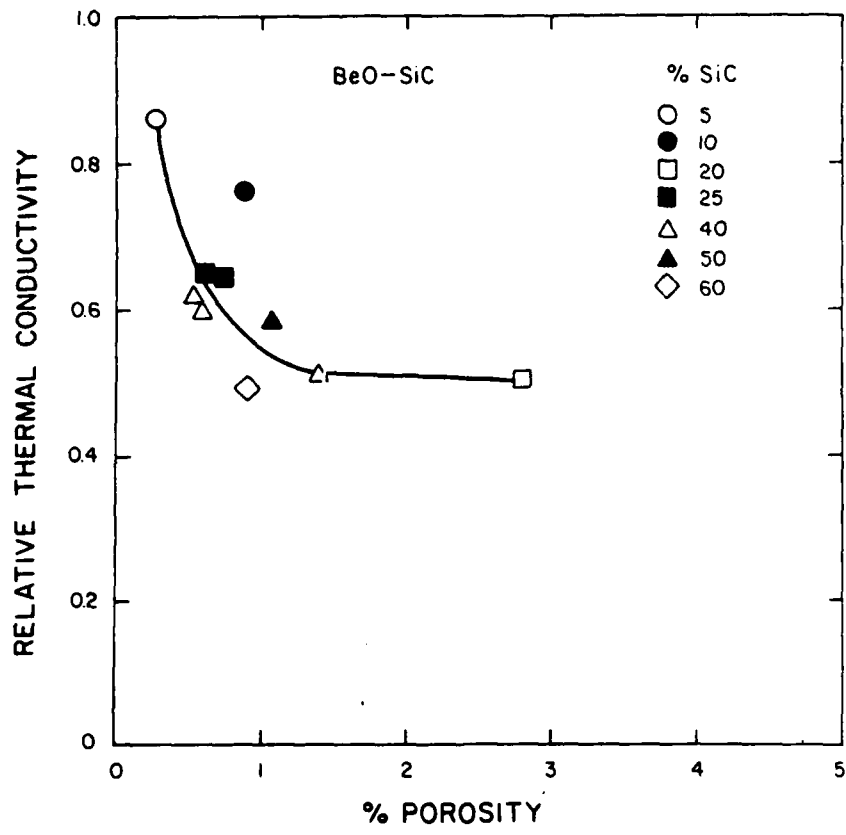
Fig. 6. Effect of pore content on the relative
thermal conductivity of microcracked
BeO-SiC composites relative to crack-
free values.
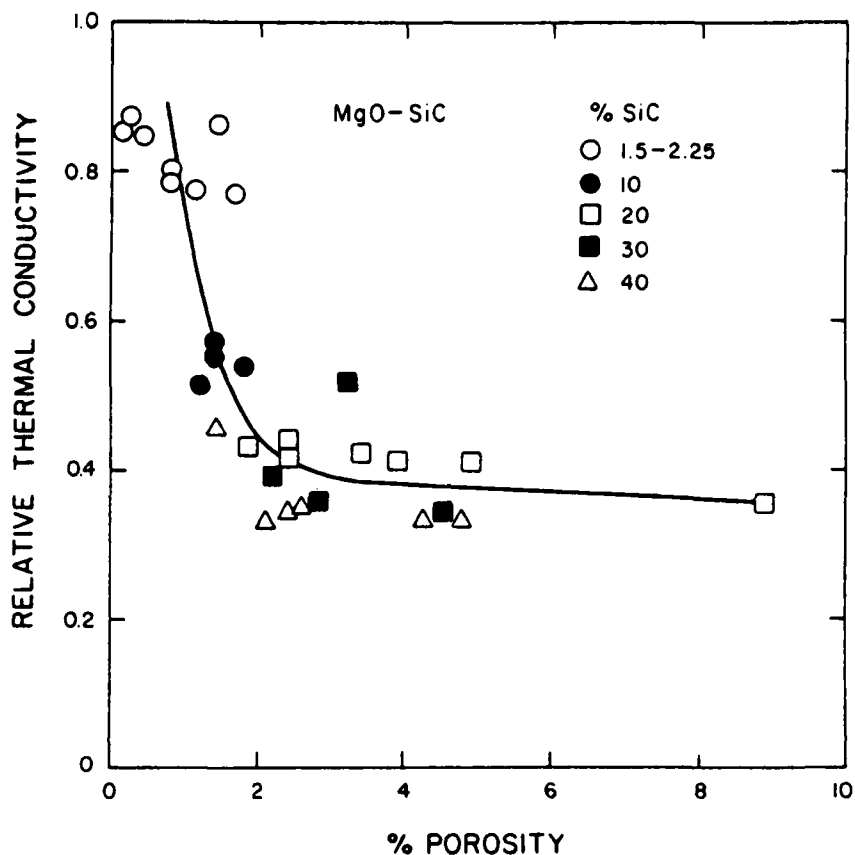
Fig. 7. Effect of pore content on the relative
thermal conductivity of microcracked
MgO-SiC composites relative to crack-
free values.

REFERENCES

1. H. J. Siebeneck, D. P. H. Hasselman, J. J. Cleveland and R. C.
    Bradt, J. Am. Ceram. Soc., 59:241 (1976).
2. H. J. Siebeneck, D. P. H. Hasselman, J. J. Cleveland and R. C.
    Bradt, J. Am. Ceram. Soc., 60:336 (1977).
3. J. P. Singh, D. P. H. Hasselman, W. M. Su, J. A. Rubin,
    R. Palicka, J. Mat. Sci., 16:141 (1981).
4. D. P. H. Hasselman, pp. 417-33 in Thermal Conductivity, Vol.
    16, Ed. by D. C. Larson, Plenum Press, New York (1983).
5. D. P. H. Hasselman, J. Comp. Mat., 12:403 (1978).

6. A. E. Powers, Conductivity in Aggregates, Knolls Atomic Power Laboratory Report KAPL-2145, March 6, 1961.

7. S. C. Cheng and R. I. Vachon, Int. J. Heat and Mass Trans., 12:249 (1969).

8. J. Francl and W. D. Kingery, J. Am. Ceram. Soc., 37:99 (1954).

9. A. Evans, Acta. Met., 26:1845 (1978).

10. D. Clarke, Acta. Met., 28:913 (1980).

11. M. V. Swain, J. Mat. Sci., 16:151 (1981).

12. Y. S. Touloukian, R. K. Kirby, R. E. Taylor, and T. Y. R. Lee, "Thermal Expansion-Nonmetallic Solids", (Thermophysical Properties of Matter, Vol. 13) IFI/Plenum Press, New York-Washington, 1977.

13. Y. S. Touloukian, R. W. Powell, C. Y. Ho, and P. G. Klemens, "Thermal Conductivity-Nonmetallic Solids", (Thermophysical Properties of Matter, Vol. 2) IFI/Plenum Press, New York-Washington, 1970.

14. Y. S. Touloukian and E. H. Buyco, "Specific Heat-Nonmetallic Solids", (Thermophysical Properties of Matter, Vol. 5) IFI/Plenum Press, New York-Washington, 1970.

15. W. J. Parker, R. J. Jenkins, C. P. Butler and G. L. Abbott, J. Appl. Phys., 32:1679 (1961).

Chapter III

RADIATIVE CONTRIBUTION TO THE THERMAL DIFFUSIVITY

AND CONDUCTIVITY OF A SILICON CARBIDE FIBER REINFORCED

GLASS-CERAMIC

L. D. Bentsen and D. P. H. Hasselman
Department of Materials Engineering
Virginia Polytechnic Institute and State University
Blacksburg, Virginia   24061   USA

J. J. Brennan
United Technologies Research Center
East Hartford, Connecticut   06108   USA

RADIATIVE CONTRIBUTION TO THE THERMAL DIFFUSIVITY AND CONDUCTIVITY OF A SILICON CARBIDE FIBER REINFORCED GLASS-CERAMIC

L. D. Bentsen and D. P. H. Hasselman
Department of Materials Engineering
Virginia Polytechnic Institute and State University
Blacksburg, Virginia 24061 USA

J. J. Brennan
United Technologies Research Center
East Hartford, Connecticut 06108 USA

ABSTRACT

The thermal diffusivity and conductivity of a silicon carbide fiber-reinforced lithium aluminosilicate glass-ceramic was measured using the laser-flash method. As indicated by the effect of specimen thickness on thermal conductivity and its positive temperature dependence, heat transfer by radiation makes a significant contribution to the total thermal conductivity. The observed dependence of the effect of specimen thickness on thermal conductivity suggests that radiative heat transfer between the carbon coated surfaces of dielectric materials for the laser-flash technique may be partially governed by the view factor between the specimen surfaces.

INTRODUCTION

Electrons, phonons, and photons represent the primary mechanisms of heat transport in solids. Each of these mechanisms displays a unique temperature dependence (1). In dielectric materials the thermal conductivity due to electron transport is generally not significant, and above room temperature the conductivity is approximately inversely proportional to the temperature as the result cf increased phonon collisions.

The thermal conductivity due to photon transport is a function of the optical absorption and emission behavior. For highly transparent materials, heat transfer can occur by direct radiation be-

tween the surfaces of the material. In this case the effective
radiative thermal conductivity for surfaces with equal emissivity
is (2):

$$K_R = (\frac{e}{2-e}) \ 4\sigma n^2 T^3 d \tag{1}$$

where e is the emissivity of the specimen surface, σ is the
Stefan-Boltzman constant, n is the index of refraction, T is the
absolute temperature, and d is the thickness of the material in
the direction of heat flow.

Heat transport by radiation can also occur by emission,
absorption, and re-emission. When the distance between absorption
and re-emission of a photon is small compared to the specimen
dimensions, the radiative conductivity becomes (2):

$$K_R = \frac{16}{3} \ \sigma n^2 T^3 l \tag{2}$$

where l is the photon mean-free-path which is equal to the recipro-
cal of the extinction coefficient.

Equations 1 and 2 indicate that the thermal conductivity due
to radiation between the specimen's surfaces, and the thermal
conductivity due to absorption and re-emission of radiation are
proportional to T^3. This implies that the radiative thermal con-
ductivity should exhibit a strong positive temperature dependence.
Equations 1 and 2 also show that the thermal conductivity due to
radiation directly across the material is directly proportional to
the specimen thickness, whereas radiative heat transfer by photon
absorption and re-emission is independent of the specimen size.

In general, the conduction of heat in dielectric materials
occurs by the combined contributions of phonon and photon transport.
Above room temperature, the negative temperature dependence of the
thermal conductivity due to phonon transport will be offset by the
positive dependence of the radiative contribution. In crystalline
dielectric materials which have a large phonon mean-free-path,
such as aluminum oxide, beryllium oxide, and diamond, the negative
temperature dependence of phonon transport generally overrides
the positive temperature dependence of radiative heat transfer up
to temperatures of some 1000°C. In highly amorphous dielectrics,
phonon transport tends to be suppressed. For these materials,
the relative contribution of radiative heat transfer can be such
that the combined thermal conductivity due to phonons and photons
produces a significant positive temperature dependence.

Such a positive temperature dependence was observed in a
feasibility study of the composite method for determining the
thermal conductivity of amorphous silicon carbide fibers contained
within a continuous matrix of a lithium aluminosilicate (LAS)

glass-ceramic (3). The experimental data indicated that radiative heat transfer within the fibers as well as the glass-ceramic matrix made significant contributions to the total thermal conductivity of the composite. A few exploratory measurements indicated the existence of the effect of specimen thickness on the thermal conductivity, suggestive of radiative heat transfer between the specimen surfaces as described by equation 1. The purpose of this study was to investigate the effect of specimen size on the thermal conductivity of the SiC-LAS composites in order to determine in further detail the nature of the radiative contribution to the total thermal conductivity.

EXPERIMENTAL PROCEDURES

Materials

The silicon carbide fibers from a commercial source* were made from an organometallic polymer by the method of Yajima (4). Chemical analysis indicated that the fibers consisted of about 65% SiC, 25% SiO_2, and 10% C. The fibers were in the form of tows of yarn containing about 500 fibers per tow. The average fiber diameter was approximately 10 μm and the density was about 2.55 $g \cdot cm^{-3}$. The degree of peak broadening in x-ray analysis showed that the fibers were nearly amorphous with a crystallite size of 2.5 to 3.0 nm.

The matrix material consisted of a lithium aluminosilicate glass-ceramic with a composition nearly identical to that of a commercial glass-ceramic**; however the 3% TiO_2 nucleating agent was replaced by about 2% ZrO_2 in order to eliminate the reactivity between the TiO_2 and the SiC. The density of the LAS was 2.52 $g \cdot cm^{-3}$.

Composites were fabricated by passing the SiC yarn through a slurry of the uncrystallized glass powder dissolved in isopropyl alcohol. After drying, the coated yarn was cut to fit a graphite die, and was hot-pressed in vacuum for 5 to 60 minutes at 1400 to 1500°C and 14 MPa. Following hot-pressing, the glass was crystallized by heat treating the composite for 1 to 2 hours at temperatures of 880 to 1100°C. Both uniaxial and 0/90 cross-ply composites were fabricated with SiC contents up to 50 vol.%. Figure 1 shows a photomicrograph of a composite with uniaxial fibers, and figure 2 shows a scanning electron fractograph of a 0/90 cross-ply composite.

---

*Nippon Carbon Company, Japan.
**C-9608, Corning Glass Works, Corning, New York.
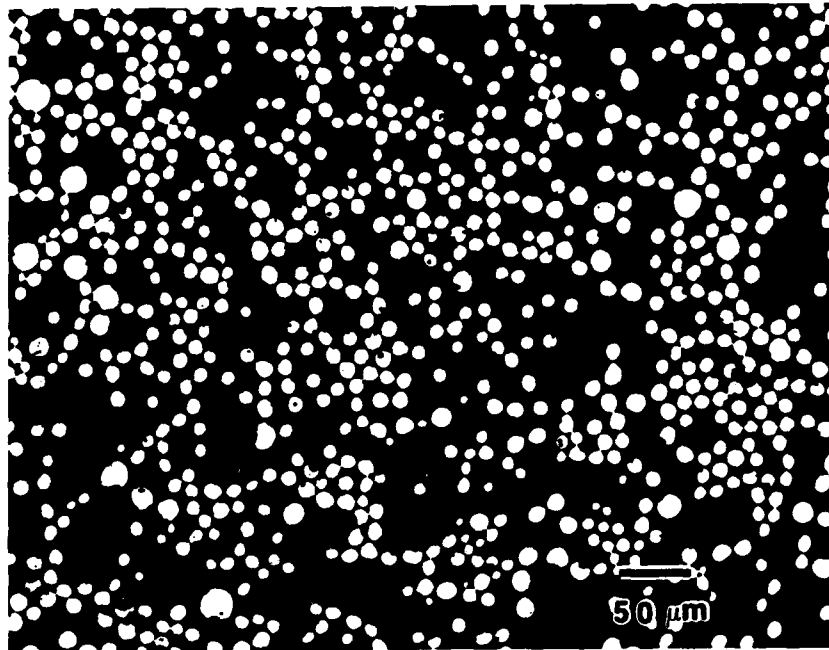
Fig. 1.   Photomicrograph of a composite of LAS glass-
          ceramic containing 48 vol.% uniaxially
          aligned SiC fibers.

Measurement and Evaluation of Thermal Properties

The laser-flash method (5) was used to measure the thermal
diffusivity of the composites and the matrix. The specimens of
the composites cut from the hot-pressed blanks were in the form
of nearly square plates about 9.5 mm on a side with thicknesses
ranging from 0.5 to 4.5 mm. Samples were cut to permit measurement
of the thermal diffusivity both parallel and perpendicular to the
fibers. Specimens of the LAS matrix were circular disks 12.8 mm
in diameter with thicknesses of 0.3 to 4.0 mm. For all samples,
direct transmission of the laser beam was prevented by coating the
specimen surfaces with carbon. The transient temperature response
of the specimen was monitored with remote optical sensors. For
measurements above room temperature, the specimens were supported
within a carbon resistance furnace containing a nitrogen atmosphere.

In the analysis of the data, corrections for heat loss were
taken into account using the method of Heckman (6). Changes in
the thickness and density of the specimens due to thermal expansion
were also accounted for. The specific heat of the fibers and the
glass-ceramic matrix was determined with differential scanning
calorimetry.

Fig. 2. Scanning electron fractograph of a composite
of LAS glass-ceramic containing 45 vol.% of
crossplied SiC fibers.

From the measured value of the thermal diffusivity of either
the fiber-free matrix or the composite, the corresponding value of
the thermal conductivity can be calculated from:

$$K = \kappa\rho c \tag{3}$$

where κ is the thermal diffusivity, ρ is the density, and c is the
specific heat. The specific heat of the composite was calculated
using the rule of mixtures and the measured specific heats of the
fibers and the matrix shown in Figure 3.

The thermal conductivity and diffusivity of the fibers were
evaluated from the corresponding data for the matrix and the com-
posites using the theory for the thermal conductivity of mixtures
with a dispersed phase in the shape of cylinders (7). For heat
flow parallel to uniaxially aligned fibers, the thermal conductivity
of the composite is:

$$K_c = K_m V_m + K_f V_f \tag{4}$$

where K is the thermal conductivity, V is the volume fraction, and
the subscripts c, m, and f refer to the composite, matrix and
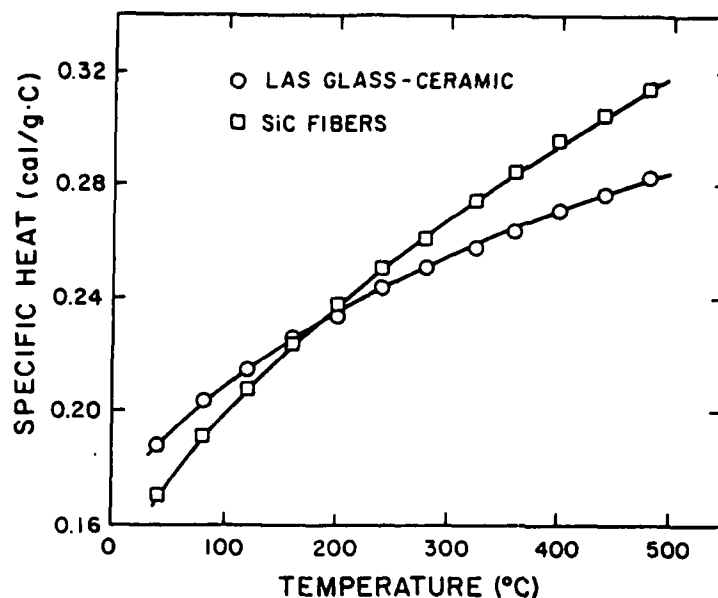
Fig. 3.   Specific heat of LAS glass-ceramic and of
          amorphous SiC fibers.

fibers, respectively. For heat flow perpendicular to the fibers,
the thermal conductivity is:

$$\left(\frac{K_m-K_c}{K_m+K_c}\right) V_m = \left(\frac{K_c-K_f}{K_c+K_f}\right) V_f \qquad (5)$$

After determining the thermal conductivity of the fibers using
equations 4 and 5, the thermal diffusivity can be calculated by
means of equation 3.

RESULTS AND DISCUSSION

Figure 4 shows the data for the effect of specimen thickness
on the thermal conductivity and diffusivity of the LAS glass-
ceramic matrix and two composites with heat flow parallel and per-
pendicular to the fiber axes. The thermal conductivity was cal-
culated using Eq. 5 and the experimental data for the thermal
diffusivity, density, and specific heat. The data indicate a
significant specimen size effect for these three materials, sug-
gestive of radiative heat transfer between the carbon-coated
surfaces of the specimens.

A similar size effect is observed for the values of thermal
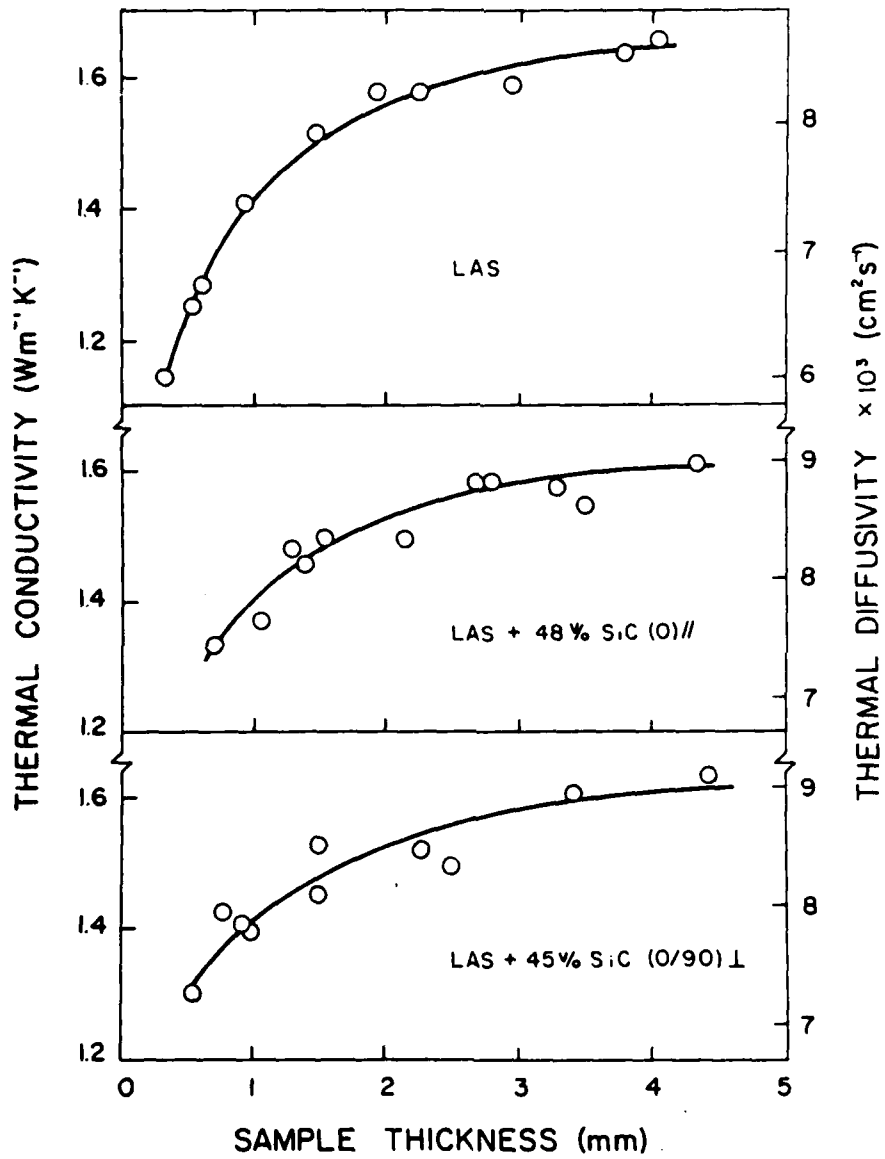
Fig. 4. Thickness dependence of the thermal diffusivity
and conductivity at 25°C for LAS glass-ceramic
and two composites of LAS with SiC fibers oriented
parallel (middle) and perpendicular (bottom) to the
direction of heat flow.

conductivity and diffusivity of the SiC fibers at room temperature
as shown in Figure 5.   These values were calculated from the ex-
perimental data for the composite and matrix samples using equations
4 and 5.   The values are essentially independent of the direction
of heat flow relative to the fibers.   This suggests that any
existing interfacial effects do not influence heat flow perpendi-
cular to the fibers.

For a quantitative interpretation of the size effect, it is
important to note that the thermal conductivity does not rise
linearly with specimen thickness, which is expected from Eq. 1 if
all the heat transfer through the specimen occurred by radiation
between the surfaces.   This indicates that additional mechanisms
of heat transfer independent of the specimen thickness also con-
tribute to the thermal conductivity.

Such mechanisms include heat transfer by phonons and by
continuous emission and absorption of photons with short mean-
free-path.   Both processes are independent of specimen thickness.
However, an additional factor to explain the observed size effect
should be considered as well.   First it should be noted that
equation 1 for the effective thermal conductivity due to radiative
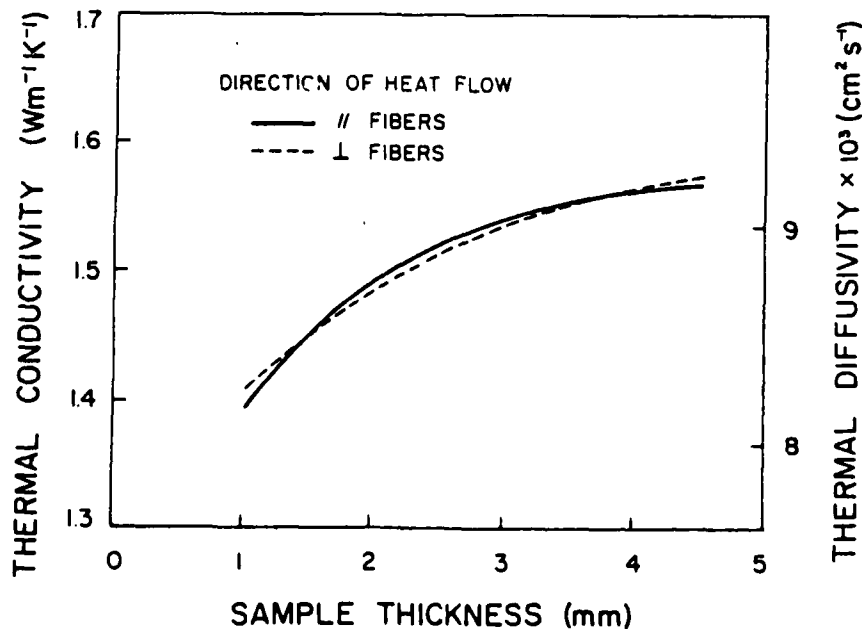

Fig. 5.   Thermal diffusivity and conductivity of SiC
          fibers at room temperature determined from
          experimental values for the LAS matrix and
          the composites.

heat transfer between sample surfaces is valid when the ratio of the length of the surface to the distance between the surfaces approaches infinity. Under this condition, all the radiation emitted by one surface is absorbed by the second surface. This condition is not met for the specimens used in this study, where in the case of the thicker specimens, the ratio is only two to three. Thus an appreciable fraction of radiation emitted hemispherically from the hotter surface will not be intercepted and absorbed by the colder surface. This condition is governed by the view factor from one surface to another, which is defined as the fraction of the total radiation emitted by the one surface that is directly incident on the other (8). For parallel circular disks of equal diameter positioned directly opposite each other, the view factor (F) can be written (9):

$$F = \frac{1}{2} \left[\frac{d^2}{r^2} + 2 - \left(\frac{d^4 + 4r^2 d^2}{r^4} \right)^{\frac{1}{2}} \right] \tag{6}$$

where r is the radius of the disks and d is the distance between them.

The effect of specimen geometry on the radiative thermal conductivity of typical carbon-coated laser-flash specimens can be taken into account by incorporating the view factor of equation 6 into equation 1, which yields:

$$K_R = \left(\frac{e}{2-e} \right) 4F\sigma n^2 T^3 d \tag{7}$$

Figure 6 shows the normalized radiative conductivity, K_R (2-e)/$4e\sigma n^2 T^3$, as a function of thickness for a range of specimen diameters, which for the LAS matrix in this study is 12.8 mm. Comparison of the data for the thermal conductivity as a function of specimen thickness shown in Figure 4 with the curve for specimen diameter of 12.8 mm shown in Figure 6 indicates that the variation in the observed thermal conductivity can be partially accounted for by the change in specimen shape with specimen thickness. Such an effect should be taken into account in the interpretation of the data for the thermal diffusivity of transparent materials measured by the laser-flash method.

Figure 7 shows the temperature dependence of the thermal conductivity for two values of thickness of specimens of the glass-ceramic matrix and two composites with heat flow parallel and perpendicular to the fiber axes. The increase in thermal conductivity with temperature for all three materials is indicative of the contribution of radiation to the total heat transfer. The relative increase in thermal conductivity with temperature, however, is well below the T^3 dependence expected if radiation were the only contributing mechanism of heat conduction. This indicates that in
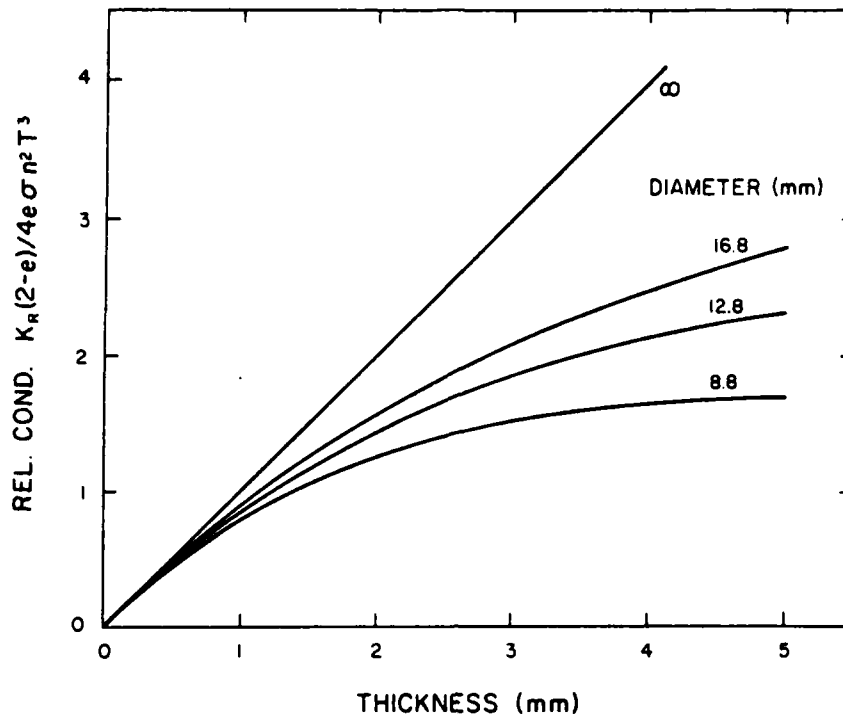
Fig. 6. Normalized thermal conductivity due to radiation between the surfaces of samples of various diameters as a function of the sample thickness.

spite of the observed specimen size effect and the positive temperature dependence, phonon transport still makes the primary contribution to the thermal conductivity. Of course, the temperature and spectral dependence of the absorption coefficient may also play a role. However, at this time no data for these effects appear to be available for these composites.

The data presented in Figure 7 indicate that the curves for the temperature dependence of the thermal conductivity for the two values of specimen thickness are nearly parallel for all three materials. This suggests that the relative effect of specimen thickness on thermal conductivity decreases with increasing temperature. This in turn suggests that heat transfer by photon emission and absorption makes a relatively larger contribution to the total thermal conductivity with increasing temperature.

It is interesting to note that compared to the present materials, the contribution of radiation to the thermal conductivity of such highly transparent materials as quartz and sapphire appears to be
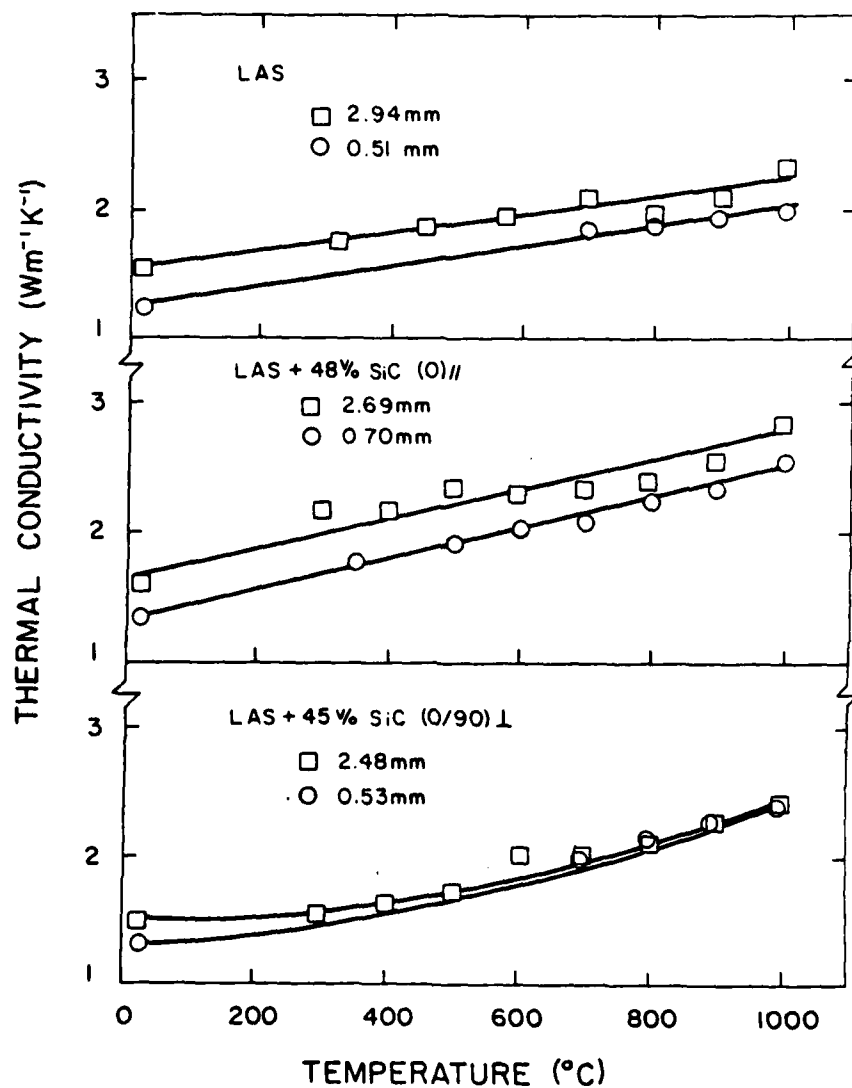
Fig. 7. Temperature dependence of the thermal conductivity of LAS glass-ceramic matrix and two composites of LAS with SiC fibers oriented parallel and perpendicular to the direction of heat flow. Data for samples of two different thicknesses are shown for each material.

much higher, as observed by Howlett (10). This suggests that the suppression of radiative heat transfer by photon scattering at optical discontinuities could play a significant role in the conduction of heat in the materials investigated in this study.

In summary, it was found that radiative heat transfer between the specimen surfaces contributes to the overall thermal conductivity of a silicon carbide fiber-reinforced lithium aluminosilicate glass-ceramic. The dependence of thermal conductivity on specimen thickness suggests that the radiative heat transfer is partially governed by the view factor between the carbon coated laser-flash specimens.

ACKNOWLEDGEMENTS

REFERENCES

1. R. Berman, "Thermal Conduction in Solids", Clarendon Press, Oxford (1976).
2. D. W. Lee and W. D. Kingery, J. Amer. Ceram. Soc., 43 (1960) 594.
3. J. J. Brennan, L. D. Bentsen and D. P. H. Hasselman, J. Mater. Sci., 17 (1982) 2337.
4. S. Yajima, K. Okamura, J. Hayashi and M. Omori, J. Amer. Ceram. Soc., 59 (1976) 324.
5. W. J. Parker, R. J. Jenkins, C. P. Butler and G. L. Abbott, J. Appl. Phys., 32 (1961) 1679.
6. R. C. Heckman, J. Appl. Phys., 44 (1973) 1455.
7. A. E. Powers, Knolls Atomic Power Laboratory, Report KAPL-2145, 1961.
8. W. A. Gray, and R. Muller, "Engineering Calculations in Radiative Heat Transfer", (Pergamon Press, New York, 1974), p. 29.
9. R. Siegel and J. R. Howell, "Thermal Radiation Heat Transfer", (McGraw-Hill, New York, 1972) p. 787.
10. S. P. Howlett, R. Taylor, and R. Morrell, "Thermal Conductivity-17", (Plenum Press, New York, 1983), p. 447, J. G. Hust, Ed.

Chapter IV

THERMAL DIFFUSIVITY ANISOTROPY
OF SiC-BN COMPOSITES

R. Ruh,[+] L. D. Bentsen,[*] and D. P. H. Hasselman[*]

[+]Air Force Wright Aeronautical Laboratory
Wright-Patterson Air Force Base, OH 45433 USA

[*]Department of Materials Engineering
Virginia Polytechnic Institute & State University
Blacksburg, VA 24061 USA

THERMAL DIFFUSIVITY ANISOTROPY OF SiC-BN COMPOSITES

R. Ruh
Air Force Wright Aeronautical Laboratory
Wright-Patterson Air Force Base, OH 45433 USA

L. D. Bentsen and D. P. H. Hasselman
Department of Materials Engineering
Virginia Polytechnic Institute & State University
Blacksburg, VA 24061 USA

ABSTRACT

The thermal diffusivity of hot pressed silicon carbide-boron nitride composites is shown to exhibit a high degree of anisotropy with respect to the hot pressing direction due to preferred orientation of the boron nitride phase. This effect is particularly pronounced at the higher boron nitride contents at both room and elevated temperature.

INTRODUCTION

Single crystals of most materials exhibit anisotropy in many of their tensor properties, including the electrical and thermal conductivity, and the elasticity.[1] While such anisotropy is most pronounced with the crystal structures of materials such as mica, graphite and boron nitride, it is also exhibited by polycrystalline aggregates of anisotropic single crystals if the grains have a preferred orientation (i.e., texture) introduced during or after manufacture. In composites, the individual components frequently are oriented preferentially. This, in addition to other variables such as the distribution of the phases, also contributes to the anisotropy of the continuum properties of the composites. This was recently demonstrated by experimental data[2] for the room temperature thermal diffusivity of hot-pressed composites of silicon nitride with a dispersed phase of boron nitride. At the highest

1

concentration of BN investigated (30 wt.%) these composites exhibited a factor of two difference in the thermal diffusivity parallel and perpendicular to the hot-pressing direction. X-ray analysis confirmed that this anisotropy resulted primarily from the preferred orientation of the boron nitride phase, probably introduced during compaction of the powders and facilitated by the plate-like shape of the individual BN particles. The purpose of this communication is to present further confirming data for the effect of the preferred orientation of boron nitride on the room temperature thermal diffusivity of hot-pressed composites of silicon carbide and boron nitride over the total range of BN content.

EXPERIMENTAL

A range of SiC-BN compositions were prepared using a sinterable β-SiC powder* and a BN powder+ with a particle size of 15 μm. The powders were mixed in a plastic ball mill with silicon nitride balls for 4 hours in isopropyl alcohol. After drying, the powders were pelletized and then uniaxially hot-pressed** in vacuum at 2100°C for 1 hour at a pressure of 35 MPa in graphite dies lined with graphite foil.++ After the specimens were removed from the die, the surfaces were ground and the density was determined from the dimensions (≈2.5 cm diameter by 1 cm thick) and the mass.

X-ray diffraction analysis of the hot-pressed blanks revealed the presence of several SiC polytypes, including 21R, 15R, 6H, 4H, and 3C.

----

* Lot S 1626, beta silicon carbide, Herman C. Starck, Goslar, Federal
  Republic of Germany.
+ B-27, Research Organic/Inorganic Chemical Corp., Belleville, NJ.
** Model 300, Vacuum Industries Div., GCA Corp., Chicago, IL.
++ Carbon Products Division, Union Carbide Corp., Chicago, IL.

2

With this multiphase assemblage it was not possible to quantify the amount of each phase present, but the SiC patterns were similar regardless of the BN content. Boron nitride was always present as the hexagonal graphite structure, and no evidence of reaction or solid solution between the SiC and BN was observed.

The effect of the concentration and the orientation of the BN on the heat transfer behavior of the composites was determined by measurements of the thermal diffusivity by the flash method[3] using a glass-Nd laser as the flash source and remote optical sensing for monitoring the transient temperature response of the specimen. At room temperature, the measurements were conducted in air, whereas at elevated temperatures, the specimen was contained within a carbon resistance furnace with a protective nitrogen atmosphere. The specimens used for these measurements were cut from the hot-pressed blanks and were in the form of square plates ≃2 mm thick with a diagonal of ≃12 mm. A number of specimens were cut from each blank in order to obtain measurements of the thermal diffusivity in directions parallel and perpendicular to the hot-pressing direction.

RESULTS AND DISCUSSION

Table I lists the composition, density, and porosity of each composite. The amount of porosity was determined from the measured density and the theoretical density based on values of 2.28 g/cm^3 for the density of boron nitride and 3.21 g/cm^3 for that of silicon carbide. As indicated by the table, the pore content generally increases with increasing BN content.

Figure 1 shows the experimental data for the thermal diffusivity at room temperature both parallel as well as perpendicular to the hot-pressing direction. The scatter in the data at a given BN content and direction of

3

heat flow indicates minor variations from specimen to specimen cut from the hot-pressed blank. For heat flow perpendicular to the hot-pressing direction, the thermal diffusivity is nearly independent of BN content. This is expected since the measured thermal diffusivity of the BN perpendicular to the hot-pressing direction is nearly the same as that of the silicon carbide. Note however that this value for the SiC (≈ 0.4 cm^2/s) is well below the value of thermal diffusivity observed for other samples[4] of SiC, which can be as high as 0.8 cm^2/s. The lower value is most likely a reflection of the nature and amount of impurities, to which the diffusivity of SiC is especially sensitive.[4]

The thermal diffusivity of the composites parallel to the hot-pressing direction decreases rapidly with increasing BN content, resulting in a maximum anisotropy ratio of about four between the thermal diffusivity in the two directions. Since the thermal diffusivity along the basal plane of boron nitride is greater than that perpendicular to the basal plane, the anisotropy observed in the composites suggests that the BN is preferentially oriented with the basal plane perpendicular to the direction of hot-pressing. For the silicon nitride-boron nitride composites investigated in an earlier study,[2] this preferred orientation was verified by x-ray analysis. In the present samples the orientation of the boron nitride can be seen in the scanning electron fractographs of the specimen containing 30 at.% BN shown in figures 2a and 2b for directions parallel and perpendicular to the hot-pressing direction. In two separate investigations[5,6] of boron nitride single crystals, the ratio of the thermal conductivity at 300 K between the direction perpendicular to the basal plane and that parallel to the basal plane was about forty and one hundred. This indicates that the orientation of the BN in the present composites, while partly preferential, is mostly random.

4

The values of thermal diffusivity for the silicon carbide also indicate a slight anisotropy. Since other high conductivity ceramics with the wurtzite crystal structure exhibit very little anisotropy in the thermal conductivity,[7,8] the observed differences in the silicon carbide data may be the result of a preferred orientation of certain particle morphologies, especially the hexagonal polytypes.

The thermal diffusivity will also be affected by the amount of porosity present. Theoretical estimates by Raleigh[9] and Maxwell[10] show that at low porosity contents, the relative decrease in thermal conductivity is 1.5 times the relative pore content. Due to the associated change in density, the corresponding relative change in thermal diffusivity should be 0.5 times the relative pore content. Assuming that this value is applicable to the present composites, the thermal diffusivity was corrected for porosity and the values are listed in table I. Because the correction is relatively small, the conclusions based on the original data remain unchanged.

A comparison of the temperature dependence of the thermal diffusivity perpendicular to the hot-pressing direction with that parallel to the hot-pressing direction is shown in figures 3a and 3b for composites with 30 and 80 at.% BN, respectively. These results indicate that for both compositions, the relative temperature dependence of the thermal diffusivity in one direction of heat flow is not significantly different from that in the other direction. This also implies that the orientation of the BN is mostly random.

The observed anisotropy of the thermal diffusivity, especially at the higher BN contents, could be of practical interest for engineering applications. This is particularly so for structures or components which, for improved energy efficiency, require high thermal insulating ability in one direction of heat flow and high thermal conduction in a perpendicular

direction, thus reducing the possibility of thermal stress failure due to spatially non-uniform heating.

ACKNOWLEDGMENTS

REFERENCES

1.   J. F. Nye, Physical Properties of Crystals, Clarendon Press, Oxford (1969).

2.   K. Niihara, L. D. Bentsen, D. P. H. Hasselman, and K. S. Mazdiyasni, "Anisotropy Effects in the Thermal Diffusivity of Si_3N_4-BN Composites", J. Am. Ceram. Soc., 64(9) C117-118 (1981).

3.   W. J. Parker, R. J. Jenkins, C. P. Butler, and G. L. Abbott, "Flash Method of Determining Thermal Diffusivity, Heat Capacity and Thermal Conductivity", J. Appl. Phys., 32(9) 1679-84 (1961).

4.   M. Srinivasan, L. D. Bentsen, and D. P. H. Hasselman, "Thermal Diffusivity of Silicon Carbide-Silicon Composites", Proc. 17th Int. Thermal Conductivity Conference, Plenum Press, New York (1983) p. 677.

5.   A. Simpson and A. D. Stuckes, "The Thermal Conductivity of Highly Oriented Pyrolytic Boron Nitride", J. Phys. C; Solid State Phys., 4, 1710-18 (1971).

6.   H. O. Pierson, "Boron Nitride Composites by Chemical Vapor

Deposition", J. Comp. Mater., 9, 228-240 (1975).

7. M. P. Borom, G. A. Slack, and J. W. Szymaszek, "Thermal Conductivity of Commercial Aluminum Nitride", Am. Ceram. Soc. Bul., 51(11)852-856(1972).

8. G. A. Slack and S. B. Austerman, "Thermal Conductivity of BeO Single Crystals", J. Appl. Phys., 42(12)4713-4717(1971).

9. Lord Raleigh, "On the Influence of Obstacles Arranged in Rectangular Order Upon the Properties of a Medium", Phil. Mag., 34, 481-507 (1892)

10. J. C. Maxwell, A Treatise on Electricity and Magnetism, I, 3rd Ed., Oxford U. Press (1904).

TABLE I. Composition, density, porosity, and mean values of thermal diffusivity at room temperature for SiC-BN composites.

| Sample No.* | BN Content | | Density (g/cm^3) | | Porosity (%) | Thermal Diffusivity (cm^{2}s^{-1}) | | | |
| | | | | | | $\perp$ HP Direction | | // HP Direction | |
	mole%	vol.%	Measured	Theoretical		Exper.	Corrected	Exper.	Corrected
494C	0	0	3.12	3.21	2.8	.4207	.4328	.3882	.3994
490C	10	8.8	3.06	3.13	2.2	.3613	.3693	.2998	.3065
483C	20	17.8	2.95	3.04	3.1	.3508	.3620	.2306	.2379
491C	30	27.1	2.84	2.96	4.0	.3837	.3995	.2113	.2200
484C	40	36.6	2.76	2.87	3.8	.3782	.3930	.1801	.1871
492C	50	46.4	2.59	2.78	6.7	.3888	.4169	.1655	.1774
383C	61.8	58.3	2.44	2.67	8.5	.3675	.4015	.1440	.1573
93C	70	66.9	2.32	2.59	10.3	.3859	.4303	.1160	.1294
85C	80	77.6	2.17	2.49	12.7	.3553	.4072	.0960	.1100
95C	90	88.6	2.04	2.39	14.5	.3544	.4143	.0883	.1032
36C	100	100.0	1.83	2.28	19.7	.3978	.4956	.0915	.1140

fers to hot-pressed blank.
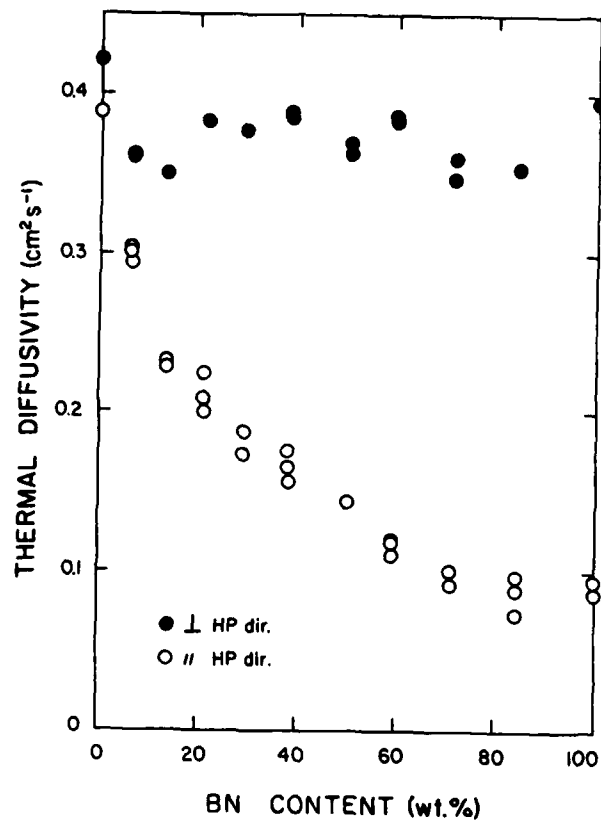
Fig. 1.   Room temperature thermal diffusivity
of silicon carbide-boron nitride
composites parallel and perpendicular
to the hot-pressing direction.

b.

a.

Fig. 2.   Scanning electron micrographs of fracture surfaces of silicon carbide containing 30 at.% boron nitride. The surfaces represent planes (a) parallel and (b) perpendicular to the hot-pressing direction.
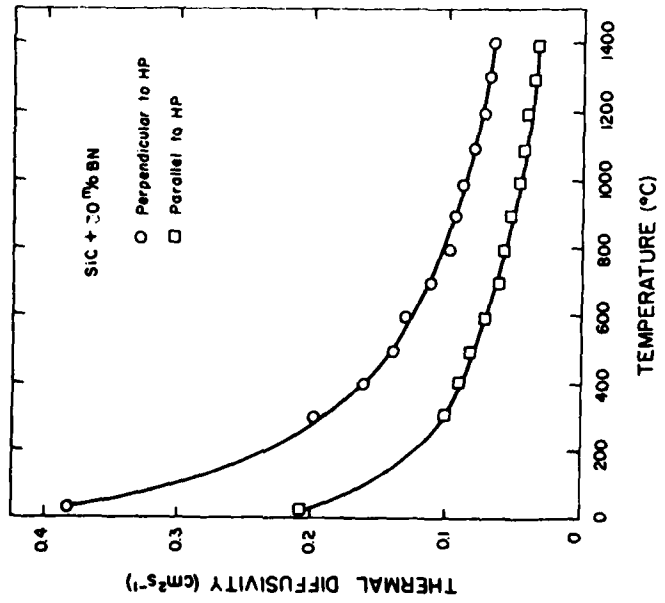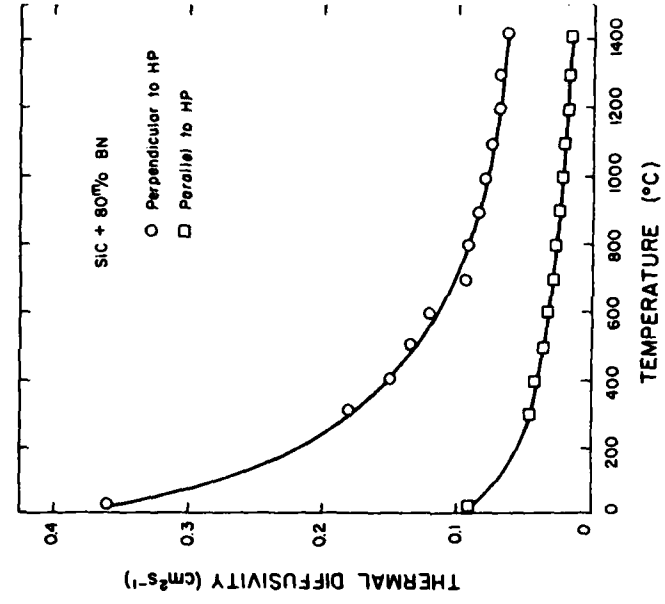
Fig. 3. Temperature dependence of the thermal diffusivity of silicon carbide with (a) 30 at.% BN and (b) 80 at.% BN measured perpendicular and parallel to the hot-pressing direction.

Chapter V

EFFECT OF CRYSTALLIZATION OF THE
GRAIN BOUNDARY PHASE ON THE THERMAL DIFFUSIVITY
OF A SIALON CERAMIC

L. D. Bentsen,[*] T. Y. Tien,[+] and D. P. H. Hasselman[*]

[*]Department of Materials Engineering
Virginia Polytechnic Institute & State University
Blacksburg, VA   24061   USA

[+]Materials and Metallurgical Engineering
The University of Michigan
Ann Arbor, MI   48109   USA

EFFECT OF CRYSTALLIZATION OF THE GRAIN BOUNDARY PHASE ON THE THERMAL DIFFUSIVITY OF A SIALON CERAMIC

L. D. Bentsen, D. P. H. Hasselman
Department of Materials Engineering
Virginia Polytechnic Institute & State University
Blacksburg, VA 24061 USA

T. Y. Tien
Materials and Metallurgical Engineering
The University of Michigan
Ann Arbor, MI 48109 USA

ABSTRACT

Crystallization of the glassy grain boundary phase in a series of Sialon ceramics fabricated using a range of hot pressing schedules increased the thermal diffusivity at room temperature by an average of about 10%. For samples made by a given hot pressing schedule, the relative difference in the thermal diffusivity between composites containing either a glassy or a crystallized grain boundary phase decreased with increasing temperature. This was attributed to enhanced phonon scattering in the crystalline grain boundary phase.

INTRODUCTION

The densification during sintering of polycrystalline ceramics for high-performance applications can be enhanced significantly by the addition of a sintering aid. This is particularly so for silicon nitride-based ceramics, which do not densify readily without the assistance of additives. For silicon nitride, such additives commonly consist of the oxides of magnesium, yttrium, or aluminum. At the fabrication temperatures, the presence of these additives results in the formation of a liquid phase at the grain boundaries. This liquid phase can act either as a lubricant to promote particle transport

1

or as a medium for material transport by solution and re-precipitation of the matrix phase. Upon cooling, the liquid at the grain boundaries and triple points becomes a glass.

The presence of this grain boundary phase, which can vary from just a few percent to over 10%, is expected to have an effect on the continuum properties of the final densified product. This effect is well known for mechanical behavior, especially at temperatures sufficiently high that the grain boundary phase can undergo significant viscous deformation.

The effect of the grain boundary phase on the continuum properties of polycrystalline aggregates also is expected to be a function of the degree of crystallinity. In terms of the objectives of this study, it should be noted that due to greatly enhanced phonon scattering, glassy(amorphous) materials generally exhibit a much lower thermal conductivity and diffusivity than their crystalline counterparts of identical composition(1-2). A polycrystalline ceramic with a grain boundary phase can be considered to be a composite. Theory(3) indicates that the thermal conductivity of composites is a function of the thermal conductivity, volume fraction, and distribution of each component. Continuous phases are particularly effective in affecting the thermal conductivity of composites. For this reason, the presence of a grain boundary phase and its degree of crystallinity are expected to have a significant effect on the thermal transport properties of polycrystalline aggregates. Experimental data are presented in support of this hypothesis.

EXPERIMENTAL

The materials for this study consisted of a β-Sialon (β-Si_3N_4 solid solution containing 5 eq.% Al, i.e., β-$Si_{6-x}Al_xO_xN_{8-x}$ where x=0.4) with a sintering aid corresponding to the composition of the mineral garnet,

i.e., $Y_3Al_5O_{12}$ (4). The samples were prepared by hot-pressing appropriate mixtures of powders of Si_3N_4[*], AIN[**], Al_2O_3[+], and Y_2O_3[++] in boron nitride coated graphite dies at a pressure of $\simeq$20 MPa in a nitrogen atmosphere at temperatures ranging from 1550 to 1690°C for time periods ranging from 15 to 120 minutes. The densities achieved were at least 99.5% of theoretical. The amount of densification aid added was approximately 10 wt.%. Following hot-pressing, the samples were annealed at 1350°C for 20 hours, which was found to result in nearly complete crystallization of the garnet grain boundary phase. Details of the x-ray and TEM studies of the crystallization process were presented in an interim technical report(4) intended for formal publication at a later date. In the "as hot-pressed" samples, β-Sialon was the only crystalline phase, whereas garnet was the only second crystalline phase in the annealed specimens.

The effect of the crystallization of the grain boundary phase on thermal transport behavior was determined by measurement of the thermal diffusivity by the flash method(5) using a glass-Nd laser as the flash source. The specimens for these measurements consisted of square plates about 6 mm on a side by about 1.5 mm thick. Measurement of the thermal diffusivity at room temperature was conducted in air; at elevated temperatures the specimens were contained in a carbon furnace with a protective nitrogen atmosphere.

RESULTS AND DISCUSSION

Figure 1a compares the data for the thermal diffusivity at room temperature prior to and following the annealing of samples hot-pressed for 30

----

[*] H. Starck, LC12, Weslar, FRG
[**] H. Starck, Weslar, FRG
[+] Alcoa, A16
[++] Molycorp, 5600

min at various temperatures. Similarly, Figure 1b compares the corresponding data for specimens hot-pressed at 1730°C for various periods of time. Both sets of data show an increase in the thermal diffusivity of about 10% after annealing, regardless of the hot-pressing conditions.

Figure 2 compares the temperature dependence of the thermal diffusivity for Sialon samples with a glassy and a crystalline grain boundary phase. Both samples were hot pressed for 30 minutes at 1690°C. The relative difference in the thermal diffusivity decreases with increasing temperature. This is expected since enhanced phonon scattering generally produces a greater relative decrease in the thermal conductivity and diffusivity of crystalline materials than for glassy materials. The data in figure 2 were obtained up to 1000°C in order to avoid crystallization of the grain boundary phase at higher temperatures. Such crystallization would lead to a *permanent increase in the thermal diffusivity of the* "as hot pressed" sample if measurements had been conducted to temperatures as high as 1200 or 1300°C. Although the temperature dependence of the thermal diffusivity was measured for only one hot pressing condition, it is anticipated that the samples for the other hot pressing conditions would exhibit a behavior similar to that shown in figure 2.

ACKNOWLEDGMENTS

REFERENCES

1. W. D. Kingery, H. K. Bowen, and D. R. Uhlmann, Introduction to Ceramics, 2nd Ed., John Wiley, 1976(1032pp.).

2. K. Chyung, G. E. Youngblood, and D. P. H. Hasselman, "Effect of Crystallization on the Thermal Diffusivity of a Cordierite Glass-Ceramic", J. Am. Ceram. Soc., 61(11-12)530-31(1978).

3. S. C. Cheng and R. I. Vachon, "The Prediction of the Thermal Conductivity of Two and Three Phase Solid Heterogeneous Mixtures", Int. J. Heat Mass Transfer, 12, 249-64(1969).

4. T. Y. Tien, "Effect of Crystallization of Grain Boundary Phase on the High Temperature Strength of Silicon Nitride Ceramics", Report to DOE, Nov. 1982.

5. W. J. Parker, R. J. Jenkins, C. P. Butler, and G. L. Abbott, "Flash Method of Determining Thermal Diffusivity, Heat Capacity and Thermal Conductivity", J. Appl. Phys., 32(9)1679-84(1961).

Fig. 1. Effect of annealing at 1350°C for 20 hours on the room temperature thermal diffusivity of β-Sialon/garnet (a) hot-pressed at various temperatures for 30 min and (b) hot-pressed at 1730°C for various lengths of time.
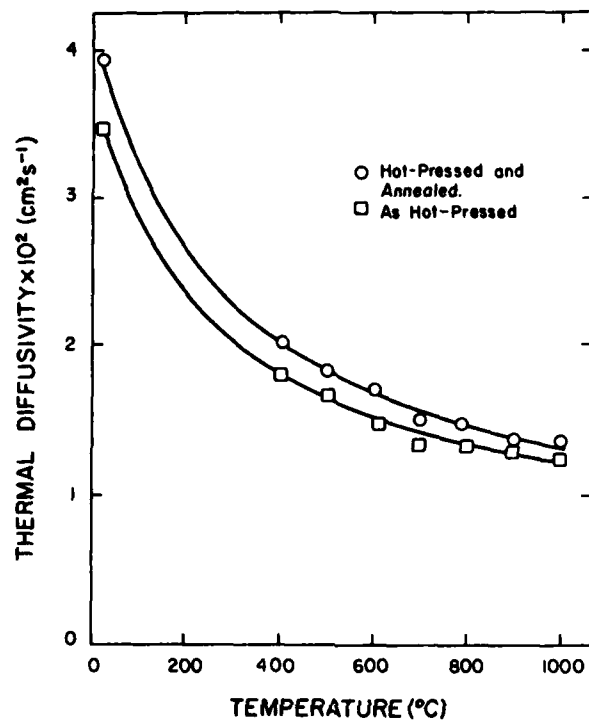
Fig. 2.   Temperature dependence of the thermal dif-
          fusivity of β-Sialon/garnet hot-pressed at
          1690°C for 30 min compared to β-Sialon/garnet
          hot-pressed at the same conditions and then
          annealed at 1350°C for 20 hours. The solid
          lines represent linear least squares fits of
          the measured thermal diffusivity to the
          reciprocal absolute temperature.

Chapter VI

EFFECT OF DROP-HEIGHT ON THE CRITICAL TEMPERATURE

DIFFERENCE (ΔT_c) FOR BRITTLE CERAMICS SUBJECTED TO

THERMAL SHOCK BY QUENCHING INTO WATER

by

J. P. Singh[*], G. Ziegler[§], D. P. H. Hasselman[*]

[*]Department of Materials Engineering
Virginia Polytechnic Institute and State University
Blacksburg, VA 24061 USA

[§]Institut fuer Werkstoff-Forschung
DFVLR, 5000 Cologne 90
Federal Republic of Germany

EFFECT OF DROP-HEIGHT ON THE CRITICAL TEMPERATURE DIFFERENCE
(ΔT_c) FOR BRITTLE CERAMICS SUBJECTED TO THERMAL SHOCK BY QUENCHING

Jitandra P. Singh, Gunther Ziegler, D. P. H. Hasselman

ABSTRACT

Values for the critical quenching temperature difference (ΔT_c) required for the initiation of thermal stress failure of soda-lime-silica glass, polycrystalline alumina, mullite and reaction-sintered silicon nitride subjected to thermal shock by quenching into water were found to be independent of the height from which the specimens were dropped. These results suggest that within the range of usual laboratory practice no close control over the drop height needs to be exercised. The relevance of the present observations in terms of the mechanism of heat transfer responsible for thermal stress failure in a water quench is briefly discussed.

The quench test is a favorite method for the measurement of the thermal stress resistance of brittle ceramics[1-7]. Usually, the method consists of dropping appropriate specimens under free-fall conditions into a fluid at or near room temperature from an oven or furnace at elevated temperature. The critical quenching temperature difference (ΔT_c) required to initiate fracture as evidenced by extensive crack formation is a measure of the thermal stress resistance of the particular ceramic being tested. Unfortunately, the quantitative interpretation of the data for ΔT_c is handicapped by uncertainties

in the relative contributions of heat transfer by convective processes, nucleate boiling and steam-film formation.

It is expected that these heat transfer mechanisms could be affected by the velocity at which the specimens hit the fluid surface, which, in turn is a function of the height over which the specimens are dropped. Very few, if any, reports on the results for ΔT_c obtained by water quenching give values for the drop-height. For this reason the purpose of this study was to obtain experimental data for this effect which should also throw a light on the dominant mechanism of heat transfer.

Four different ceramic materials were selected, as listed in Table 1, together with the specimen size, geometry and values for the relevant material properties, corresponding to the approximate mean value at the initial temperature of the specimens at $\Delta T = \Delta T_c$. Five specimens were quenched simultaneously from a range of values of height and temperature difference (ΔT) from an electrically heated laboratory oven into a water bath held at 33°C. Each specimen was tested only once in order to eliminate the possible effect of fatigue on ΔT_c. The circular specimens hit the surface in a horizontal position, whereas the square specimens of silicon nitride, tested in another laboratory, hit the surface in a vertical position. Following quenching, the strength retained by the specimens was measured in 4-point bending at a cross-head speed of 0.05 cm/min. with an inner and outer span for the circular specimens of 1.6 and 5.0 cm, respectively. For the silicon nitride, the corresponding values were 2 and 4 cm, respectively. The value of ΔT_c was defined by the range and mean of the values of quenching temperature difference (ΔT) at which 1 or 5 of the five specimens tested exhibited a significant strength loss. At values of ΔT near ΔT_c, ΔT was varied over 10°C intervals in order to define ΔT_c as closely as possible.

The experimental results are shown in Fig. 1. For all four materials no significant difference exists between the value of ΔT_c over the total range of values of height used.[*] In view of the square root dependence of specimen velocity on drop-height, the range of velocities involved a factor in excess of six. During their transit from the oven to the water bath, the specimens should lose some heat to the air by convection or by radiation. This effect, however, would serve to increase ΔT_c with increasing height, other effects being absent. Due to the very low heat transfer coefficient, the loss of heat to the air by convection (8) should have a negligible effect on ΔT_c. The slight apparent increase in ΔT_c with increasing height for the mullite and silicon nitride specimens which require the higher values for the initial specimen temperature possibly may be attributed to radiative heat loss during the transit to water bath. However, from the dependence of radiative heat transfer on absolute temperature it is easily calculated that significant changes in ΔT_c due to radiative heat losses would occur only for initial specimen temperatures well in excess of 1000°C for the range of values of drop-height used in this study. Regardless of the details, these experimental results must be considered as rather gratifying as they suggest that for the range of quenching conditions for a water bath generally encountered in practice, close control over the drop-height need not be exercised.

The implications of the present results for the mechanisms of heat transfer can be speculated on briefly. The independence of ΔT_c from drop-

---

[*]It is not the purpose of this study to compare the values of ΔT_c for the four materials because of the differences in geometry involved. It should be noted, however, that the relative order of ΔT_c is the same as the order of the parameters (8,9): $\sigma_f(1-\nu)/\alpha E$ and $\sigma_f(1-\nu)K/\alpha E$.

height suggests that the mechanism of heat transfer responsible for the thermal fracture is not governed by the velocity at which the specimens hit the surface and the corresponding forced convective heat transfer coefficient. From heat transfer theory[10], this latter quantity can be calculated to vary by a factor of about two for the range of drop-heights used. This, in turn suggests that the transfer of heat is controlled by either forced convection corresponding to the "terminal" velocity at which the specimen falls through the water (which is independent of the drop-velocity) or by nucleate boiling or steam-film formation. In fact, for the circular samples of aluminum oxide for which ΔT_c is not strongly affected by sub-critical crack growth as demonstrated by computer simulation[13], the value of ΔT_c calculated from the heat transfer coefficient for the free-fall velocity[6,14] and the appropriate thermo-elastic equation, agrees very well with the observed value. Such agreement, however, must be concerned fortuitous as for the initial specimen temperature nucleate boiling and steam-film formation are expected to play a significant role. In fact, the effective heat transfer coefficient in the presence of steam-film formation[4,5] is of approximately the same magnitude as the one calculated for free-fall conditions. As indicated by experimental evidence[11,12], the rate of heat transfer by nucleate boiling and steam-film also is relatively independent of the relative velocity between the water and the hot surface. For this reason, ΔT_c for heat transfer by these latter mechanisms would also be independent of specimen velocity (i.e., drop-height).

ACKNOWLEDGMENT
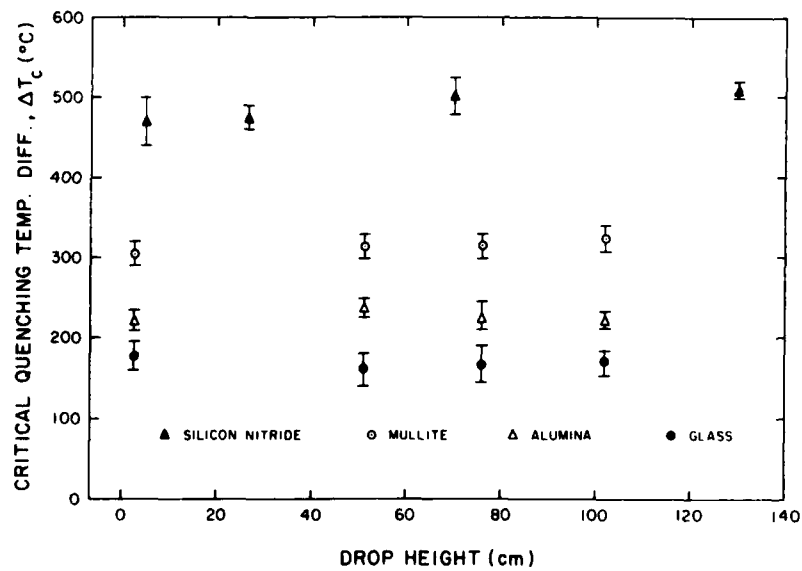
Fig. 1. Effect of drop-height on the critical quenching
temperature difference ΔT_C required to initiate
thermal stress fracture in four ceramic materials.

TABLE 1. CERAMIC MATERIALS

	Soda-Lime-Silica Glass*	Polycrystalline Alumina[+]	Polycrystalline Mullite[§]	Reaction-Sintered Silicon Nitride**
Geometry:	Solid Circular Cylinder	Solid Circular Cylinder	Hollow Concentric Circular Cylinder	Solid Square Cylinder
Dimensions:	Diam.: 5.3 mm	Diam.: 6.35 mm	O.Diam.: 9.1 mm I.Diam.: 3.3 mm	Side: 5 mm
Young's Modulus E(GPa):	70.3	393	69	153
Tensile Strength (MPa):	66.5	271	69	186
Coef. Thermal Exp, $\alpha°C^{-1}(\times10^6)$:	9.3	7.4	5.3	2.5
Poisson's Ratio (ν)	0.25	0.27	0.20	0.22
Thermal Conductivity $K(J.m^{-1}°C^{-1}sec^{-1})$:	1.05	15	5.87	27.7

* R-6, Owens-Corning
[+] 998 Alumina, McDanel Porcelain, Beaver Falls, PA.
[§] MV-20, McDanel Porcelain, Beaver Falls, PA.
** Made at DFVLR, Cologne, FRG.

REFERENCES

1. R. W. Davidge and G. Tappin, "Thermal Shock and Fracture in Ceramics", Trans. Brit. Ceram. Soc., 66 (8) 405-22 (1967).

2. D. P. H. Hasselman, "Strength Behavior of Polycrystalline Alumina Subjected to Thermal Shock", J. Amer. Ceram. Soc., 53, 9, 490-95 (1970).

3. T. K. Gupta, "Strength Degradation and Crack Propagation in Thermally Shocked Al_2O_3", J. Amer. Ceram. Soc., 55 (5) 249-53 (1972).

4. P. F. Becher, D. Lewis, III, K. R. Carman and C. A. Gonzales, "Thermal Shock Resistance of Ceramics: Size and Geometry Effects in Quench Tests", Amer. Ceram. Soc. Bull., 59 (5) 542-548 (1980).

5. J. P. Singh, Y. Tree and D. P. H. Hasselman, "Effect of Bath and Specimen Temperature on the Thermal Stress Resistance of Brittle Ceramics Subjected to Thermal Quenching", J. Mat. Sc., 16, 2109-2118 (1981).

6. J. P. Singh, J. R. Thomas, Jr., and D. P. H. Hasselman, "Analysis of Effect of Heat Transfer Variables on Thermal Stress Resistance of Brittle Ceramics Measured by Quenching Experiments", J. Amer. Ceram. Soc., 63 (3-4) 140 (1980).

7. K. Niihara, J. P. Singh and D. P. H. Hasselman, "Observations on the Characteristics of a Fluidized Bed for the Thermal Shock Testing of Brittle Ceramics", J. Mat. Sc., 17, 2553-59 (1982).

8. W. D. Kingery, "Factors Affecting Thermal Shock Resistance of Ceramic Materials", J. Amer. Ceram. Soc., 38 (1) 3-15 (1955).

9. D. P. H. Hasselman, "Figures-Of-Merit for the Thermal Stress Resistance of High-Temperature Brittle Materials, A Review", Ceramurgia International 4 (4) 147-150 (1978).

10. A. J. Chapman, Heat Transfer, 3rd Ed., McMillan Publishing Com. Inc., New York, 1974.

11. W. H. McAdams, W. E. Kennel, C. S. Minden, Rudolf Carl, P. M. Picornell and J. E. Dew, "Heat Transfer at High Rates to Water with Surface Boiling", Ind. and Eng. Chemistry, 41, 1945-53 (1949).

12. F. Kreith and M. Summerfield, "Heat Transfer to Water at High Flux Densities With and Without Surface Boiling", Trans. ASME, 71, 805-15 (1949).

13. D. P. H. Hasselman and K. R. McKinney, unpublished results.

14. H. R. Perry and C. H. Chilton, pp. 10-13 in Chemical Engineers Handbook, 5th Ed., McGraw-Hill, New York (1973).

Chapter VII

EFFECT OF THERMAL DIFFUSIVITY ON MAGNITUDE

OF THERMAL STRESS IN A BRITTLE CERAMIC SUBJECTED

TO RAPID THERMAL CYCLING

by

T. D. Nguyen[*], J. R. Thomas[*] and D. P. H. Hasselman[†]

[*]Department of Mechanical Engineering
[†]Department of Materials Engineering
Virginia Polytechnic Institute and State University
Blacksburg, VA 24061 USA

ABSTRACT

A study was conducted of the effect of the magnitude of the thermal diffusivity on the thermal stresses in a ceramic plate subjected to thermal cycling by changes in ambient temperature involving convective heat transfer, at frequency sufficiently high that thermal equilibrium (i.e., temperature uniformity) is not achieved within each cycle. The results obtained indicate that at any specific value of the Biot number the magnitude of maximum thermal stress within any cycle decreases with decreasing thermal diffusivity and increases with increasing plate thickness. The approximate expression for the thermal stress resistance parameter appropriate for very high cycling frequencies and low values of the Biot number indicates that good thermal stress resistance under these conditions requires a high value for the specific heat per unit volume.

I. INTRODUCTION

Ceramic materials for structural purposes frequently exhibit high values of Young's modulus and coefficient of thermal expansion and relatively low values of tensile strength. This combination of properties, together with a high degree of brittleness, make structural ceramics highly susceptible to catastrophic failure under the influence of steady-state or transient thermal stresses usually encountered during normal use at elevated temperatures. For this reason, it is imperative for design purposes that the variables which influence the magnitude of thermal stress and the resulting failure are well understood. For this purpose a number of analytical studies have appeared in the ceramics literature.[1-11] These studies have permitted the derivation of so-called thermal stress "resistance parameters" or "figures-of-merit" which permit the selection of the ceramic from among a number of candidate materials with optimum thermal stress resistance for a specific thermal environment and failure mode.

The derivations of the thermal stress resistance parameters for ceramic materials presented to date, without exception, have considered steady-state heat flow, or in the case of transient heat transfer, situations in which initial and/or final thermal equilibrium is attained. In practice, however, situations involving thermal shock are encountered in which the ceramic is not in a state of thermal equilibrium. For instance, this is the case for ceramic components of internal combustion or turbine engines, which involve thermal cycling of such frequency that no thermal equilibrium is attained within the time-duration of each cycle. It is anticipated that for these conditions, the thermal stress

1

resistance parameters will differ from those appropriate to steady-state heat flow or those which involve thermal equilibrium following or preceding transient heat flow.

It is the purpose of this study to develop an analysis of the material properties which affect thermal stress failure of ceramic components subjected to rapid thermal cycling and to establish the appropriate thermal stress resistance parameters.

II. THEORY

The geometry selected for this study consists of an infinite flat plate of thickness 2a located in the y-z plane with $-a \leq x \leq a$. The plate is exposed to an ambient environment, with heat transfer to and from the plate taking place by Newtonian convection. The plate is subjected to rapid thermal cycling by changes in the temperature of the ambient alternating instantaneously between upper and lower temperatures T_f and T_o, respectively, for equal duration with a total period of Δt illustrated schematically in Fig. 1.

A solution of the heat conduction equation;[12]

$$\kappa \partial^2 T / \partial x^2 = \partial T / \partial t \tag{1a}$$

is required for each time interval:

$$\left(\frac{m-1}{2}\right)\Delta t \leq t \leq \frac{m}{2}\Delta t \tag{1b}$$

where κ is the thermal diffusivity and m refers to the mth half-cycle with $m = 1, 2, 3 \ldots \infty$, subject to the boundary condition of symmetry:

$$\partial T / \partial x = 0 \text{ at } x = 0 \tag{2}$$

2

with Newtonian convection at the surfaces $x = \pm\, a$,

$$-k\left(\frac{\partial T}{\partial x}\right)_{x=a} = h\left[T(a,t) - T_\infty(t)\right] \tag{3}$$

where k is the thermal conductivity and h is the heat transfer coefficient (assumed to be the same for heating and cooling) and $T_\infty = T_f$ or T_o, for the heating or cooling phase of the cycle, respectively.

The initial conditions are different for each time interval, but, in general, the initial temperature distribution for each time interval will be identical to the distribution at the end of the preceding interval. The solution is found by standard techniques.[12] In the mth half-cycle, we find

$$T(x,t) = T_m + \sum_{\ell=1}^{\infty} C_{\ell m} e^{-\kappa\lambda_\ell^2 t} \cos(\lambda_\ell x) \tag{4}$$

where

$$T_m = \begin{cases} T_o, & m \text{ even;} \\[2em] T_f, & m \text{ odd} \end{cases}$$

The eigenvalues λ_ℓ are solutions of the transcendental equation:

$$\lambda_\ell a \,\tan\,(\lambda_\ell a) = \beta \tag{5}$$

with Biot number

$$\beta = \frac{ha}{k} \tag{6}$$

The expansion coefficients C_ℓ for the mth time interval are

$$C_{\ell m} = \frac{2(T_f - T_o)\beta \,\sin\,\lambda_\ell a}{\lambda_\ell a(\beta + \sin^2\lambda_\ell a)}\left[\sum_{j=0}^{m=1} (-1)^{(m-j)} e^{-j\kappa\lambda_m^2 \Delta t/2}\right], \quad m \geq 1 \tag{7}$$

The thermal stress is computed from the temperature distribution according to:[13]

$$\sigma_{yz}(x,t) = \frac{\alpha E}{1-\nu}\left[-T(x,t) + \frac{1}{2a}\int_{-a}^{a}T(x',t)dx' + \frac{3x}{2a^3}\int_{-a}^{a}T(x',t)x'dx'\right], \quad (8)$$

to yield, for the mth half-cycle,

$$\sigma_{yz}(x,t) = \frac{\alpha E}{1-\nu}\sum_{\ell=1}^{\infty}C_{\ell m}e^{-\kappa\lambda_\ell^2 t}\left(\frac{\sin \lambda_\ell a}{\lambda_\ell a} - \cos \lambda_\ell a\right), \quad (9)$$

where $C_{\ell m}$ is given by Eq. (7) and α is the thermal expansion coefficient, E is Young's modulus, and ν is Poisson's ratio.

The temperature was calculated in terms of the non-dimensional temperature, T^*:

$$T^* = (T - T_o)/(T_f - T_o) \quad (10)$$

and the stress in terms of the non-dimensional stress, σ^*:

$$\sigma^* = \sigma(1-\nu)/\alpha E(T_f - T_o) \quad (11)$$

the non-dimensional time, t^*:

$$t^* = \kappa t/a^2 \quad (12)$$

and the non-dimensional period for each cycle:

$$\Delta t^* = \kappa\Delta t/a^2 \quad (13)$$

4

For convenience, these non-dimensional quantities will be referred to simply as temperature, stress, time and period, respectively.

III. NUMBERICAL RESULTS AND DISCUSSION

Figures 2a and 2b, for $\beta = 2.5$, show the distribution of the temperatures and stresses encountered during the first cycle for a range of values of time, t^*, for a value of the cycling period $\Delta t^* = 50$. The corresponding value of frequency is sufficiently low that during the heating and cooling phases of the cycle thermal equilibrium (i.e., temperature uniformity at T_f and T_o, respectively) is achieved. The numerical values for the temperature and stresses agree with other literature data[13-15], which supports the validity of the theory presented above. For purposes of further discussion it should be noted that the data shown in Fig. 2, because of the large value of the period Δt^* (i.e., low frequency), will not vary from cycle-to-cycle, regardless of the number of cycles to which the plate is subjected.

Figures 3a and 3b, for a value of $\beta = 2.5$, show the temperature and stress distribution for a range of values of t^* during the first cycle, with a period $\Delta t^* = 1.0$. This value of period is sufficiently brief that within the cycle thermal equilibrium is not achieved. This is clearly evident from the data presented because the value of temperature (T^*) does not attain the value of unity.

In general, after a sufficient number of cycles, a condition will be achieved to which, for a specific value of time for any cycle, no cycle-to-cycle variation in temperature or thermal stress is found. For convenience, this condition will be referred to as cycle-to-cycle equilibrium.

Figures 4a and 4b show the distribution of the temperature and stress, respectively, during a cycle for which such cycle-to-cycle equilibrium was attained for a vlaue of $\beta = 2.5$ and $\Delta t^* = 1.0$, identical to the values of Fig. 3. Comparison of the data given in Fig. 4 with those in Fig. 3 shows that the magnitude of the maximum compressive stresses during the equilibrium cycle are below those encountered during the first cycle, and conversely for the tensile stress. This effect arises because during heating in the first cycle the value of tensile stress at the center of the plate rises slower than the compressive stress in the surface. For this particular value of β if the value of Δt^* is smaller than 0.2, the cooling phase will be initiated well before tensile stress could reach a peak value, if heating had been continued. It should be noted that for the thermal cycling conditions for the data in Fig. 4, the stress at any instant of time may exhibit a maximum at a position in the plate not necessarily at the center or surface. However, it was found that the maximum value of stress encountered during any complete cycle occurs in the surface, except for tensile stress in the first complete cycle which for values of Δt^* between 0.1 and 1.0 may occur in the center.

Figure 5 shows the envelope of the absolute value of the maximum values of the tensile and compressive stresses from the first cycle until cycle-to-cycle equilibrium is approached for values of Δt^* and β identical to those for Figs. 3 and 4. As can be seen for the latter condition the magnitudes of the maximum tensile and compressive stresses are identical. This is expected because at cycle-to-cycle equilibrium the spatial- and time-averaged temperature of the plate lies mid-way between the upper and lower ambient temperatures between which the plate is being cycled.

6
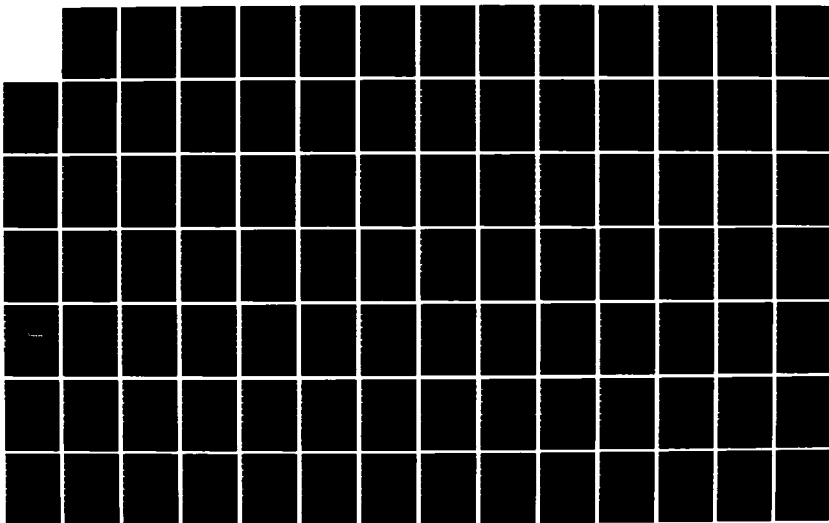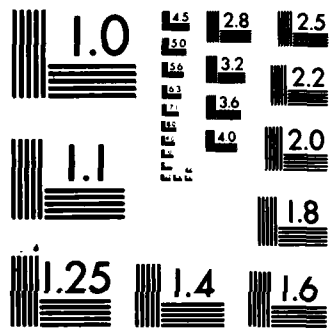
MICROCOPY RESOLUTION TEST CHART

NATIONAL BUREAU OF STANDARDS 1963-A

Figures 6a and 6b give the maximum values of the compressive and tensile thermal stresses at the surface and center of the plate, respectively, during the heating phase of the first cycle as a function of the cycling period, Δt^*, and a range of value of the Biot number, β. In general, as found earlier for a specific case (Fig. 3), the absolute values of the compressive stresses exceed the corresponding values of the tensile stresses.

Figures 7a and 7b show the tensile and compressive stresses, respectively, in the surface of the plate during the cooling phase of the first cycle as a function of the cycling period, Δt^*, and a range of values of the Biot number. Of interest to note is that at the lowest values of the cycling period (i.e., high cycling frequency) the stresses in the surface are compressive throughout the cycle.

The opposite effect can be seen in Figs. 8a and 8b, in which we give the values for the maximum compressive and tensile stresses, respectively, at the center of the plate, during the cooling phase of the first cycle, as a function of the cycling period Δt^* and for a range of values of Biot number. In this case, at the lower values of cycling period (high frequency) the center of the plate remains in a state of tension throughout the first cycle.

The values for the maximum tensile (or compressive) stress in the surface and center of the plate, at the condition of cycle-to-cycle equilibrium as a function of the period Δt^* and a range of values for the Biot number are shown in Figs. 9a and 9b, respectively. The stresses in the surface are significantly higher than those at the center.

7

In terms of the objectives of this study, it is of interest to note that, as indicated by the data presented in Figs. 6, 7, 8 and 9, at least qualitatively the magnitude of maximum stress within any cycle decreases with decreasing cycling period Δt^*, or in other words the maximum stress decreases with increasing cycling frequency. Since Δt^* is defined as $\kappa \Delta t / a^2$, where Δt is the period in real time, this conclusion implies that for any given value of Δt and a, low thermal stress can be achieved by choosing materials with a value of thermal diffusivity as low as possible, other variables being constant. This conclusion is in direct contrast with the general concept that for good thermal stress resistance, high thermal diffusivity is desirable. Of course, high thermal diffusivity is appropriate for heating or cooling conditions involving initial and/or final thermal equilibrium. The requirement of low thermal diffusivity as concluded from the present analysis is appropriate for thermal cycling at frequencies for which thermal equilibrium is not achieved within each cycle.

Of interest to note also, as indicated by the dependence of the magnitude of stress on Δt^* at high frequencies, is that at any given value of Biot number the stresses decrease with increasing plate thickness. This effect also is opposite to the general effect of dimensions on the magnitude of thermal stress, as indicated for instance by the dependence of stress on Biot number. It is postulated that at least qualitatively, high thermal inertia is required for low magnitude of thermal stress. Of course, high thermal inertia is achieved by large plate thickness, as well as by low thermal diffusivity.

It is appropriate to establish the applicability of the present results to ceramic practice, by means of a numerical example. It will be assumed that the value for the Biot number is $\beta = 1$. At this value the magnitude of Δt^* for which the value of stress at cycle-to-cycle equilibrium is approximately one half the value attained for $\Delta t^* \to \infty$ corresponds to $\Delta t^* \approx 0.3$, with corresponding value of frequency $f = (\Delta t)^{-1} = \kappa/0.3a^2$. For silicon nitride with $\kappa \approx 0.1$ cm.^{2}s^{-1} and a value of $a = 0.25$ cm, this frequency is approximately 5 cps or 300 cpm, well within the range encountered during normal operation of an internal combustion engine. For the above reasons, it is predicted that structural ceramics with very low thermal diffusivity such as zirconia or micro-cracked multi-oxide ceramics should show very good thermal stress resistance under conditions of rapid thermal cycling.

As indicated in Fig. 6, the tensile stresses increase with increasing number of cycles to which the ceramic is subjected. This implies that if tensile failure is of primary concern, as it usually is, failure more likely will occur when conditions of cycle-to-cycle equilibrium are reached rather than during the first few cycles.

This conclusion needs revision if the plate originally is at the higher temperature and is subjected to cooling during the initial phase of the first cycle. If so, the signs of all the stress values reported are reversed, and the magnitude of the tensile stresses during the first cycle exceeds that for cycle-to-cycle thermal equilibrium. Under this condition, tensile failure is more likely to occur during the first few, rather than subsequent cycles. Obviously, these conclusions would need to be re-examined if significant thermal fatigue effects are present.

9

For purposes of material selection, it is convenient to derive an appropriate "thermal stress resistance parameter" on the basis of which, from among a number of candidates, the material can be selected with optimum thermal stress resistance for any specific failure criterion and mechanism of heat transfer. Because of the specific dependence of σ^* on Δt^* found in the present study, no simple linear analytical expression was found by curve-fitting or other method from which the appropriate thermal stress resistance parameter could be obtained. Nevertheless, a very approximate derivation of such a parameter can be presented. This derivation will concentrate on the dependence of stress on Δt^* at the condition of cycle-to-cycle equilibrium.

The data in Fig. 9 illustrate that at low values of Δt^* (high frequencies) the magnitude of stress increases with increasing Δt^*. If to a first approximation a linear dependence can be assumed, the stress can be written:

$$\sigma \approx \frac{A\alpha E\Delta T\kappa(\Delta t)}{(1-\nu)a^2} \tag{14}$$

The data in Fig. 9 also indicate that at the lower values of the Biot number ($\beta < 1$) the magnitude of maximum stress is directly proportional to the value of the Biot number, β. Incorporating this effect in eq. 14, yields:

$$\sigma \approx \frac{B\alpha E\Delta T\kappa(\Delta t)h}{(1-\nu)ak} \tag{15}$$

where B is another constant.

Thermal stress failure in brittle ceramics usually occurs in tension, Equating the stress, σ, in eq. 15, to the tensile strength, S_t, an expression can be obtained for the maximum range of temperature difference ΔT_{max} to which the plate can be subjected for a given value of ΔT:

$$\Delta T_{max} \approx - \left\{ \frac{S_+(1-\nu)k}{\alpha E \kappa} \right\} \left\{ \frac{a}{B(\Delta t)h} \right\} \qquad (16)$$

which yields the thermal stress resistance parameter:

$$\frac{S_+(1-\nu)k}{\alpha E \kappa} \qquad (17)$$

Because, by definition $\kappa = k/\rho c$ (where ρ is the density and c is the specific heat), this parameter can be written also as:

$$\frac{S_+(1-\nu)\rho c}{\alpha E}$$

which indicates that for thermal cycling at high frequency, materials should have a high specific heat per unit volume. At least qualitatively, this conclusion seems physically realistic since a high specific heat per unit volume limits the range of temperature variation in the plate within any given thermal cycle. Also, high specific heat per unit volume is in accordance with the earlier hypothesis that high thermal inertia is required to minimize the stresses.

In summary, the present results indicate under conditions of thermal cycling of such frequency that thermal equilibrium is not achieved within each cycle, materials with low values of thermal diffusivity should exhibit better thermal stress resistance than materials with high values of thermal diffusivity.

The notation S_+ for tensile strength follows the original notation used by Kingery (footnote 1).

ACKNOWLEDGMENT

REFERENCES

1. W. D. Kingery, "Factors Affecting Thermal Stress Resistance of Ceramic Materials", J. Amer. Ceram. Soc., 38 (1) 3-15 (1955).

2. W. R. Buessum, "Resistance of Ceramic Bodies to Temperature Fluctuations", Sprechsaal, 93 (6) 137-141 (1960).

3. W. B. Crandall and J. Ging, "Thermal Shock Analysis of Spherical Shapes", J. Amer. Ceram. Soc., 38 (1) 44-45 (1955).

4. D. P. H. Hasselman, "Approximate Theory of Thermal Stress Resistance of Brittle Ceramics Involving Creep", J. Amer. Ceram. Soc., 50 (9) 454-57 (1967).

5. D. P. H. Hasselman, "Thermal Shock by Radiation Heating", J. Amer. Ceram. Soc., 46 (5) 229-34.

6. D. P. H. Hasselman, "Theory of Thermal Shock Resistance of Semitransparent Ceramics Under Radiation Heating", J. Amer. Ceram. Soc., 49 (2) 103-04 (1966).

7. D. P. H. Hasselman, "Elastic Energy at Fracture and Surface Energy as Design Criteria for Thermal Shock", J. Amer. Ceram. Soc., 46 (11) 535-40 (1963).

8. D. P. H. Hasselman, "Unified Theory of Thermal Shock Fracture Initiation and Crack Propagation in Brittle Ceramics", J. Amer. Ceram. Soc., 52 (11) 600-04 (1969).

9. D. P. H. Hasselman, "Role of Physical Properties in Post-Thermal Buckling Resistance of Brittle Ceramics", J. Amer. Ceram. Soc., 61, 178 (1978).

10. D. P. H. Hasselman, "Role of Physical Properties in the Resistance of Brittle Ceramics to Fracture in Thermal Buckling", J. Amer. Ceram. Soc., 62 (3-4) 125-28 (1979).

REFERENCES (Continued)

11. D. P. H. Hasselman, J. R. Thomas, Jr., M. P. Kamat and K. Satyamurthy, "Thermal Stress Analysis of Partially Absorbing Brittle Ceramics Subjected to Radiation Heating", J. Amer. Ceram. Soc., 63 (1-2) 21-25 (1980).

12. H. S. Carslaw and J. C. Jaeger, Conduction of Heat in Solids, Oxford at the Clarendon Press, 2nd Eds. 1960, 510 pp.

13. B. A. Boley and J. H. Weiner, Theory of Thermal Stresses, John Wiley and Sons, N.Y. 1960 (586 pp).

14. M. P. Heisler, "Transient Thermal Stresses in Slabs and Circular Pressure Vessels", J. Appl. Mech. 20 (2) 261-269 (1953).

15. P. J. Schneider, Temperature Response Charts, John Wiley and Sons, Inc., NY, 1963 (153 pp).
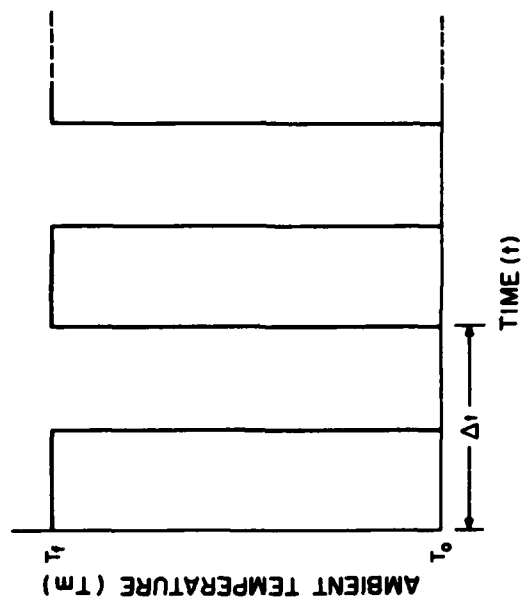
Fig. 1. Cyclic variation with period Δt of ambient temperature surrounding ceramic plate subjected to convective heat transfer.
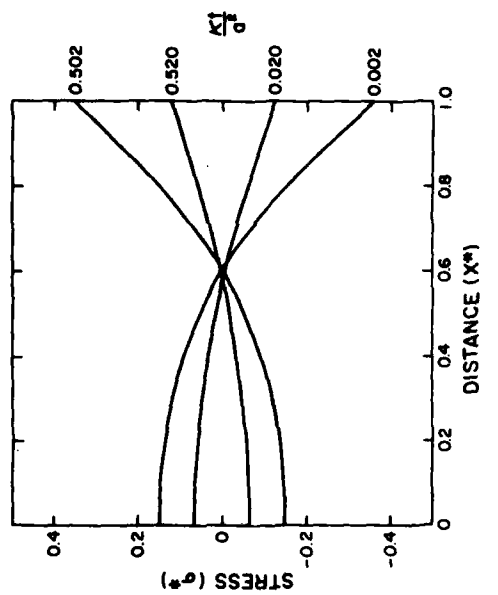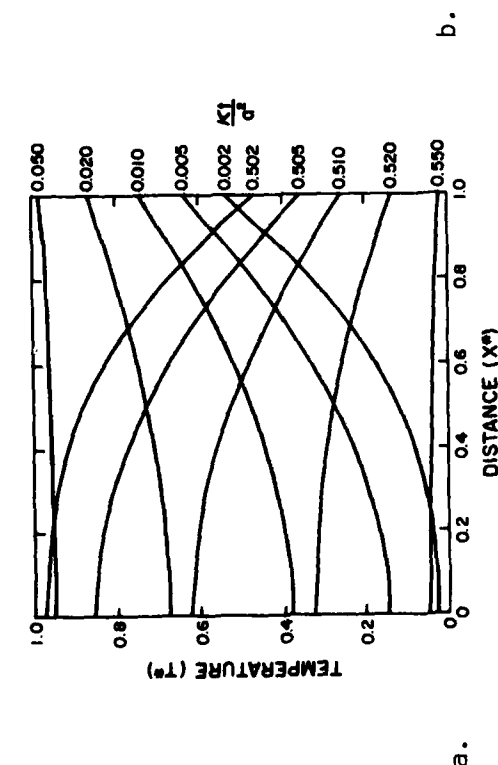
Fig. 2. Temperature (a) and stress (b) distributions for Biot number, $\beta = 2.5$, for a range of values of time (t^*) during the first cycle in a plate subjected to thermal cycling with period $\Delta t^* = 50$, such that within each cycle the plate comes to thermal equilibrium.
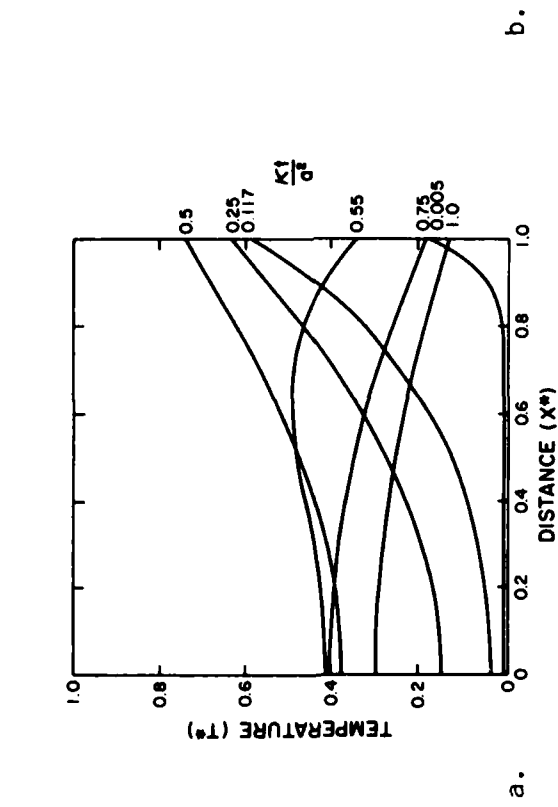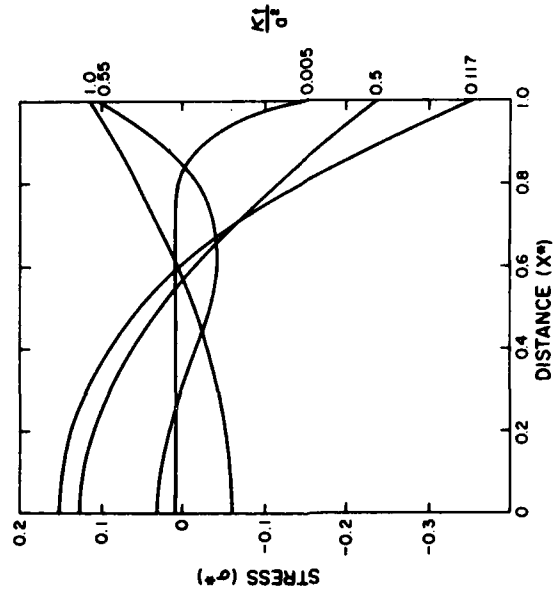
Fig. 3. Temperature (a) and stress (b) distributions for Biot number, $\beta = 2.5$, for a range of values of time (t^*) in a plate subjected to thermal cycling with a period $\Delta t^* = 1$, for which the plate does not reach thermal equilibrium within the cycle.
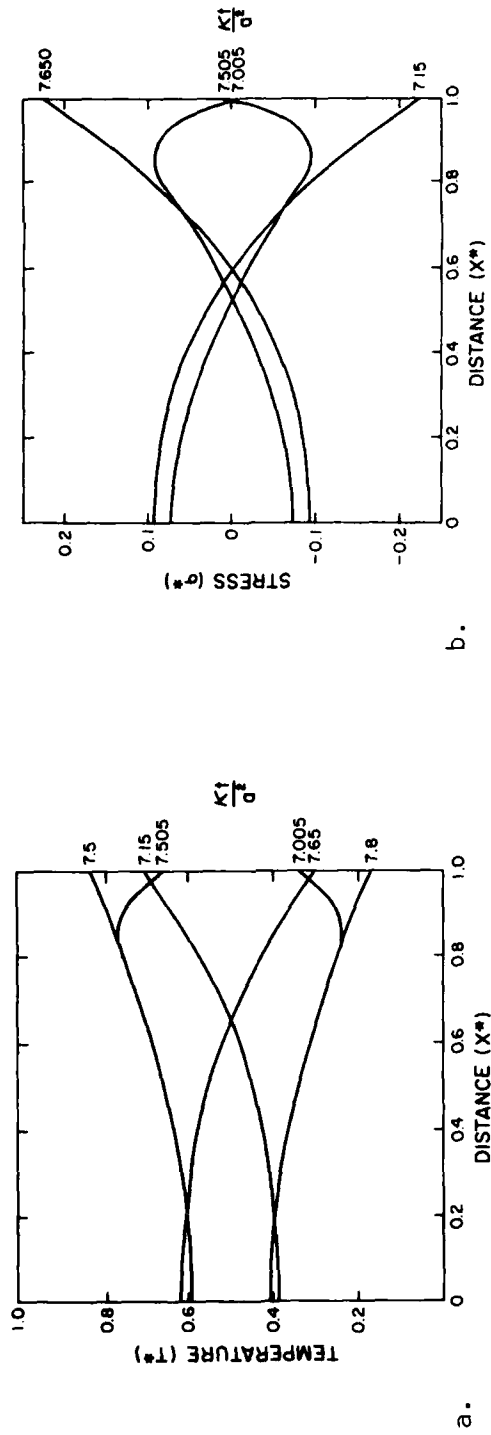
Fig. 4.   Temperature (a) and stress (b) distributions for Biot number, β = 2.5 for a range of values of time t* in a plate subjected to thermal cycling after sufficient cycles that cycle-to-cycle thermal equilibrium is achieved for period Δt* = 1.
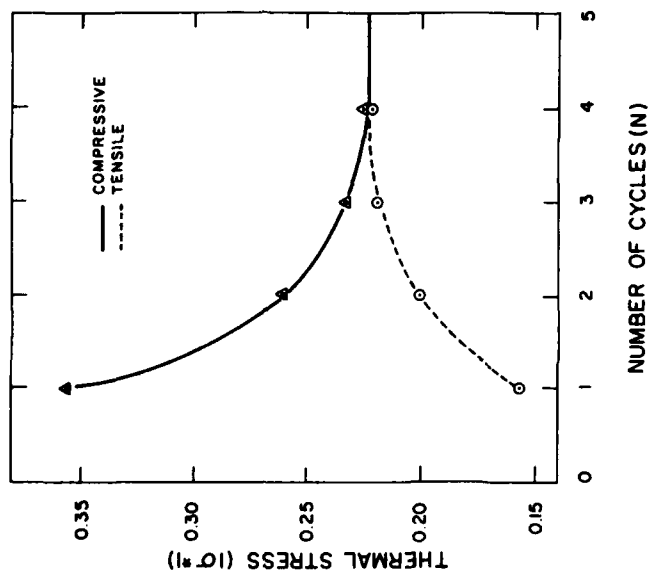
Fig. 5. Envelope of maximum stress for Biot number $\beta = 2.5$ in surface of plate subjected to thermal cycling with period $\Delta t^* = 1$ from the first cycle to cycle-to-cycle thermal equilibrium.
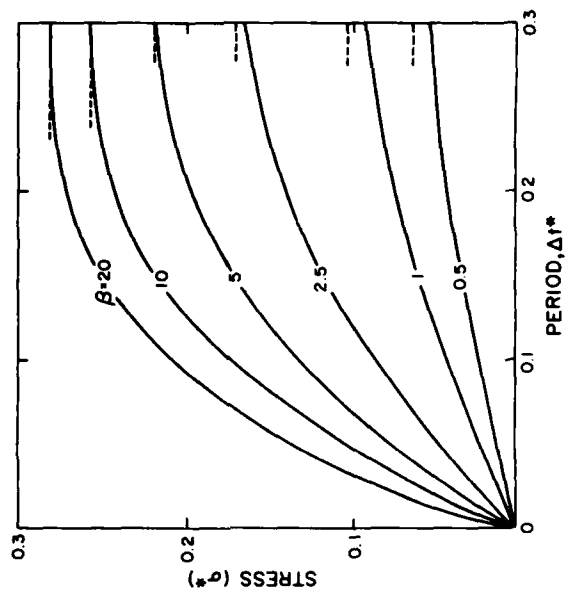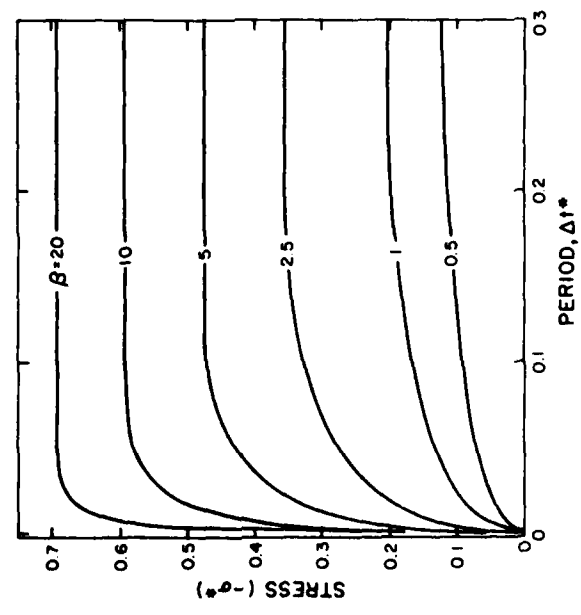
Fig. 6. Maximum value of stress in surface (a) and center (b) of plate subjected to thermal cycling, during the heating phase of the first cycle, as a function of the period Δt^* for a range of values of Biot number, β. Dotted lines indicate the asymptotic values of stress for values of the period Δt^* for which thermal eqiulibrium occurs during first cycle.
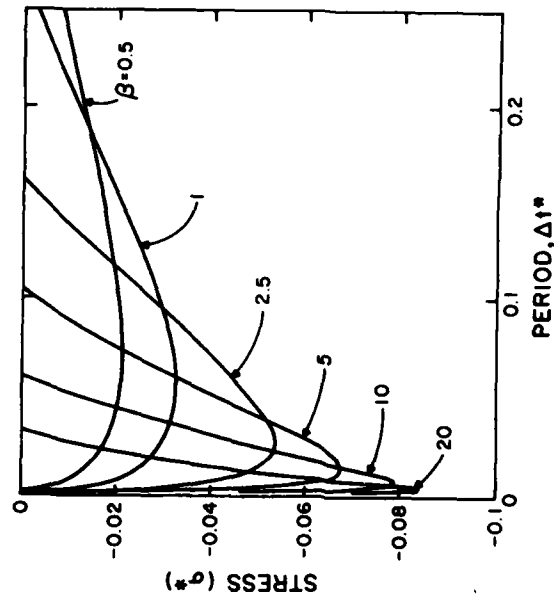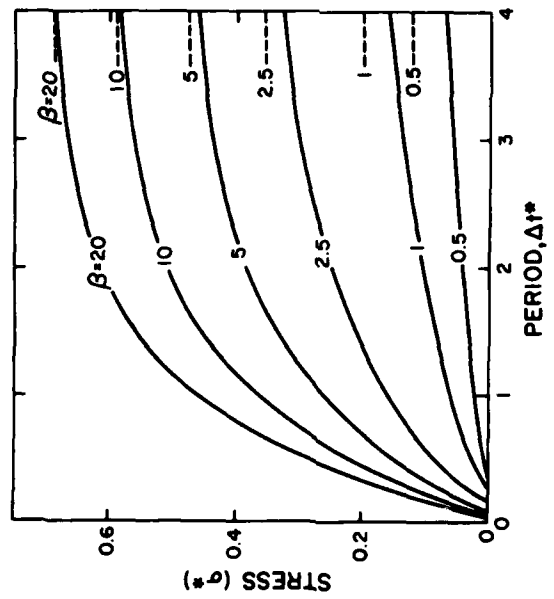
Fig. 7. Maximum value of tensile (a) and compressive (b) stresses in surface of plate subjected to thermal cycling, during the cooling phase of the first cycle, as a function of the period Δt^* for a range of values of Biot number, β. (Dotted lines indicate the asymptotic values of stress for values of Δt^* for which thermal equilibrium occurs during first cycle). Fig. (a) is the continuation of Fig. (b) as the period increases.
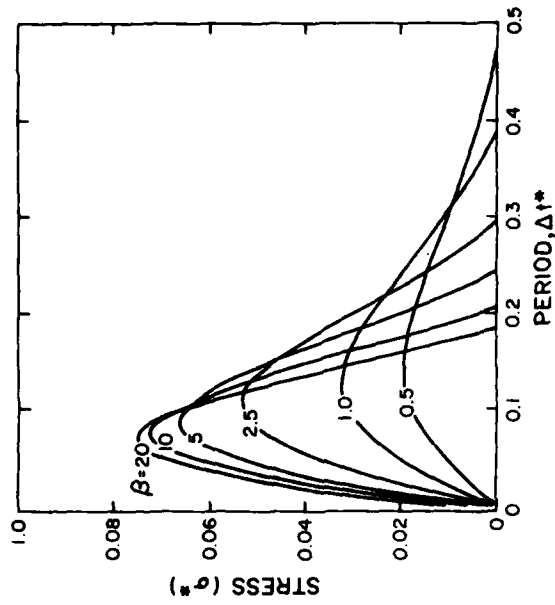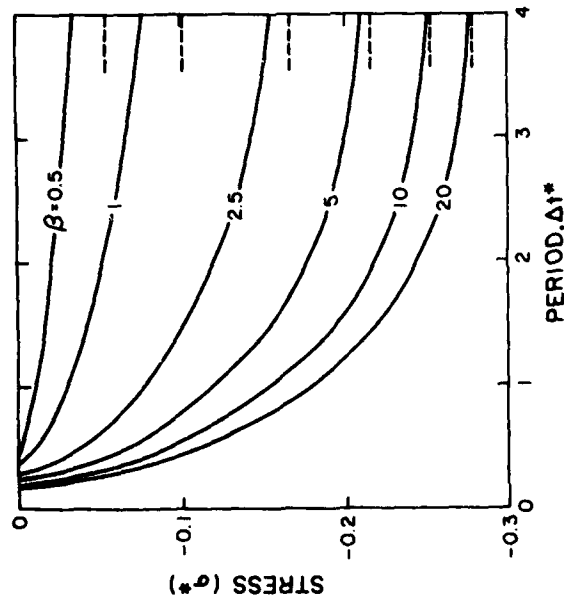
Fig. 8. Maximum value of compressive (a) and tensile (b) stresses in center of plate subjected to thermal cycling during the cooling phase of the first cycle as a function of the period Δt^* for a range of values of Biot number. (Dotted lines indicate the asymptotic values of stress for values of Δt^* for which thermal equilibrium occurs during first cycle). Fig. (a) is the continuation of Fig. (b) as period increases.
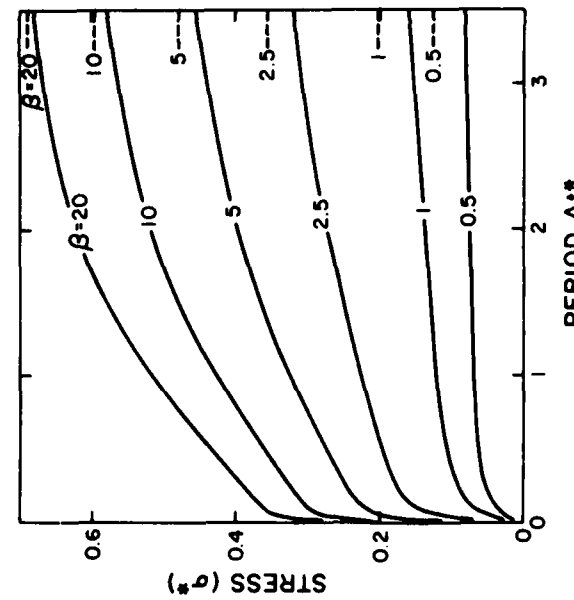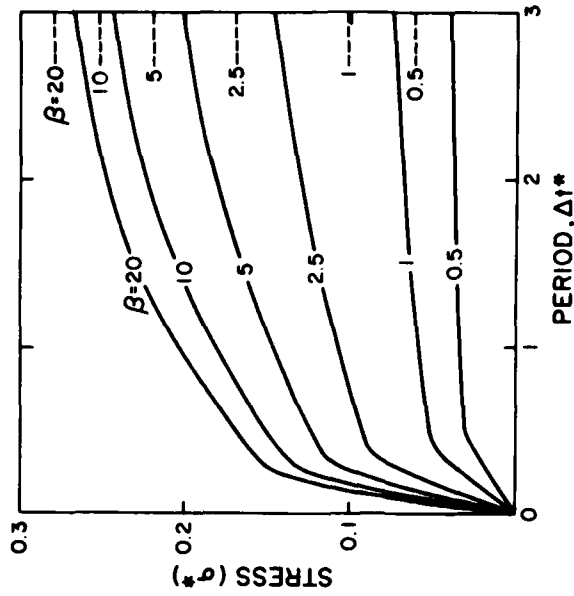
Fig. 9. Maximum stress in surface (a) and center (b) of plate subjected to thermal cycling at cycle-to-cycle equilibrium as a function of period Δt^* for a range of values of Biot number, β. (Dotted lines denote asymptotic values of stress for value of Δt^* for which plate comes to thermal equilibrium within cycle.)

Chapter VIII

ROLE OF MATERIAL PROPERTIES IN THE
THERMAL STRESS FRACTURE OF BRITTLE CERAMICS
SUBJECTED TO CONDUCTIVE HEAT TRANSFER

by

H. Hencke*, J. R. Thomas, Jr.,* D. P. H. Hasselman

*Department of Mechanical Engineering
Department of Materials Engineering
Virginia Polytechnic Institute and State University
Blacksburg, VA 24061 USA

ABSTRACT

An analysis is presented of the thermal stresses in brittle ceramics subjected to thermal shock by quenching into a liquid medium in which conduction is the primary mechanism of heat transfer. The magnitude of maximum stress was shown to be a function of the coefficient of thermal expansion, Young's modulus and Poisson's ratio of the ceramic as well as the values of the thermal conductivity, specific heat and density of the ceramic and quenching medium. The magnitude of thermal stress was shown to be independent of specimen size and on cooling to occur at the instant of cooling ($t = 0$). Appropriate thermal stress resistance parameters were derived.

I. INTRODUCTION

Brittle structural ceramics for use at high temperatures are very susceptible to catastrophic failure due to transient or steady-state thermal stresses, which inevitably arise under normal or unusual operating conditions involving non-uniform temperature contributions.[1,2] A fundamental understanding of the factors which affect thermal stress fracture of brittle ceramics is imperative for reliable performance and failure analysis. As an alternative, information on the thermal fracture behavior of ceramic materials can be obtained by experimental means. One test for this purpose which is highly popular because of its simplicity, consists of quenching appropriate specimens from an oven at high temperature into a fluid medium such as water,[3,4,5] oil,[6] fused salts[7] or fluidized bed[8,9] maintained at a lower temperature. The critical quenching temperature difference (ΔT_c) required to initiate thermal stress fracture represents a quantitative measure of the thermal stress resistance of the particular ceramic.

The quantitative interpretation of such data, without exception, as far as these authors are aware, is based on thermo-elastic theory for heat transfer by convective means. The assumption of heat transfer by convection whether by natural convection for stationary specimens or by forced convection for moving specimens,[10] implies the transport of heat by relative motion (shear) within the fluid. It should be noted that the quantitative understanding of convective heat transfer is based on meas-

2

urement during steady-state conditions. In this respect it should be noted also that the maximum thermal stresses (i.e., fracture) during quenching from a higher to a lower temperature occurs a relatively brief time after the specimen is inserted into the fluid[3,7]. For specimens in the form of rods with circular or square cross-section with diameter or sides of a few mm and values of thermal diffusivity ranging from 0.02 to 0.2 cm.^{2}sec^{-1}, common for many structural ceramics, the time-to-maximum stress (i.e., time-to-fracture) is of the order of 0.01 seconds. It seems unlikely that steady-state conditions for convective heat transfer could be established in a time span of this small magnitude.

In order to provide a justification for the objectives of this study, it should also be recognized that a thin layer of the fluid in immediate contact with the specimen is stationary with respect to the hot surface. Any heat lost from the specimen must be removed by conduction through this stagnant layer. Such conduction of heat requires a temperature gradient through this layer and also results in an increase in temperature of this layer. This temperature increase, in turn, requires an amount of heat which is a function of the specific heat and density of the fluid.

As indicated by the values of peak thermal stress and associated transient temperature distributions[11,12,13] on cooling, tensile thermal stresses in the surface of sufficient magnitude to cause fracture requires the removal of heat from a relatively

3

thin surface layer of the ceramic specimen which is a small fraction of the total thermal energy stored within the specimen. Depending on the relative values of specific heat and density of the specimen and fluid medium the heat removed from the specimen surface sufficient to cause fracture can be of the order of the amount of heat absorbed by the stagnant layer. If this hypothesis is correct it appears conceivable that thermal fracture in a quenching experiment may not require the transport of heat by convection, in the usual sense. Indeed, if this statement can be proven to be true, quantitative interpretation of experimental data for ΔT_c should be based on conductive heat transfer within the fluid, rather than by convective heat transfer as has been common practice.

For the reasons outlined above thermal stress fracture in quenching experiments by purely conductive processes appears deserving of attention. It is thought that during a quench, thermal fracture by convection and conduction are competitive processes, depending on the relative values of the thermal conductivity, density and specific heat of the specimen and fluid medium as well as the value of the fluid viscosity. However, in order to assess the dominant mechanism of heat transfer responsible for thermal stress fracture in a quench, an analytical solution for the thermal stresses generated by conductive heat transfer is required.

The purpose of this study was to derive such solutions and to assess their relevance to the quenching method for the meas-

4

urement of thermal stress resistance of brittle structural ceramics.

II. ANALYSIS

In view of its relevance to quenching studies a circular cylinder was chosen as a suitable geometry for the present analysis. The cylinder, at initial temperature T_o, was assumed to be submerged instantaneously into a fluid at temperature T_f. The thermal contact between the cylinder and fluid was considered to be perfect so that the heat transfer was not impeded by a contact resistance. The transfer of heat within the cylinder and fluid was assumed to occur in a radial direction only. For purposes of simplification the cylinder was assumed to be infinitely long, so that end effects could be ignored. For this reason the solutions to be obtained are expected to describe the conditions near the center of quenching specimens with a length large compared to the diameter. The solutions for the transient temperatures were obtained first, from which the thermal stresses were then readily obtained.

A. Transient Temperatures

The transient temperatures are obtained by solution of the heat conduction equations[14]:

$$\kappa_1 \frac{1}{r} \frac{\partial}{\partial r} \left(r \frac{\partial \theta_1}{\partial r} \right) = \frac{\partial \theta_1}{\partial t} \tag{1}$$

and

$$\kappa_2 \frac{1}{r} \frac{\partial}{\partial r} \left(r \frac{\partial \theta_2}{\partial r} \right) = \frac{\partial \theta_2}{\partial t} \tag{2}$$

5

where $\theta(r,t) = T - T_f$, κ is the thermal diffusivity, r is the radial coordinate and the subscripts 1 and 2 refer to the cylinder and medium, respectively.

The solution of eqs. 1 and 2 must satisfy the boundary conditions:

$$\theta_1 (r,0) = \theta_o \;\; ; \;\; \theta_2(r,0) = 0 \tag{3}$$

$$\frac{\partial \theta_1}{\partial r} (0,t) = 0 \;\; ; \;\; \lim_{r \to \infty} \theta_2(r,t) = 0 \tag{4}$$

$$\theta_1(R,t) = \theta_2(R,t) \tag{5}$$

$$k_1 \frac{\partial \theta_1}{\partial r} (R,t) = k_2 \frac{\partial \theta_2}{\partial r} (R,t) \tag{6}$$

where $\theta_o = T_o - T_f$, R is the radius of the cylinder and k is the thermal conductivity.

A general solution of eqs. 1 and 2, subject to the boundary conditions given by eqs. 3 thru 6, was presented by Carslaw and Jaeger[15] and worked out in detail by Hencke[16]. The final solution, for purposes of general convenience, was expressed in terms of the thermal conductivity ratio, K

$$K = k_1/k_2 \tag{7}$$

the thermal diffusivity ratio, A

$$a^2 = \kappa_1/\kappa_2 \tag{8}$$

the non-dimensional time, t^*

$$t^* = \kappa_1 t/R^2 \tag{9}$$

the non-dimensional radial distance, r^*

$$r^* = r/R \tag{10}$$

and the non-dimensional temperature, T^*

$$T^* = (T - T_f)/(T_o - T_f) \tag{11}$$

For convenience, the last three non-dimensional quantities will be referred to as time, distance and temperature, respectively.

The solutions for the temperatures T_1^* and T_2^* in the cylinder and surrounding liquid, respectively, are:

$$T_1(r^*, t^*) = \frac{4}{\pi^2} K \int_0^\infty \exp(-\mu^2 t^*) \, \frac{J_o(\mu r^*) \, J_1(\mu) \, d\mu}{\mu^2 [\Phi^2(\mu) + \Omega^2(\mu)]} \tag{12a}$$

and

$$T_2(r^*, t^*) = \frac{2}{\pi} K \int_0^\infty \exp(-\mu^2 t^*) \, \frac{J_1(\mu) \, [J_o(a\mu r^*) \Phi(\mu) - Y_o(a\mu r^*) \Omega(\mu)] \, d\mu}{\mu [\Phi^2(\mu) + \Omega^2(\mu)]} \tag{12b}$$

where

$$\Phi(\mu) = K \, J_1(\mu) Y_o(a\mu) - a \, J_o(\mu) \, Y_1(a\mu) \tag{13}$$

$$\Omega(\mu) = K \, J_1(\mu) J_o(a\mu) - a \, J_o(\mu) \, J_1(a\mu) \tag{14}$$

where μ is the variable of integration which arises from inverting the Laplace transform solutions[16] of eqs. 1 and 2, and J_o, J_1, Y_o, and Y_1 are the Bessel functions of the first and second kind.

The temperatures T_1^* and T_2^* were obtained most conveniently by numerical evaluation of the integrals in eqs. 12a and 12b.

B. Thermal Stresses

General expressions for the thermal stresses in long circular cylinders with arbitrary radial temperature distributions are

7

given by Boley and Weiner[13]. The stress distribution consists of radial, tangential and axial stresses. From the point of view of thermal stress failure the maximum stresses are of primary interest. Examination of the general solutions shows that the axial stresses exceed the radial and tangential stresses throughout the volume of the cylinder and are equal to the tangential stresses at the cylinder surface $(r = R)$.

In general, the axial stress is given by [13]:

$$\sigma_z = \frac{\alpha E}{(1-\nu)} \; [\; \frac{2}{R^2} \int_0^R Tr'dr' - T] \tag{15}$$

where α is the coefficient of linear thermal expansion, E is Young's modulus and ν is Poisson's ratio.

For convenience the results will be reported in terms of the non-dimensional stress σ_z^*, defined as:

$$\sigma_z^* = \frac{\sigma_z(1-\nu)}{\alpha E(T_o - T_f)} \tag{16}$$

In this notation, substitution of eq. (12a) into eq. (15) yields:

$$\sigma_z^*(r^*, t^*) = \frac{8}{\pi^2} K \int_0^\infty \exp(-\mu^2 t^*) \; \frac{J_1^2(\mu)d\mu}{\mu^3[\Phi^2(\mu) + \Omega^2(\mu)]}$$

$$- T_1^*(r^*, t^*) \tag{17}$$

which can be evaluated numerically as eqs. 12.

III. NUMERICAL RESULTS AND DISCUSSION

The magnitude of the transient temperatures and stresses are illustrated most conveniently by means of a few numerical examples. For two of these examples the thermal conductivity of the cylinder will be taken to be much higher or much lower than the thermal conductivity of the fluid. For the third example the thermal conductivity of the cylinder and fluid will be assumed to be equal. The stress was also found to be a function of the volumetric heat capacity ratio, $A = \rho_1 c_1 / \rho_2 c_2$ of the cylinder and the fluid. However, in order to keep the number of numerical examples to a reasonable number, the volumetric heat capacities ratio was taken as unity.

For a cylinder being cooled, figs. 1a, 1b, and 1c show the transient temperature distributions in the cylinder and fluid for values of the thermal conductivity ratio, $K = 100$, 1 and 0.01, respectively, for a range of values of time, t^*. Comparison of these data indicates that at the higher value of K the temperatures within the cylinder at any instant of time remain fairly uniform. This effect arises because the heat loss from the cylinder is controlled primarily by the much lower value of the thermal conductivity of the fluid. In contrast, at the value of $K = 0.01$, because of the much higher value of the thermal conductivity of the surrounding liquid, the resulting rapid surface cooling of the cylinder results in a relatively high degree of

non-uniformity of the temperature distribution within the cylinder. For K = 1 the degree of cooling of the cylinder and heating of the fluid at the surface are comparable.

In general, the magnitude of thermal stresses is a function of the degree of non-linearity of the temperature distribution. For this reason, the differences in the temperature distributions for the three values of thermal conductivity ratio shown in fig. 1 should be reflected in differences in the magnitude of the thermal stresses.

Figures 2a, 2b and 2c show the distributions of the thermal stresses within the cylinder for the same values of the thermal conductivity ratio and t* as those for the temperature distribution shown in figs. 1a, 1b and 1c. As expected for cooling, the maximum tensile stresses are found at the surface of the cylinder (r = R), whereas the maximum compressive stresses are found at the exact center, r = 0. For heating, the signs of the stresses are reversed.

The maximum value of thermal stress was obtained by calculating the stresses as a function of time. These results are shown in figs. 3a, 3b and 3c, with the stresses in the surface being tensile or compressive for cooling and heating, respectively. The stresses in the surface reach their maximum value at t* = 0. In contrast, the stresses at the center of the cylinder reach their maximum value after some time has elapsed.

It was found that the maximum value of stress in the surface could be expressed by a simple relation:

$$\sigma^*(R) = (N_k^{1/2} + 1)^{-1}$$

10

where N_k is referred to as the conductive heat transfer number defined by:

$$N_k = \frac{k_1 \rho_1 c_1}{k_2 \rho_2 c_2}$$

where k, ρ and c are the thermal conductivity, density and specific heat, respectively, and the subscripts 1 and 2 refer to the cylinder and liquid medium, respectively. Figure 4a shows the maximum thermal stress in the surface as expressed by eq. 18, as a function of the quantity N_k.

The "critical quenching temperature difference, ΔT_c" required for the initiation of thermal stress fracture obtained in a quenching experiment is a measure of the thermal stress resistance of the ceramic being tested. At the value of $\Delta T = \Delta T_c$, the maximum tensile stress equals the tensile strength (S_t) of the ceramic. By equating this value of thermal stress to the tensile strength, as is common practice in the development of thermal stress failure theories , with the aid of eq. 18 an expression for ΔT_c in terms of the relevant material properties can be derived:

$$\Delta T_c = \frac{S_t (1-\nu)}{\alpha E} \left[\left(\frac{k_1 \rho_1 c_1}{k_2 \rho_2 c_2} \right)^{1/2} + 1 \right] \tag{20}$$

For two limiting conditions, eq. 20 permits the derivation of thermal stress resistance parameters for the selection of the ceramic with the optimum thermal stress resistance.

11

For $k_1\rho_1c_1/k_2\rho_2c_2 >> 1$, the appropriate parameter in terms of the properties of the cylinder quenched into a given fluid is:

$$\frac{S_t(1-\nu)(k\rho c)^{1/2}}{\alpha E} \qquad (21)$$

For $k_1\rho_1c_1/k_2\rho_2c_2 >> 1$, the appropriate parameter is:

$$S_t(1-\nu)/\alpha E \qquad (22)$$

The maximum tensile stress at the center of the cylinder encountered during heating could be plotted most conveniently as a function of the thermal conductivity ratio (K) and the volumetric heat capacity ratio, A, as shown in fig. 4b. Because of the relatively complex dependence of the stresses on K and A, the derivation of thermal stress resistance parameters of simple form was not feasible.

The relevance of the above results to the interpretation of quenching data can be demonstrated by means of a numerical example which compares the magnitude of the thermal stresses attained by convective and conductive heat transfer. For this example, four different liquid media were selected with widely different convective and conductive heat transfer properties, namely silicone oil, water, mercury and sodium. Convective heat transfer can occur by natural (free) or forced convection. The latter

12

process is governed by the relative speed between the cylinder and the fluid medium. Depending on the choice of speed almost any value for the forced convective heat transfer coefficient can be obtained. The value of speed at which the specimen hits the fluid surface, at least for a water bath, was shown in a recent study[17] to have no effect on ΔT_c. Perhaps a more appropriate value of speed is the terminal velocity at which the specimen falls through the fluid medium under the influence of gravity[10]. Liquid metal media such as lead and mercury, however, have a density higher than the density of many ceramic specimens. This difference in density would not permit quenching by the usual free-fall method, as the specimen would float only partially submerged on the surface of the fluid. For such media with high density it appears more suitable to rapidly immerse the specimen, attached to a suitable specimen holder, in the fluid after which it is held stationary. Under this condition the specimen is subject to heat flow by natural convection, which was the heat transfer conditions selected for the numerical example to be presented subsequently.

The heat transfer coefficient under conditions of free convection for a circular cylinder held in a horizontal stationary position was calculated from equations given by Holman[18].

For the silicone oil and water baths the heat transfer coefficient is givey by[18]:

$$h = 0.53(N_{Gr} \cdot N_{Pr})^{1/4}(K_f/d)$$

where N_{Gr} is the Grashof number:

13

$$N_{Gr} = g\beta(T_o - T_f)d^3/v_f{}^2$$

in which g is the gravitational constant, β is the coefficient of volumetric thermal expansion, d is the diameter of the cylinder, and v_f is the viscosity of the fluid.

The Prandtl number, N_{Pr}, is defined by:

$$N_{Pr} = v_f/\kappa_f$$

where κ_f is the thermal diffusivity of the fluid.

For the liquid metals, the heat transfer coefficient is[18]:

$$h = 0.53(N_{Gr} N_{Pr}{}^2)^{1/4}(k_f/d)$$

Because the values of h given by eqs. 23 and 26 are a function of the temperature difference itself, the quantity $(T_o - T_f)$ was taken to be 200°C for all calculations. The actual value of $(T_o - T_f)$ can be obtained experimentally or by the method of successive approximations. For the water bath the heat transfer coefficient was assumed to result from free convection only, without the additional contribution from nucleate boiling or steam-film formation. The diameter D of the cylinder was taken to be 6.35 and 12,7 mm (0.25 and 0.5 inch), respectively, which represent dimensions typical for specimens encountered in laboratory practice.

The thermal stresses for conductive heat transfer were calculated by means of eqs. 18 and 19. The property values for the water, mercury and sodium for both the convective and conductive heat transfer were taken from values tabulated by Chapman[19] for

14

assumed film temperatures of 140, 150 and 200°C, respectively. The data for a typical silicone oil with a viscosity of $10^{-4} m^2 s^{-1}$ were taken from data sheets provided by a manufacturer.*

Table I lists the values for the heat transfer parameters for the silicone oil, water, mercury and sodium required for the calculation of the convective heat transfer coefficient.

Table II compares the values of maximum thermal stress (σ^*) for three different materials with property values typical for a glass, polycrystalline aluminum oxide and silicon carbide at a temperature corresponding approximately to the initial specimen temperature during an actual quench. Comparison of these stress values indicates that for all quenching media, the stresses for conductive heat transfer are comparable to or exceed the stress values for natural convection by a considerable margin. It should be emphasized that this conclusion is valid only for the specific condition of natural convection chosen for the mode of convective heat transfer. In practice, under the right conditions of forced convection, almost any value of heat transfer coefficient and corresponding values of stress (σ^*) approaching unity can be achieved.

However, if the quenching test is conducted by holding the specimen stationary in a non-stirred fluid, the data for σ^* in Table II indicate that the possibility of thermal fracture by conductive heat tranfer definitely must be considered in the analysis of the experimental data. Especially for liquid metal

---

* Dow-Corning, Midland, Michigan

15

baths with their much higher thermal conductivity used for quenching of specimens with low thermal conductivity, conductive heat transfer may well be the primary mechanism for thermal stress failure. The relative contributions of convective and conductive heat transfer also are expected to be affected by specimen size. For convective heat transfer the maximum value of thermal stress increases with specimen size, which has no effect on the peak stress for conductive heat transfer. This suggests that, especially for small specimens commonly used for laboratory studies, the contribution of conductive heat transfer should not be overlooked. If indeed conductive heat tranfer is the primary cause for failure, any observed effect of specimen size on ΔT_c is attributable to the statistical nature of brittle fracture, such as expressed by the Weibull theory[20]. Even if the magnitudes of peak stress due to convective and conductive heat transfer are comparable, failure may still be due to the conductive heat transfer for which the maximum value occurs at $t = o$; whereas for convective heat transfer[11,12,13], for all values of the Biot number $\beta < \infty$, the maximum stress occurs at $t > o$. Verification of the analytical results of this study is handicapped by the absence of appropriate data in the open literature. The only available data[21] for specimens held stationary were obtained for glass thermally cycled in water as the quenching medium for which the interpretation of the data is complicated by extensive sub-critical crack growth and quantitative uncertainties of nucleate boiling and steam-film formation. The acquisi-

16

tion of the necessary experimental data with major emphasis on liquid metals is intended to be the subject of a future study.

As a final comment it should be noted that eq. 20 for ΔT was based on the assumption that failure would occur at a value of maximum tensile stress equal to a well-defined value of tensile strength without regard to the underlying variables which govern or contribute to tensile failure. It should be noted that making this assumption has been common practice in the development of thermal stress failure theories of brittle ceramics[1,22,23,24,25]. It is well known, however, that tensile failure of brittle materials is subject to statistical and/or fracture-mechanical variables. For this reason for a quantitative application of the results of this study, a separate detailed analysis of the tensile failure stress will be required for the specific ceramic being considered and for the specific thermal conditions to which it is being subjected.

In summary, an analysis was conducted of the variables which affect thermal stress failure of brittle ceramics subjected to conductive heat transfer. The magnitude of the peak thermal stress was shown to be a function of the coefficient of thermal expansion, Young's modulus and Poisson's ratio of the ceramic as well as the values of the thermal conductivity, specific heat and density of the ceramic and surrounding medium. Appropriate thermal stress resistance parameters were derived.

Acknowledgements

References

1. W. D. Kingery, "Factors Affecting Thermal Shock Resistance of Ceramic Materials", J. Amer. Ceram. Soc. 38 (1) 3-15 (1955).

2. D.P.H. Hasselman, "Unified Theory of Thermal Shock Fracture Initiation and Crack Propagation of Brittle Ceramics", J. Amer. Ceram. Soc., 52 (11) 600-04 (1969).

3. R. W. Davidge and G. Tappin, "Thermal Shock and Fracture in Ceramics", Trans. Brit. Ceram. Soc., 66 (8) 405-22 (1967).

4. D.P.H. Hasselman, "Strength Behavior of Polycrystalline Alumina to Thermal Shock", J. Amer. Ceram. Soc., 53 (9) 490-95 (1970).

5. P. F. Becher, D. Lewis, III, K. R. Carman and C. A. Gonzales, "Thermal Shock Resistance of Ceramics: Size and Geometry Effects in Quench Tests", J. Amer. Ceram. Soc. Bull., 59 (5) 542-48 (1980).

6. J. P. Singh, Y. Tree, D.P.H. Hasselman, "Effect of Bath and Specimen Temperature on the Thermal Stress Resistance of Brittle Ceramics Subjected to Thermal Quenching", J. Mat. Sc., 16, 2109-18 (1981).

7. W. B. Crandall and J. Ging, "Thermal Shock Analysis of Spherical Shapes", J. Amer. Ceram. Soc., 38 (1) 44-54 (1955).

8. D.P.H. Hasselman, E. P. Chen, C. L. Ammann, J. E. Doherty and C. C. Nessler, "Fracture Prediction of the Thermal Fatigue of Silicon Nitride", J. Amer. Ceram. Soc., 58, 513 (1975).

9. K. Niihara, J. P. Singh and D.P.H. Hasselman, "Observations on the Characteristics of a Fluidized Bed for the Thermal Shock Testing of Brittle Ceramics", J. Mat. Sc., 17, 2553-59 (1982).

10. J. P. Singh, J. R. Thomas, Jr., and D.ᵖ.H. Hasselman, "Analysis of Effect of Heat Transfer Variables on Thermal Stress Resistance of Brittle Ceramics Measured by Quenching Experiments", J. Amer. Ceram. Soc., 63 (3-4) 140 (1980).

11. J. C. Jaeger, "On Thermal Stresses in Circular Cylinders", Philos. Mag., 36 (257) 418-28 (1945).

12. M. P. Heisler, "Transient Thermal Stresses in Slabs and Circular Pressure Vessels", J. Apl. Mech., 20 (2) 261-69 (1953).

13. B. A. Boley and J. H. Weiner, Theory of Thermal Stresses, John Wiley and Sons, 1960 (586 pp.).

14. H. S. Carslaw and J. C. Jaeger, Conduction of Heat in Solids, 2nd Ed. Oxford, at the Clarendon Press (1959).

15. Ref. 14, p. 347.

16. H. Hencke, "A Theoretical One-Dimensional Analysis of the Transient Temperature and Stress Distributions in a Long Cylinder Subjected to Conductive Cooling and Heating", M.S. Thesis, Department of Mechanical Engineering, Virginia Polytechnic Institute and State University (1983).

17. J. P. Singh, G. Ziegler, D.P.H. Hasselman, "Effect of Drop-Height on the Critical Temperature Difference (ΔT_c) for Brittle Ceramics Subjected to Thermal Shock by Quenching into Water", J. Amer. Ceram. Soc. (in review)

18. J. P. Holman, Heat Transfer, 5th Ed., McGraw-Hill, New York (1981).

19. A. J. Chapman, Heat Transfer, 3rd Ed., McMillan Publishing Company, New York (1974).

20. W. Weibull, "A Statistical Distribution Function of Wide Applicability", J. Appl. Mech. 18, 293-97 (1951).

21. D.P.H. Hasselman, R. Badaliance, K. R. McKinney and C. H. Kim, "Fracture Prediction of the Thermal Fatigue Resistance of a Glass", J. Mat. Sc. 11, 458-64 (1976).

22. D. P. H. Hasselman, "Thermal Shock by Radiation Heating", J. Amer. Ceram. Soc., 46, 229-34 (1963).

23. D. P. H. Hasselman, "Approximate Theory of Thermal Stress Resistance of Brittle Ceramics Involving Creep", J. Amer. Ceram. Soc., 50, 454-57 (1967).

24. D. P. H. Hasselman, "Thermal Stress Resistance of Brittle Refractory Ceramics: A Compendium", Amer. Ceram. Soc. Bull., 49(12) 1933-37 (1970).

25. D. P. H. Hasselman, J. R. Thomas, Jr., M. P. Kamat and K. Satyamurthy", Thermal Stress Analysis of Partially Absorbing Brittle Ceramics Subjected to Radiation Heating", J. Amer. Ceram. Soc., 63 (1-2) 21-25 (1980).

TABLE I. HEAT TRANSFER PARAMETERS REQUIRED FOR THE CALCULATION OF FREE CONVECTIVE HEAT TRANSFER COEFFICIENTS FOR A VARIETY OF LIQUID QUENCHING MEDIA.

| Liquid Medium	Film Temperature (°C)	Cylinder Diam (mm)	Grashof No. N_{Gr}	Prandtl No. N_{Pr}	Heat Transfer Coefficient* $h(J.m^{-2}.s^{-1}.K^{-1})$
Silicone Oil	140	6.35	0.184×10^6	14.7	525
		12.7	0.147×10^7		441
Water	140	6.35	0.329×10^7	1.24	2,569
		12.7	0.263×10^8		2,160
Mercury	150	6.35	0.394×10^8	0.013	8,754
		12.7	0.316×10^9		7,361
Sodium	200	6.35	0.105×10^7	0.0074	18,410
		12.7	0.837×10^7		15,480

* Based on $(T_o - T_f) = 200°C$.

TABLE II. COMPARISON OF THERMAL STRESSES (σ*) DUE TO CONVECTIVE AND CONDUCTIVE HEAT TRANSFER FOR A TYPICAL GLASS, POLYCRYSTALLINE ALUMINA AND SILICON CARBIDE QUENCHED IN DIFFERENT FLUID MEDIA.

Quenching Medium	Cylinder Diam (mm)	Glass*		Alumina*		SiC*	
		Convection	Conduction	Convection	Conduction	Convection	Conduction
Silicone oil	6.34	0.19(1.3)§	0.21§	0.02(0.11)§	0.06	0.006(0.03)§	0.03
	12.7	0.27(2.3)	0.21	0.04(0.19)	0.06	0.011(0.06)	0.03
Water	6.35	0.45(6.5)	0.48	0.90(0.54)	0.18	0.03(0.16)	0.11
	12.7	0.53(11)	0.48	0.15(0.92)	0.18	0.05(0.27)	0.11
Mercury	6.35	0.60(22)	0.72	0.24(1.9)	0.50	0.10(0.55)	0.26
	12.7	0.63(37)	0.72	0.33(3.1)	0.50	0.15(0.93)	0.26
Sodium	6.35	0.65(47)	0.85	0.37(3.9)	0.68	0.18(1.1)	0.43
	12.7	0.66(78)	0.85	0.45(6.5)	0.68	0.25(1.9)	0.43

* Assumed property values: Glass: K_s = 1.25 W/m^{o}K, ρ_s = 2,475 kg/m^3, c_s = 1050 J/kg^{o}K; Alumina: K_s = 15 W/m^{o}K, ρ_s = 3960 kg/m^3, c_s = 1047 J/kg^{o}K; Silicon Carbide: K_s = 50 W/m^{o}K, ρ_s = 3,200 kg/m^3, c_s = 1,050 J/kg^{o}K.

§ Values for the Biot number calculated from the data for the heat transfer coefficient listed in Table I.

22
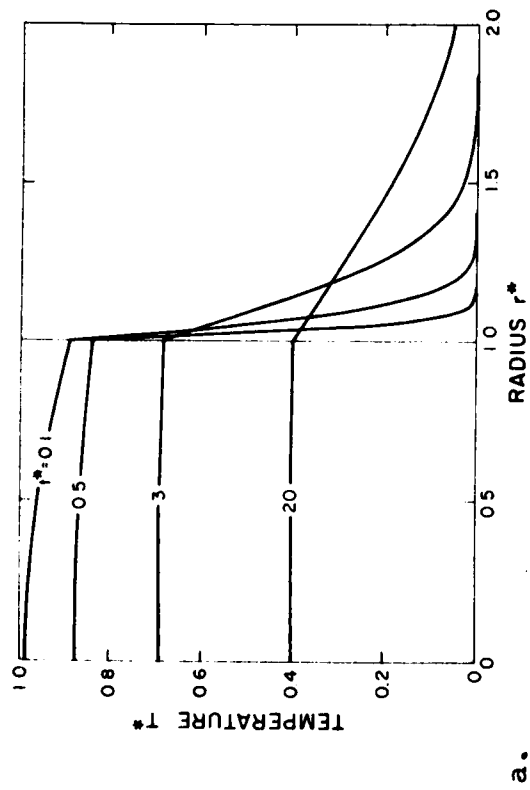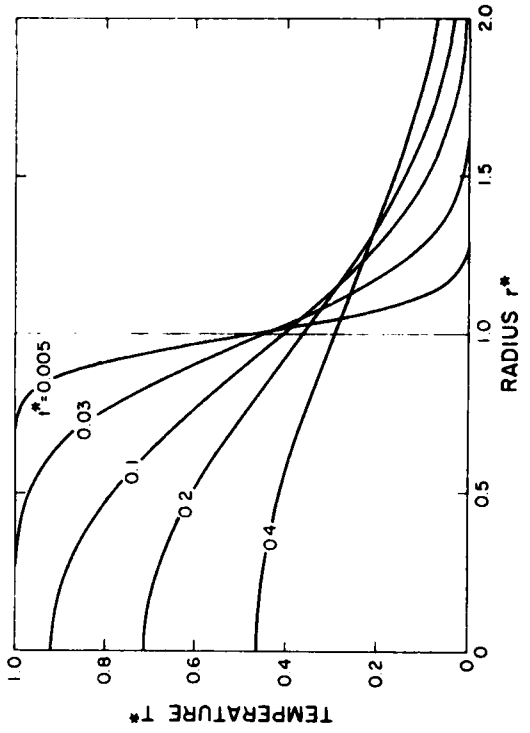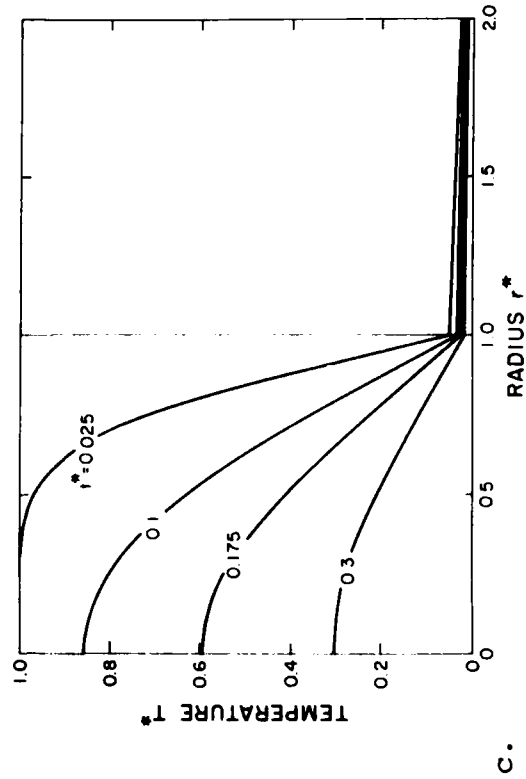
Fig. 1. Transient temperature distributions in and around solid circular cylinder subjected to thermal shock by quenching in a liquid medium with conductive heat transfer for a range of values of time and thermal conducive ratio: a, K = 100; b, K = 1 and c, K = 0.01. (Volumetric heat capacity ratio, A = 1).
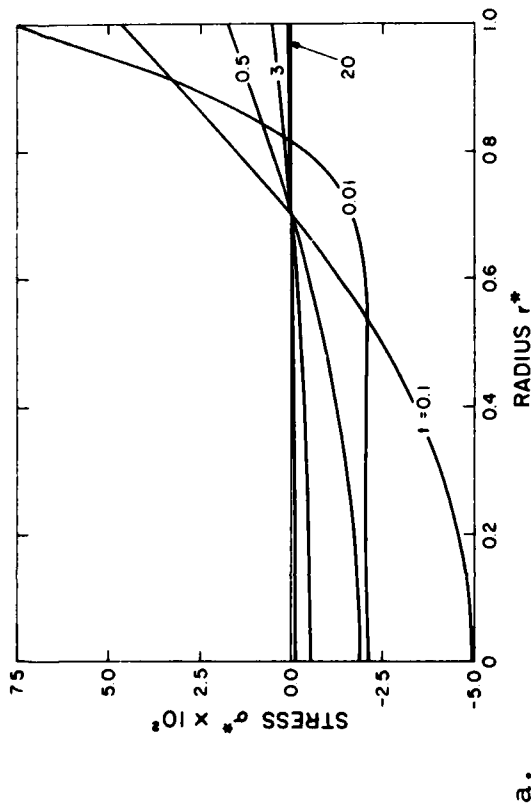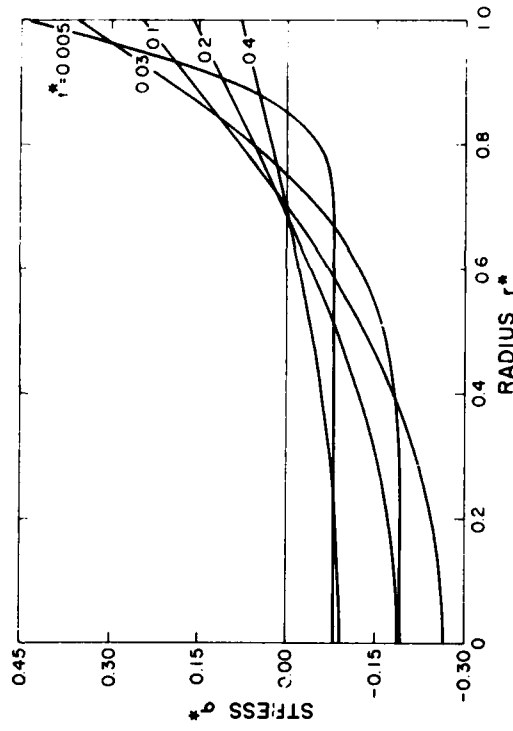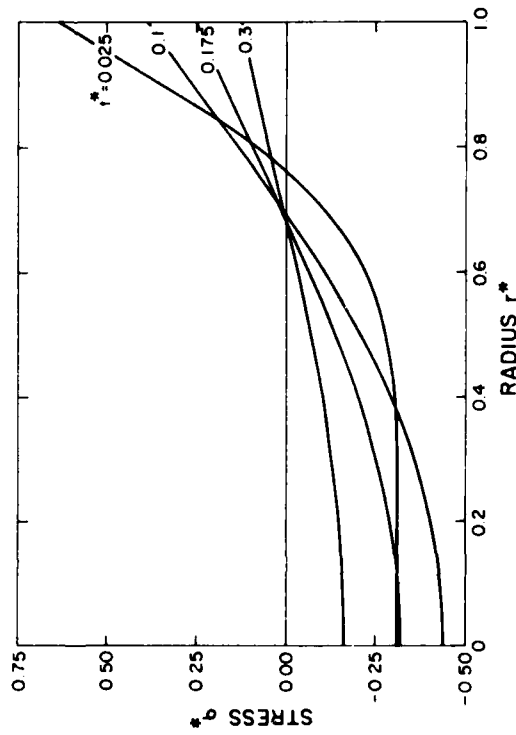
Fig. 2. Distribution of transient thermal stresses in solid circular cylinder subjected to thermal shock by quenching in liquid medium with conductive heat transfer for a range of values of time and thermal conductivity ratios: a, K = 100; b, K = 1 and c, K = 0.01. (Volumetric heat capacity ratio, A = 1).
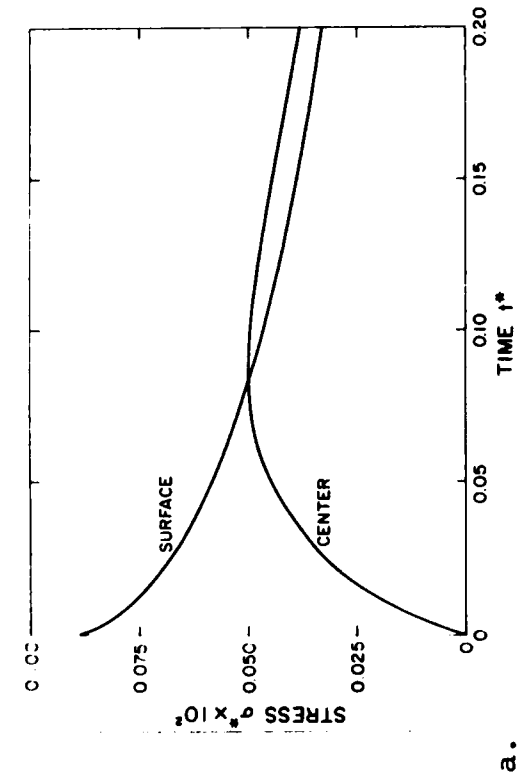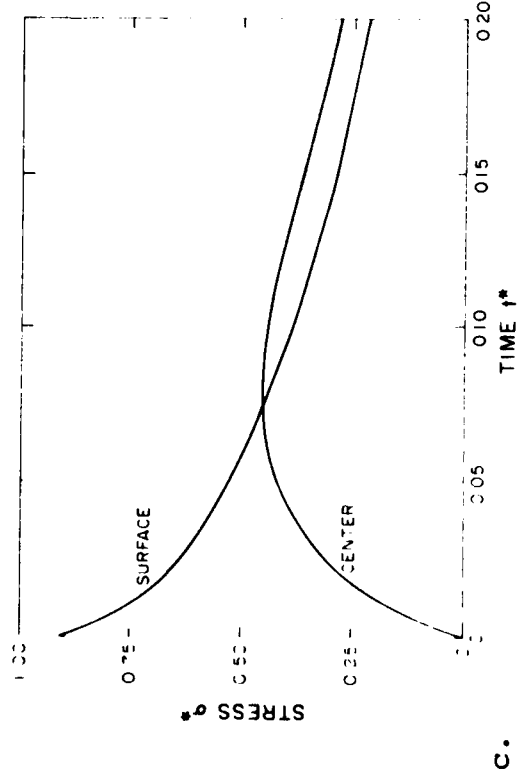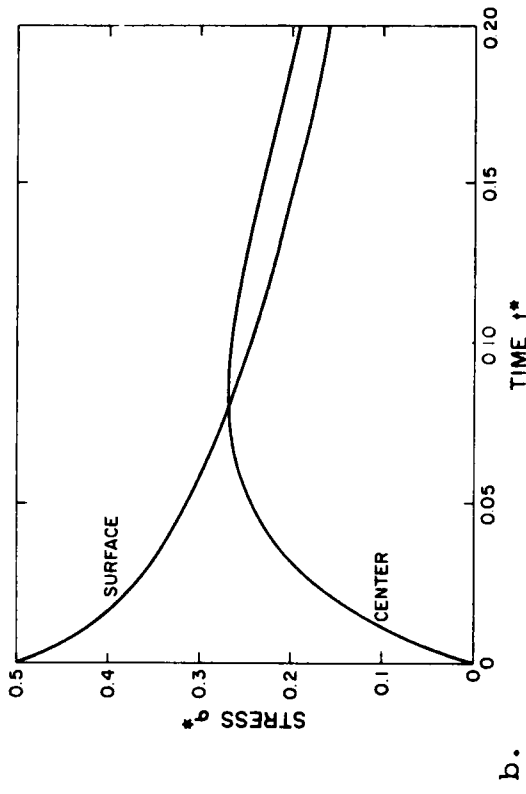
Fig. 3. Time dependence of stresses in surface and center in solid circular cylinder subjected to thermal shock by quenching into liquid medium with conductive heat transfer for values of the thermal conductivity ratio: a, K = 100; b, K = 1 and c, K = 0.01. (Volumetric heat capacity ratio, A = 1). (On cooling, stress is tensile in surface and compressive in center with the converse on heating).

b.

a.
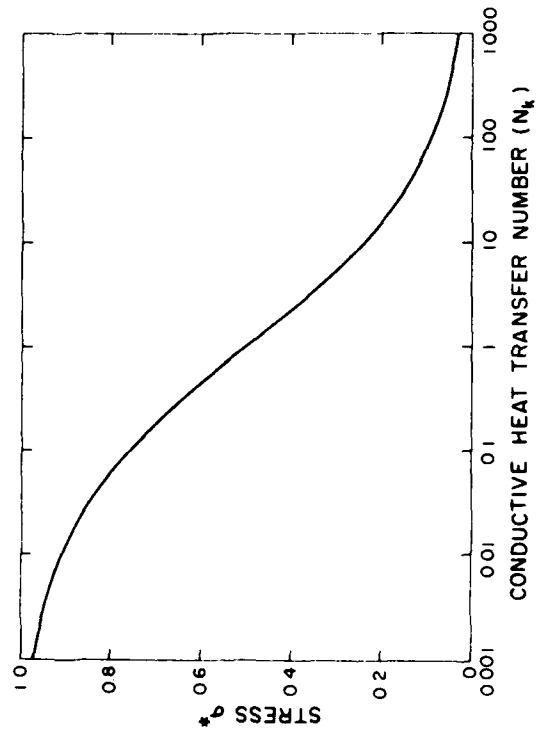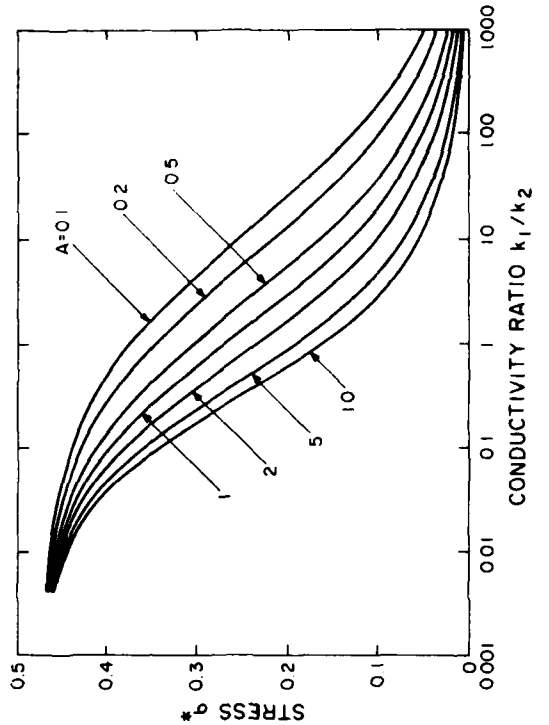
Fig. 4. Maximum stresses in: a, surface and b, center of a solid circular cylinder subjected by thermal shock by quenching into a liquid medium with conductive heat transfer. (A = ratio of volumetric heat capacity, $\rho_1 c_1 / \rho_2 c_2$).

Chapter IX

CRITERIA FOR THE THERMAL STRESS FAILURE

OF BRITTLE STRUCTURAL CERAMICS

by

D. P. H. Hasselman and J. P. Singh

Department of Materials Engineering
Virginia Polytechnic Institute and State University
Blacksburg, Virginia 24061 USA

TABLE OF CONTENTS

CONTENTS (CONT'D)

List of Symbols

A. Material Properties

α	–	coefficient of linear thermal expansion
$\Delta\alpha$	–	coefficient of thermal expansion mismatch
A	–	constant in $V = AK^n \exp(-Q/RT)$
c	–	specific heat
ε	–	emissivity ($\varepsilon = 1-r$)
E	–	Young's modulus
η	–	viscosity
G, γ	–	fracture surface energy
K	–	thermal conductivity
K_{Ic}	–	mode I critical stress intensity factor
K_{IIc}	–	mode II critical stress intensity factor
κ	–	thermal diffusivity
λ_o	–	cut-off wavelength for dielectric
n	–	constant in $V = AK_I^n \exp(-Q/RT)$
ν	–	Poisson's ratio
Q	–	activation energy for sub-critical crack growth
r	–	reflectivity ($r = 1-\varepsilon$)
ρ	–	density
σ_c	–	compressive strength
σ_t	–	tensile strength
μ	–	absorption coefficient

B. Environmental, geometric variables and physical constants

a — crack size

A — cross-sectional area of column

b — thickness of plate, column, radius of cylinder, sphere, spherical cavity or crack

β — Biot number, $\beta = bh/K$

C, C', c — geometric constants, neutral axis to outer fiber distance.

d — thickness of column

∇ — temperature gradient

∇_{max} — maximum temperature gradient

F_{λ_0} — fracture of total energy from black-body radiation below frequency, λ_0

H_{max} — maximum rate of internal heat generation

h — convective heat transfer coefficient

I — cross-sectional moment of inertia of column

K_I — mode I stress intensity factor

K_{Ii} — initial mode I stress intensity factor

K_{II} — mode II stress intensity factor

ℓ — crack half-length

L — length of column, rod

N — number of cracks per unit area or volume

N_f — number of cycles to failure

Q_{max} — maximum heat flux or flow, activation energy

$\dot{Q}_{max}$ — maximum rate of change of heat flux or flow

ρ — Stefan-Boltzmann constant

R — gas constant

σ — stress

T_{max} — maximum temperature of black-body radiation, maximum temperature reached during thermal cycle

B. Environmental, geometric variables and physical constants (continued)

ΔT_c -   critical temperature difference

ΔT_{max} -   maximum temperature difference

$\dot{\Delta T}_{max}$ -   maximum rate of change of ΔT_{max}

t -   time

t^* -   time-to-maximum stress

t_f -   time-to-failure

CRITERIA FOR THE THERMAL STRESS
FAILURE OF BRITTLE STRUCTURAL
CERAMICS

D.P.H. Hasselman and J.P. Singh

Department of Materials Engineering
Virginia Polytechnic Institute and
       State University
Blacksburg, Virginia 24061   USA

A survey is presented of the current understanding of the
response of brittle structural ceramic materials to thermal
stresses. The figures-of-merit available at this time for the
ceramic with optimum thermal stress resistance for a number
of thermal boundary conditions and failure criteria are
reviewed. These figures-of-merit include those for the
initiation of thermal stress fracture as well as those
appropriate for crack propagation and arrest. Experimental
data for a selection of brittle ceramics are presented
for purposes of illustration of a number of features of the
nature of thermal stress fracture of these materials.

INTRODUCTION

Structural materials for numerous applications encountered
in industry, aerospace and other areas of technology may be
required to provide satisfactory service at elevated tempera-
tures. Such applications include process vessels and crucibles
in the metal-working and chemical process industry, heat exchangers,
heat-regenerators or recuperators, components for energy-conversion

devices such as turbine engines, components or structure for high-speed aerospace purposes, and many others. In addition to high temperature, the materials used in many of the above applications also are subjected to corrosion, erosion and mechanical loads. Obviously, for long-term performance, the materials selected for these applications should exhibit high melting point, good corrosion and erosion resistance, excellent retention of load-bearing capability as well as resistance to creep at high temperature.

The only class of materials which can satisfy the above requirements is known as "structural ceramics". Such ceramic materials include the metal oxides, carbides, nitrides, silicides and similar compounds as well as carbon and graphite. The advantageous properties of these materials at high temperature basically derive from the high strength of the bond between the atoms. Such bonding usually is of ionic and/or covalent type. Most unfortunately, this type of atomic bonding also causes these ceramic materials to be exceedingly brittle. This brittleness introduces a great deal of difficulty in the manufacture and successful use of structural ceramics in those applications which require close design tolerances and high load-bearing requirements.

Structures or components which operate at elevated temperatures invariably will be subjected to transient or steady-state heat flow at some time during normal use. Such heat flow usually will involve non-linear temperature distributions which inevitably will give rise to thermal stresses. The combination of the relevant properties of structural ceramics (i.e., low thermal conductivity,

high Young's modulus) is such that these thermal stresses are of considerable magnitude. Because of the high degree of brittleness, these thermal stresses are not relieved by non-linear deformation. This behavior in combination with a low fracture stress renders structural ceramics highly susceptible to thermal stress failure. Furthermore, the extent of crack propagation, which frequently occurs in a highly unstable manner, can be very extensive. In extreme cases, the size of the cracks can exceed the dimensions of the structure or component. For this reason, thermal stress failure can be catastrophic, rendering the material completely incapable of continued satisfactory service. Such failure is demonstrated in Fig. 1, which shows a series of thermally shocked spherical test specimens of zirconium carbide with varying amounts of graphite dispersed phase. The specimen on the left which contains no graphite literally exploded on fracture. The presence of the graphite phase inhibited this mode of failure, although the initiation of fracture was not suppressed.

Such catastrophic thermal stress failure of brittle structural ceramics constitutes a major handicap in the successful design of components or structures intended for high-temperature operation. It is ironic that the very class of structural materials, which in view of a combination of very excellent properties is most eminently suited for high-temperature use, is most susceptible to catastrophic thermal stress failure.

For these reasons, the development, design and selection of materials for high-temperature application requires a great deal of care. The role of the pertinent material properties and other

Fig. 1.   Catastrophic thermal stress fracture in sphere
          of zirconium carbide (left).   Other spheres
          contain a dispersed phase of graphite, which
          inhibits unstable mode of crack propagation
          (for additional details, the reader is referred
          to reference [1]).

variables which affect the magnitude of thermal stress in any specific heat flow environment must be well understood, both qualitatively as well as quantitatively. All possible modes of failure must be considered. Furthermore, a detailed understanding of the factors which control crack propagation following the initiation of fracture is essential for predicting service performance following thermal stress failure.

The purpose of this paper is to present the state-of-the-art understanding of the thermal stress failure of brittle structural ceramics. The point of view of the materials engineer or scientist responsible for the ceramics with optimum thermal stress resistance is emphasized. The underlying thermo-elastic theory is covered by other studies of this series. Much of the experimental work in the area of thermal stress fracture of brittle structural materials was done under poorl defined heat transfer conditions. For this reason, no exhaustive review of these results will be presented. Instead, for the purpose of clarity and convenience of the more theoretically oriented reader of this series only those experimental data which will illustrate a particular phenomenon of thermal failure will be presented.

CRITERIA FOR OPTIMUM THERMAL STRESS RESISTANCE

General

At this time the selection of materials with optimum thermal stress resistance is based on two distinctly different (as will be shown) criteria.

The first criterion is based on the objective that the magnitude of thermal stress relative to the failure stress be reduced as much as possible. In other words, the basic premise of this criterion is to avoid the initiation of fracture. On the basis of this

criterion, appropriate selection rules for materials with optimum thermal stress resistance can be developed. For this purpose, simple expressions for the maximum heat transfer conditions based on the most simplifying assumptions were derived to indicate the relative role of the pertinent material properties in governing thermal stress resistance. From these expressions appropriate figures-of-merit expressed in terms of these material properties then form the basis for comparison for the relative thermal stress resistance of candidate materials for a specific application. Critical to note is that the derivation of such figures-of-merit should not be regarded as design calculations which is so only for the most simple case.

In view of the high susceptibility of brittle structural ceramics to catastrophic thermal stress failure, the derivation of such figures-of-merit for optimum thermal stress resistance appears to have received greater attention for purpose of high-temperature technology than in other fields of science or engineering. In this respect, then, one of the major objectives of this paper is to review the thermal stress figures-of-merit derived to date.

The above approach in which the thermal stresses are kept as small as possible relative to the failure stress (or alternatively: the stress intensity factor is kept below the critical stress intensity factor) is common practice in the area of structural engineering. Most, if not all, readers of this paper should have no reason to take issue with this criterion. In practice, however, materials can be subjected to thermal stresses which can be an order-of-magnitude or more above the stress required for fracture. Clearly, under such conditions the initiation of failure cannot be avoided. Order-of-

magnitude improvements in the failure stress of brittle materials at the current state of technology is not expected within the near or even distant future. At first sight, then, it appears that in terms of conventional engineering practice no solutions for conditions of excessive thermal stresses appear to be available.

Nevertheless, a solution, believed to be unique to high temperature technology, is based on the criterion that since the initiation of fracture cannot be avoided, the resulting crack propagation should be limited as much as possible. Basically this criterion relies on the arrest of cracks after the onset of propagation and is commonly used in so-called "refractory practice". Refractories are the type of materials used as linings of blast-furnaces, kilns, thermal storage units, and other large structures which must operate at elevated temperature for long duration and for many of which heat insulation is a critical aspect of their performance.

The latter criterion also can be used to derive appropriate figures-of-merit. These, of course, because of their basically different foundation are expected to differ from those derived from the criterion that the initiation of thermal fracture must be avoided. In this respect, then, the second objective of this paper is to present the state-of-the-art understanding of the material properties and other variables which control crack arrest during thermal stress failure. In the view of these writers, this latter problem represents the most promising area for further theoretical work.

DERIVATION OF FIGURES-OF-MERIT

General Approach

The major objective of the derivation of figures-of-merit is to establish the role of the pertinent material properties which affect thermal stress failure and to develop appropriate rules for the selection of candidate materials with optimum thermal stress resistance for a particular thermal environment, mode of heat transfer and failure. Since such derivations are not made for design purposes, they can be based on the most simplifying assumptions, geometries and boundary conditions. All material properties will be assumed to be independent of temperature and position within the material. With one exception, linear elastic behavior till fracture will be assumed throughout. Since the geometry does not affect the relative role of the material properties for any given thermal environment, the appropriate figure-of-merit will be given for a single geometry only, in order to avoid redundancy. Poisson's ratio generally plays a lesser role in establishing the magnitude of thermal stress than other material properties as it usually occurs in factors of the form $(1-\nu)$ or $(1-2\nu)$. For this reason, again, to avoid redundancy, a single expression involving Poisson's ratio will be given for any given thermal environment and failure criterion.

Brittle structural materials generally exhibit a ratio of tensile-to-compressive failure stress equal to an order of magnitude or so. For this reason, thermal stress failure far more

likely will occur under the influence of a tensile thermal stress than by the compressive thermal stresses. Such tensile failure will be assumed throughout with the exception of the case of external constraints, which result in a compressive thermal stress only. For the figures-of-merit for limited crack propagation, the derivation will be based on either mode I tensile or mode II shear crack-opening.

The general approach taken in the development of a specific figure-of-merit for a given heat transfer condition and mode of failure, is to derive or obtain from the literature the appropriate expression for the thermal stresses in terms of the relevant parameters such as geometry, size and boundary conditions. These latter can include the rate of heating, magnitude of heat flux and many others. The maximum value of thermal stress should not exceed the failure stress (such as the tensile strength). By substitution of this latter value for the maximum stress, followed by rearrangement, an expression is obtained for the maximum thermal conditions (i.e., maximum rate of heating) to which the material can be subjected without fracture. Implicit in such an approach is the assumption that the safety factor equals unity. For higher values of the safety factor, the appropriate expression can be obtained by a simple division.

In the final expressions which have appeared in the literature, the relevant material properties and other parameters such as geometry and dimensions usually are uncoupled; this permits the easy extraction of the appropriate figure-of-merit. For the

convenience of the reader and to keep this report within reason-
able size, the final expression for the maximum thermal condition
will be given together with the appropriate literature reference
if available. For those cases which involve more complex materi-
als-related phenomena such as sub-critical crack growth and
others, with which some of the readers may not be fully familiar,
a brief explanation will be given as well.

The above assumptions and approach permit expressing the
figures-of-merit in simple analytical form. For those cases
where the stress depends non-linearly on some relevant parameter
(as in the case for the dependence of the thermal stress on
optical thickness of partially transparent materials subjected to
radiation heating) limiting conditions are selected such that the
figure-of-merit can be expressed in simple algebraic form. For
the more general case, the reader is referred to the original
study. For the thermal conditions and failure criteria, figures-
of-merit derived and reported in the literature are listed
below.

Figures-of-Merit for the Resistance to the Initiation of Thermal Stress Fracture

A. Uniform temperature or steady-state heat flow

Case 1. Flat plate at uniform temperature constrained from in-plane
expansion.

The flat plate initially stress-free is at uniform tempera-
ture and is prevented from thermal expansion by rigid constraints
at the edges of the plate. The plate will be considered to be
sufficiently thick so that failure due to elastic instability

(i.e., thermal buckling) is avoided. The plate undergoes a uniform temperature change ΔT. For a positive coefficient of thermal expansion (as is usually the case for most materials) the stresses in the plate will be tensile or compressive depending on whether ΔT is negative or positive. The maximum value of ΔT to which the plate can be subjected is:

$$\Delta T_{max} = \sigma_t(1-\nu)/\alpha E \qquad \text{cooling} \qquad (1a)$$

$$\Delta T_{max} = \sigma_c(1-\nu)/\alpha E \qquad \text{heating} \qquad (1b)$$

ΔT_{max} of eqs. 1a and 1b is independent of the size of the plate and has a geometric constant equal to unity.

The appropriate figures-of-merit are:

$$\sigma_t(1-\nu)/\alpha E \qquad \text{and} \qquad \sigma_c(1-\nu)/\alpha E \qquad (1c)$$

For a uniaxial or triaxial constraint the term $(1-\nu)$ in eq. 1c is replaced by unity and $(1-2\nu)$, respectively.

Case 2. Composite structures.

High levels of thermal stress even under isothermal conditions can be generated in composites and structures composed of strongly bonded dissimilar materials with mismatches in their coefficients of thermal expansion. Such a composite or structure will be stress-free only at the temperature at which the materials which constitute the composite or structure were fabricated or joined. A change from this value of temperature creates thermal stress, as each individual material is prevented from free expansion by the other material(s). Such stresses usually are

undesirable, with the possible exception of the bi-metallic strip for which the resulting deformation can be used to advantage for the operation of a thermostat.

A simple expression can be given for the stresses which result from a mismatch in the coefficients of thermal expansion for a composite structure consisting of a thin coating on an underlying thick substrate. The magnitude of the stresses in the coating equals [2]:

$$\sigma = E\Delta\alpha\Delta T/(1-\nu) \tag{2a}$$

where $\Delta\alpha$ is the difference in the coefficients of thermal expansion of the substrate and the coating and ΔT is the difference in temperature at which the coating was joined to the substrate and the new temperature to which the composite is heated or cooled. For other composite structures such as inclusions [3,4] and concentric rings or cylinders, the expressions for the stresses which result from a mismatch in the coefficients of thermal expansion are more complex and involve the elastic properties of all individual components or materials. Regardless of the geometry, however, the magnitude of these stresses is proportional to the quantities $\Delta\alpha$ and ΔT and can be negative or positive depending on the sign of $\Delta\alpha$ and ΔT.

For failure in tension, eq. 2a can be rearranged to yield the maximum temperature difference to which the coating and sub-strate can be subjected:

$$\Delta T_{max} = \sigma_t(1-\nu)/(\Delta\alpha)E \tag{2b}$$

Because ΔT_{max} of eq. 2b is independent of size, the appropriate figure-of-merit for this case of thermal stress failure is identical to ΔT_{max}.

Case 3. Concentric hollow cylinder. Radially outward steady-state
heat flow.

The concentric hollow cylinder infinite in extent with inner
and outer radius of a and b, respectively, is subjected to radi-
ally outward heat flow. This results in a radial distribution of
temperature with a temperature difference ΔT between the inner
and outer surfaces. The cylinder is not constrained externally.
From the solutions of Timoshenko and Goodier [5], the maximum
value of temperature difference (ΔT_{max}) across the cylinder wall
which can be permitted is:

$$\Delta T_{max} = \frac{\sigma_t (1-\nu)}{\alpha E}\left[2\ln\left(\frac{b}{a}\right)\right]\left[1 - \frac{2a^2}{b^2-a^2}\ln\left(\frac{b}{a}\right)\right]^{-1} \tag{3a}$$

By noting that the heat flux, q per unit length of the cyl-
inder can be related to the temperature difference ΔT across the
wall by:

$$q = 2\pi K\Delta T/\ln(b/a) \tag{3b}$$

where K is the thermal conductivity, eq. 3a for ΔT_{max} can be
rearranged to yield an expression for the maximum heat
flux per unit length, q_{max}, to which the cylinder can be subjected
given by:

$$q_{max} = \frac{4\pi\sigma_t (1-\nu) K}{\alpha E}\left[1 - \frac{2a^2}{b^2-a^2}\ln\left(\frac{b}{a}\right)\right]^{-1} \tag{3c}$$

For a cylinder of finite length, the tensile stresses exhi-
bit their maximum value at the end of the cylinder in the tangen-
tial direction. The appropriate values of ΔT_{max} and q_{max} can be
obtained by dividing eqs. 3a and 3c by [6]:

$$\left[1 + \frac{(1 - \nu^2)^{\frac{1}{2}}}{\sqrt{3}} - \nu\right] \tag{3d}$$

The figures-of-merit for ΔT_{max} and q_{max} of eqs. 3a and 3c are:

$$\sigma_t (1-\nu)/\alpha E \quad \text{and} \quad \sigma_t (1-\nu) K/\alpha E \tag{3e}$$

Case 4. Uniform internal heat generation.

Thermal stresses of high magnitude can be caused by the non-uniform temperature distributions resulting from internal heat generation. This occurs, for instance, in such components as nuclear fuel elements, and in materials subjected to micro-wave heating, nuclear or solar radiation.

For steady-state, spatially uniform internal heat genera-tion, the role of material properties can be obtained from the solutions for a solid circular cylinder [7]. The maximum rate of internal heat generation per unit volume (H_{max}) which can be withstood is:

$$H_{max} = 8\sigma_t (1-\nu) K/\alpha E b^2 \tag{4a}$$

with the corresponding figure-of-merit:

$$\sigma_t (1-\nu) K/\alpha E \tag{4b}$$

Eq. 4a indicates that in order to reduce the possibility of tensile thermal fracture, the cylinder radius (b) should be kept as small as possible.

Case 5. Thermal discontinuities.

Steady-state heat flow in materials with a linear tempera-ture distribution and absence of external constraints will result

in zero thermal stress. If, however, such materials contain inclusions with heat conduction properties different from the matrix materials, the temperature field near these inclusions will be disturbed to be non-linear. This, as indicated by Florence and Goodier [8] for a spherical cavity and by Tauchert [9] for a general inclusion, will result in a thermal stress field in the immediate vicinity around the inclusion. From the solution for the spherical cavity, the maximum temperature gradient which can be imposed without incurring the risk of tensile failure, can be derived:

$$\nabla_{max} = 2\sigma_t(1-\nu)/\alpha E b \tag{5a}$$

where ∇ is the temperature gradient in the absence of the cavity and b is the cavity radius.

The heat flux (q) can be related to the temperature gradient by: $q = K\nabla$. Accordingly, eq. 5a can be rewritten in terms of the maximum allowable heat flux, q_{max}:

$$q_{max} = 2\sigma_t K(1-\nu)/\alpha E b \tag{5b}$$

Eqs. 5a and 5b yield the figures-of-merit:

$$\sigma_t(1-\nu)/\alpha E \quad \text{and} \quad \sigma_t K(1-\nu)/\alpha E \tag{5c}$$

Case 6. Thermal buckling. Straight column with uniform temperature.

From the solutions of Fridman [10], and Burgemeister and Stuep [11], the critical temperature difference (ΔT_c) required for thermoelastic instability can be expressed as:

$$\Delta T_c = C_1 \pi^2 I/L^2 \alpha A \tag{6a}$$

where I is the cross-sectional moment of inertia, L is the length of the column, α is the coefficient of thermal expansion and A is the cross-sectional area.

The value of the constant C_1 depends on the boundary conditions and is equal to unity for a column for which both ends are free to rotate. For a column where the ends are not permitted to rotate the value of C_1 is 4.0 and for a column with one end free and the other end restrained from rotation its value is 0.25.

Eq. 6a reveals that the critical temperature difference is an inverse function of the coefficient of thermal expansion only. A thermal buckling resistance figure-of-merit can be defined as:

$$\alpha^{-1} \tag{6b}$$

Case 7. Post-thermal buckling. Straight column at uniform temperature.

When the temperature rise in a straight column with ends free to rotate exceeds the critical temperature ΔT_c, it does not fail immediately, but exhibits post-thermal buckling analyzed by Boley and Weiner [12]. It will fail only when the maximum bending stresses in the column exceed the tensile strength. Under this condition, the maximum temperature difference, ΔT_c over which a column with square cross-section can be heated, is given by [13]:

$$\Delta T_{max} = \Delta T_c + \sigma_t^2 L^2 / \pi^2 \alpha E^2 d^2 \tag{7a}$$

Eq. 7a suggests the post-thermal buckling figure-of-merit:

$$\sigma_t^2 / \alpha E^2 \tag{7b}$$

B. Transient heat flow

Case 8. Convective Newtonian heat transfer. Instantaneous change in ambient temperature.

An infinitely long solid circular cylinder initially at thermal equilibrium is subjected to an instantaneous change ΔT in ambient temperature under conditions of Newtonian convective heat transfer. Under these conditions the maximum tensile stress occurs at the surface of the cylinder.

From the solutions of Jaeger [14] and Manson and Smith [15] the maximum change ΔT_{max} in ambient temperature for a range in values of the Biot number $0 < \beta \leq 10$ to a good approximation can be expressed:

$$\Delta T_{max} = \frac{1.45\sigma_t(1-\nu)}{\alpha E}(1 + 3.41/\beta) \tag{8a}$$

where $\beta = Rh/K$ with R being the radius, h the heat transfer coefficient and K the thermal conductivity.

Eq. 8a indicates that the relative effect of the Biot number on ΔT_{max} is a function of its magnitude.

For $3.41/\beta << 1$ eq. 8a becomes:

$$\Delta T_{max} \simeq 1.45\sigma_t(1-\nu)/\alpha E \tag{8b}$$

Similarly for $3.41/\beta << 1$, eq. 8a becomes

$$\Delta T_{max} \simeq 4.95\sigma_t(1-\nu)K/\alpha Ebh \tag{8c}$$

Eqs. 8b and 8c suggest the figures-of-merit:

$$\sigma_t(1-\nu)/\alpha E \qquad ; \qquad \sigma_t(1-\nu)K/\alpha E \tag{8d}$$

The relative influence of the above figures-of-merit on ΔT_{max} depends on the magnitude of the Biot number.

Case 9. Controlled rate of heating.

An infinite flat plate is asymmetrically cooled by a constant rate ($\dot{T}$) of surface temperature. From the solutions of Buessum [16] the maximum rate of cooling so that tensile fracture can be avoided is:

$$\dot{T}_{max} = 3\sigma_t(1-\nu)\kappa/\alpha Eb^2 \tag{9a}$$

where b is the half-thickness of the plate, and κ is the thermal diffusivity.

Eq. 9a yields the figure-of-merit:

$$\sigma_t(1-\nu)\kappa/\alpha E \tag{9b}$$

Radiative Heat Transfer

Case 10. Opaque materials.

A solid sphere initially at thermal equilibrium at low temperature is suddenly subjected to black-body radiation at temperature T. If thermal stress fracture occurs for surface temperatures of the sphere low enough that emitted radiation can be neglected, the solutions of Hasselman [17] show that the maximum radiative heat flux q_{max} the sphere can be subjected to is:

$$q_{max} = 5\sigma_t(1-\nu)K/\alpha E\epsilon b \tag{10a}$$

where b is the radius of the sphere and $\epsilon = 1-r$ where r is the reflectivity.

Eq. 10a can be rewritten in terms of the maximum radiation temperature, T_{max} to which the sphere can be subjected.

$$q_{max} = \rho(T_{max}^4 - T^4) \tag{10b}$$

where T is the surface temperature of the sphere and ρ is the Stefan-Boltzmann constant.

For $T_{max} >> T$:

$$q_{max} \approx \rho T_{max}^4 \tag{10c}$$

Substitution of eq. 10c for q_{max} in eq. 10a followed by rearrangement yields:

$$T_{max} = (5/\rho b)^{1/4} \{\sigma_t(1-\nu)K/\alpha E\epsilon\}^{1/4} \tag{10d}$$

Equations 10a and 10d yield the figures-of-merit:

$$\sigma_t(1-\nu)K/\alpha E\epsilon \quad ; \quad \{\sigma_t(1-\nu)K/\alpha E\epsilon\}^{1/4} \tag{10e}$$

Case 11.   Semi-transparent materials.

The material is assumed to be completely transparent below a value of wavelength (λ_o) and totally opaque above this wavelength [18]. Thermal stresses will arise only for radiative heat transfer with wavelength $\lambda \geq \lambda_o$. Solution for q_{max} and T_{max} can be obtained from the earlier example of a totally opaque sphere initially at low temperature suddenly subjected to black-body radiation:

$$q_{max} = 5\sigma_t(1-\nu)K/\alpha E\epsilon b(1-F_{\lambda_o}) \tag{11a}$$

and

$$T_{max} = \{5\sigma_t(1-\nu)K\}^{1/4}/\{\alpha E\epsilon b\rho(1-F_{\lambda_o})\}^{1/4} \tag{11b}$$

where F_{λ_o} is the fraction of energy in the black-body spectrum for $\lambda \leq \lambda_o$.

Eqs. 11a and 11b lead to the figures-of-merit:

$$\sigma_t(1-\nu)K/\alpha E\epsilon(1-F_{\lambda_o}) \quad ; \quad \{\sigma_t(1-\nu)K/\alpha E\epsilon(1-F_{\lambda_o})\}^{1/4} \qquad (11c)$$

Semi-absorbing materials.

Radiative heat transfer is considered which penetrates into a material with an intensity (q) as a function of depth of penetration (x) given by:

$$q = q_o\epsilon \ \exp(-\mu x) \qquad (12a)$$

where q_o is the intensity of the incoming radiation, $\epsilon = 1-r$ where r is the reflectivity and μ is the absorption coefficient. The resulting spatially non-uniform internal heat generation gives rise to thermal stress. Solutions for the magnitude of these stresses were obtained in a number of studies [19-21] specifically for an infinite flat plate originally at thermal equilibrium subjected simultaneously to normally incident thermal radiation and cooled by Newtonian convection. Temperatures were considered to remain low enough that re-emitted radiation over the total thermal history was negligible compared to the intensity of the incoming radiation.

Appropriate figures-of-merit of simple analytical form were derived for the limiting conditions of the heat transfer coefficient h = 0, ∞ and optical thickness, $\mu a \to 0$, ∞ (where a is the plate half-thickness) under conditions at which the plate has reached thermal eqiuilbrium after long-term radiation.

Case 12. Asymmetric heating and cooling. h= 0; $\mu a \to \infty$.

The maximum heat flux (q_{max}) to which the plate can be subjected in order to avoid tensile failure:

$$q_{max} = 12\sigma_t(1-\nu)K/\alpha E\epsilon a \tag{12b}$$

Case 13. Asymmetric heating and cooling. h = 0; $\mu a \to 0$

$$q_{max} = \sigma_t(1-\nu)K/\alpha E\epsilon\mu a^2 \tag{13a}$$

Case 14. Asymmetric heating and cooling. h = ∞; $\mu a \to 0$.

$$q_{max} = \frac{3.677\sigma_t(1-\nu)K}{\alpha E\epsilon\mu a^2} \tag{14a}$$

Case 15. Symmetric heating and cooling. h = 0; $\mu a \to \infty$

$$q_{max} = 6\sigma_t(1-\nu)K/\alpha E\epsilon a \tag{15a}$$

Case 16. Symmetric heating and cooling. h = 0; $\mu a \to 0$.

$$q_{max} = 180\sigma_t(1-\nu)K/7\alpha E\epsilon\mu^3 a^4 \tag{16a}$$

Eqs. 12b thru 16a yield the figures-of-merit,

$$\sigma_t(1-\nu)K/\alpha E\epsilon \quad ; \quad \sigma_t(1-\nu)K/\alpha E\epsilon\mu^3 \quad ; \quad \sigma_t(1-\nu)K/\alpha E\epsilon\mu$$

C.   Time-to-failure

In practice, situations can be encountered in which the time period required for satisfactory performance is of the order of the period of time required for the thermal stresses under transient heat transfer conditions to rise to their maximum value. This is the case, for instance, for components of aerospace structures, with a time of performance on the order of seconds. If thermal stress fracture does not occur over the time period over which this component is expected to provide satisfactory service, it is considered to be safe even at longer values of time.

Case 17.   Sphere subjected to an instantaneous rise in temperature.

The time period (t^*) required for the tensile thermal stresses at the center of the sphere to reach their maximum value as calculated by Gruenberg [22] is given by:

$$t^* = 0.0574 \ b^2/\kappa \tag{17a}$$

where b is the sphere radius. Eq. 17a indicates that the time of maximum stress is an inverse function of the thermal diffusivity. This latter statement is generally true for thermal stresses encountered in convective heat transfer involving an instantaneous change in ambient temperature. For these conditions, the magnitude of maximum stress is uniquely defined by the value of the Biot number [12,14]. However, the actual time period required for the stresses to reach a prescribed value is an inverse function of the thermal diffusivity. Accordingly, the figure-of-merit appropriate for having large times-to-failure is

defined by:

$$\kappa^{-1} \tag{17b}$$

D. Thermoviscoelastic stress relaxation

Under conditions of mechanical stress, materials can exhibit slow deformation by creep. Such creep deformation also is expected to occur under conditions of thermal stress. Ceramic materials will exhibit creep by diffusional processes at levels of temperature at which vacancy concentrations and mobility become appreciable. These temperatures correspond to about one half to two thirds of the melting point of the material.

Creep deformation under conditions of thermal stress generally is favorable as it leads to stress relaxation. For this reason, the occurrence of creep reduces the probability of failure by thermal stresses. The magnitude of thermal stresses due to external constraints will decrease with increasing time. Therefore, thermal stress relaxation by creep leads to an increase in the thermal condition (i.e., ΔT_{max}, q_{max}, etc.) to which a material can be subjected without thermal stress failure, to a value greater than if no stress relaxation occurred.

In general, the higher the creep rate, the more rapidly thermal stress relaxation will occur, with a corresponding greater thermal stress resistance. The derivation of analytical expressions for the magnitude of thermal stress affected by creep is highly complex, if possible at all. In general, the kinetics of creep is a function of the temperature as well as stress. For this reason, in a body subjected to non-isothermal conditions,

thermal stress relaxation can occur by a multitude of mechanisms. Complex numerical methods based on finite element principles are required for such calculations (Poritsky and Fend [23]). For these reasons, derivations of expressions for the purposes of obtaining figures-of-merit for thermal stress relaxation in general cannot be obtained unless grossly simplifying assumptions are introduced. Even then, such an analysis should be limited to steady-state heat flow.

In such an analytical study [24], it was noted that the rate of creep in a thermally stressed structure corresponding to the stress at the position of lowest temperature represents a lower bound on the rate of thermal stress relaxation. This concept was applied to a hollow circular cylinder undergoing steady-state heat flow, treated earlier. It was pointed out that as thermal stress relaxation occurred, the values of the maximum temperature difference or heat flux across the wall could be increased, at a rate such that the maximum value of tensile thermal stress remained constant.

Case 18. Hollow cylinder. Radial outward heat flow.

The maximum rate of rise of the temperature difference $(\Delta \dot{T})_{max}$ across the cylinder wall for a ceramic material undergoing linear creep was derived to be [24]:

$$(\Delta \dot{T})_{max} = \sigma_t (1-\nu)/C\alpha\eta \tag{18a}$$

where η is the effective viscosity which relates the creep rate $(\dot{\varepsilon})$ to the stress by $\dot{\varepsilon} = \sigma/\eta$ and

$$C = [2\ln(\frac{b}{a})]^{-1}[1 - \frac{2a^2}{b^2-a^2}\ln(\frac{b}{a})] \tag{18b}$$

Similarly, the heat flux per unit length can be increased at a rate:

$$\dot{q}_{max} = \sigma_t (1-\nu) K / C' \alpha \eta \qquad (18c)$$

where

$$C' = [1 - \frac{2a^2}{b^2-a^2} \ln \frac{b}{a}]/4\pi \qquad (18d)$$

Eqs. 18a and 18c suggest that materials which exhibit maximum thermal stress relaxation should be selected on the basis of the figures-of-merit:

$$\frac{\sigma_t (1-\nu)}{\alpha \eta} \quad \text{and} \quad \frac{\sigma_t (1-\nu) K}{\alpha \eta} \qquad (18e)$$

Important to note is that equations 18a and 18c represent lower bounds on the rate of rise of ΔT_{max} or q_{max}. As time progresses and the changes in ΔT and q involve changes in the absolute temperature, these rates can be modified. Also, critical to note is that thermal stress relaxation under non-isothermal conditions can lead to the generation of residual stresses of magnitude comparable to the original thermal stress whenever conditions of thermal equilibrium are achieved on cessation of the flow of heat.

E. Thermal Fatigue

Brittle ceramic materials under conditions of static or cyclic stress can exhibit the growth of cracks at levels of stress intensity factor below the critical stress intensity factor

(i.e., for $K_I < K_{Ic}$). This phenomenon is referred to as sub-critical crack growth. If for a given stress value or history, the total extent of crack growth is sufficient for the crack to become critical, failure will ensue. For constant or cyclic stress, this mode of failure is referred to as static or cyclic fatigue, respectively.

Subcritical crack growth can also occur under conditions of steady-state or cyclic thermal stress. The resulting failure is referred to as "thermal fatigue". Such fatigue behavior can be predicted from fracture-mechanical principles. Basically, this methodology requires a knowledge of the size and geometry of the propagating crack, the kinetics of crack growth as well as the stress and temperature history to which the material is being subjected. In principle, with this information, the time or number of cycles required for the propagating crack to become critical (i.e., the time to failure) can be calculated for any stress and temperature history.

Case 19. Steady-state heat flow.

An expression for the time to failure under conditions of a constant thermal stress was derived [25] as follows:

The time-to-failure (t_f) for a brittle material subjected to a constant tensile stress (σ) is given by [26].

$$t_f = [2/\sigma^2 Y^2 \int_{K_{Ii}}^{K_{Ic}} [K_I dK_I / V] \tag{19a}$$

where Y is a geometric constant which relates the value of tensile stress to the mode I stress intensity factor, K_I by:

$$K_I = \sigma Y a^{1/2} \tag{19b}$$

where a is the crack size. $K_{Ii} = K_I(t = 0)$ and V is the crack
velocity which for many brittle materials can be expressed
as:

$$V = AK_I^n \exp (-Q/RT) \tag{19c}$$

where A and n are constants and Q is the activation energy for
the particular mechanism responsible for the crack growth.
An expression for the thermal stresses can be assumed to take the form:

$$\sigma = C\alpha E\Delta T/(1-\nu) \tag{19d}$$

where C is a geometric constant. For instance, for a hollow
circular cylinder subjected to steady-state radial heat flow,
the quantity C is given by eq. 3a presented in an earlier section
of this report.

Substitution of eq. 19d into eq. 19a and assuming that
$K_{Ii} << K_{Ic}$, where $K_{Ii} = K_I$ at t=0 results in:

$$t_f = 2(1-\nu)^n \exp (Q/RT)/[C\alpha E\Delta TY]^n A(n-2)a_i^{(n-2)/2} \tag{19e}$$

where $a_i = a$ at $t = 0$.

Eq. 19a can be rewritten in terms of the time-to-failure at
a given level of heat flux (q) by using the relation $q = C_1 K\Delta T$
where C_1 is another constant and K is the thermal conductivity.
This yields:

$$t_f = 2(1-\nu)^n C_1^n K^n \exp (Q/RT)/C\alpha EqY)^n A(n-2)a_i^{(n-2)/2} \tag{19f}$$

The appropriate thermal fatigue figures-of-merit can be obtained from eqs. 19e and 19f by the deletion of the constant C and C_1, ΔT and q, respectively.

One should be careful to note that the above approach is based on the implicit assumption that the thermal stress intensity factor can be calculated from the value of thermal stress obtained from thermoelastic principles for a continuum and the crack size and geometry as given by eq. 19b. This assumption is expected to lead to reliable results as long as the crack size is small (say $\leq$ 1%) relative to the size of the component or structure which is the case for high-strength structural ceramics. For crack sizes, however, which are an appreciable fraction of the body size, the above approach will lead to an over-estimate of the thermal stress intensity factor, due to the effect of the crack on the effective compliance. As will be shown later, this effect is very critical for the promotion of crack arrest. Such dependence can be established by analytical or numerical techniques as those employed by Stahn et al [27,28], Stern [29] and Emery and co-workers [30,31]. Since the present approach neglects the effect of the crack on the compliance, the expressions for the time-to-failure, in fact, are conservative.

Case 20. Cyclic temperature variation.

The prediction of thermal fatigue behavior under conditions of cyclic temperature variation is far more complex than for steady-state heat flow. Under cyclic conditions, both the stresses as well as the temperature vary continuously as governed by the mode of heat transfer, geometry and other variables.

The magnitude of absolute temperatures encountered is very critical in view of the thermally activated nature of sub-critical crack growth. For these reasons, the prediction of thermal fatigue under cyclic conditions is most conveniently performed by the numerical integration of eq. 19a. This method was followed successfully in a number of earlier studies, as will be indicated later in the section of experimental results. Such numerical integration, however, does not give a direct feel to the materials engineer for the relative role of the material properties and could handicap an intelligent choice of the candidate material with optimum thermal fatigue resistance for any given application.

A semi-empirical equation based on eq. 19a was proposed [32] for the number of cycles (N) required for failure of a solid circular cylinder under conditions of cyclic change in ambient temperature involving Newtonian convective heating and cooling. Sub-critical crack growth was assumed prominent during the cooling cycle. The cylinder was assumed to have attained thermal equilibrium between cycles. The number of cycles to failure (N) is:

$$N = \frac{C\kappa \, (\exp \, Q/RT_{max})}{A\sigma_{max}^2 R^2 Y^2 (n-2) K_{Ii}^{(n-2)}} \tag{20a}$$

where C is a constant to be evaluated by numerical integration of eq. 19a. T_{max} is the maximum temperature encountered by the material, which in this case is the higher of the two temperatures between which the cylinder is being cycled. σ_{max} is the maximum value of tensile thermal stress encountered in the cylinder

during the cooling part of the cycle. K_{Ii} is the maximum

value of mode I stress intensity factor during the first cycle:

$$K_{Ii} = \sigma_{max} Y a_i^{1/2} \qquad (20b)$$

where a_i is the initial crack size.

Substitution of eq. 20b into eq. 20a yields:

$$N = \frac{C\kappa \, \exp(Q/RT_{max})}{AR^2 \sigma_{max}^n \, Y^n (n-2) a_i^{(n-2)/2}} \qquad (20c)$$

with σ_{max} for a solid circular cylinder (see case 8) given

by:

$$\sigma_{max} = \alpha E \Delta T / 1.45(1-\nu)\{1+3.41/\beta\} \qquad (20d)$$

Figures-of-Merit for the Resistance to Crack Propagation $(K \geq K_c)$

General

As mentioned earlier in the introduction, thermal environ-
ments can be encountered in practice which are of such severity
that even in the best materials, the onset of thermal stress
fracture cannot be avoided. For such conditions, good thermal
stress resistance of brittle structural materials is based on
their ability to retain their geometry and physical characteris-
tics so that continued satisfactory performance can be rendered,
in spite of being fractured. Experimental tests of thermal
stress resistance based on this criterion may measure the relative
loss in load-bearing ability such as the loss of tensile strength
due to a single thermal cycle, the number of cycles required to
cause complete fracture or the loss in weight due to a single
thermal shock due to surface spalling and similar criteria.

Clearly, thermal shock resistance based on these latter criteria is governed by the extent of crack propagation following the initiation of thermal stress fracture. The derivation of figures-of-merit appropriate to such criteria requires the understanding of the pertinent material properties which affect the propagation of cracks in thermal stress fields. The literature studies concerned with this latter problem are fewer in number than those which deal with the analysis of thermal stresses and the onset of crack propagation.

Case 21. Flat plate with Griffith crack. Steady-state heat flow perpendicular to plane of crack.

From the solutions of Florence and Goodier [8], the maximum temperature gradient (∇_{max}) permitted to avoid crack instability can be derived to be:

$$\nabla_{max} = 8(\gamma/2\pi a^2 E \ell^3)^{1/2} \tag{21a}$$

where γ is the total energy required to create unit area of fracture surface and ℓ is the half-length of the crack.

Eq. 21a leads to the figure-of-merit:

$$(\gamma/\alpha^2 E)^{1/2} \tag{21b}$$

Eq. 21a can be rewritten in terms of the maximum heat flow (Q_{max}) per unit width of the plate:

$$Q_{max} = 8(\gamma K^2/2\pi\alpha^2 E \ell^3)^{1/2} \tag{21c}$$

with the corresponding figure-of-merit:

$$(\gamma K^2/\alpha^2 E)^{1/2} \tag{21d}$$

Case 22:   Three-dimensional solid with penny-shaped crack.
Steady-state heat flow perpendicular to crack.

From the solutions of Nowinski [33], the maximum temperature gradient (∇_{max}) to avoid crack instability in terms of fracture-mechanical principles can be written:

$$\nabla_{max} = \frac{3\pi^{1/2}(1-\nu)K_{IIc}}{\alpha E b^{3/2}} \tag{22a}$$

where K_{IIc} is the mode II critical stress intensity factor and b is the radius of the crack.

The figure-of-merit is:

$$\frac{(1-\nu)K_{IIc}}{\alpha E} \tag{22b}$$

Clearly, from a general point of view this case is identical to the previous case 21 because the critical stress intensity factor K_c can be related to the fracture energy γ and Young's modulus, E by:

$$K_c = (2\gamma E)^{1/2} \tag{22c}$$

This latter expression permits conversion of equations for the crack stability in thermal stress field expressed in terms of energy principles to fracture-mechanical concepts and vice-versa.

Case 23: Flat plate with N parallel non-interacting*cracks of equal size per unit area. Plate is cooled by temperature difference ΔT and prevented from shrinking by uniaxial rigid constraints perpendicular to plane of cracks. Crack stability.

The maximum temperature difference (ΔT_{max}) by which the plate can be cooled to prevent crack instability is [34]:

$$\Delta T_{max} = (2\gamma/\pi\alpha^2 E\ell)^{1/2}(1 + 2\pi N\ell^2) \tag{23a}$$

For $2\pi N\ell^2 \ll 1$:

$$\Delta T_{max} = (2\gamma/\pi\alpha^2 E\ell)^{1/2} \tag{23b}$$

For $2\pi N\ell^2 \gg 1$:

$$\Delta T_{max} = (2\gamma/\pi\alpha^2 E\ell)^{1/2}(2\pi N\ell^2) \tag{23c}$$

Taking N as a material property, the appropriate figures-of-merit are:

$$(\gamma/\alpha^2 E)^{1/2} \quad \text{and} \quad (\gamma N^2/\alpha^2 E)^{1/2} \tag{23d}$$

ΔT_{max} of eq. 23a exhibits a minimum at a value of crack-length:

$$\ell_m = (6\pi N)^{-1/2} \tag{23e}$$

---

*For crack-interaction in plane of crack propagation, the reader is referred to the study of Singh et al. [35].

For the purpose of further discussion, it should be noted that if the initial crack length, $\ell_o > \ell_m$ the crack will propagate in a stable manner with the crack-length and ΔT related by means of eq. 23b. If, however, $\ell_o < \ell_m$ the crack will propagate in an unstable (dynamic) mode as described below.

Case 24: Flat plate with N parallel non-interacting cracks of equal size per unit area. Plate is cooled by temperature difference ΔT and prevented from shrinking by uniaxial constraints perpendicular to plane of cracks. Unstable crack propagation.

This case is identical to Case 23 considered above, with the exception that the initial crack size $\ell_o \ll \ell_m$ (eq. 23e).

On crack instability at ΔT_{max} given by eq. 23a the final crack length (ℓ_f) which results from unstable crack propagation is:

$$\ell_f = (4\pi N\ell_o)^{-1} \tag{24a}$$

Eq. 24a indicates that ℓ_f is inversely proportional to the initial crack length, ℓ_o and the crack density, N but independent from all other material properties. This latter conclusion requires modification when the fracture energy or stress intensity factors for the onset of crack propagation and arrest are not the same.

Eq. 24a, by means of the Griffith equation can be rewritten in terms of the original tensile strength, σ_t^2, which yields:

$$\ell_f = \sigma_t^2/8N\gamma E \tag{24b}$$

The appropriate figure-of-merit is:

$$\sigma_t^2/N\gamma E \tag{24c}$$

Again, by using the Griffith equation, eq (24b) can be rewritten in terms of the tensile strength retained (σ_f) follow-ing unstable crack propagation as a function of the original strength (σ_t):

$$\sigma_f = (\gamma E/\sigma_t)(16N/\pi)^{1/2} \tag{24d}$$

This latter result indicates that the tensile load-bearing ability retained following dynamic crack propagation is inversely proportional to the corresponding load-bearing ability prior to crack propagation. This conclusion has considerable practical implications.

Figure 2 illustrates the crack stability and propagation behavior described by eqs. 23 and 24 for two values of crack den-sity. Although a very simple mechanical model was used for these derivations, the general behavior shown in Fig. 2 has led to the prediction of a number of fracture phenomena in the ther-mal stress failure of brittle materials. These will be presented in a subsequent section devoted to experimental behavior.

The absence of crack-interaction was assumed throughout in the above discussion. Nevertheless such interactions can be taken into account as shown by Singh and co-workers [35] for an array of co-planar cracks based on the solutions of Yokobori and
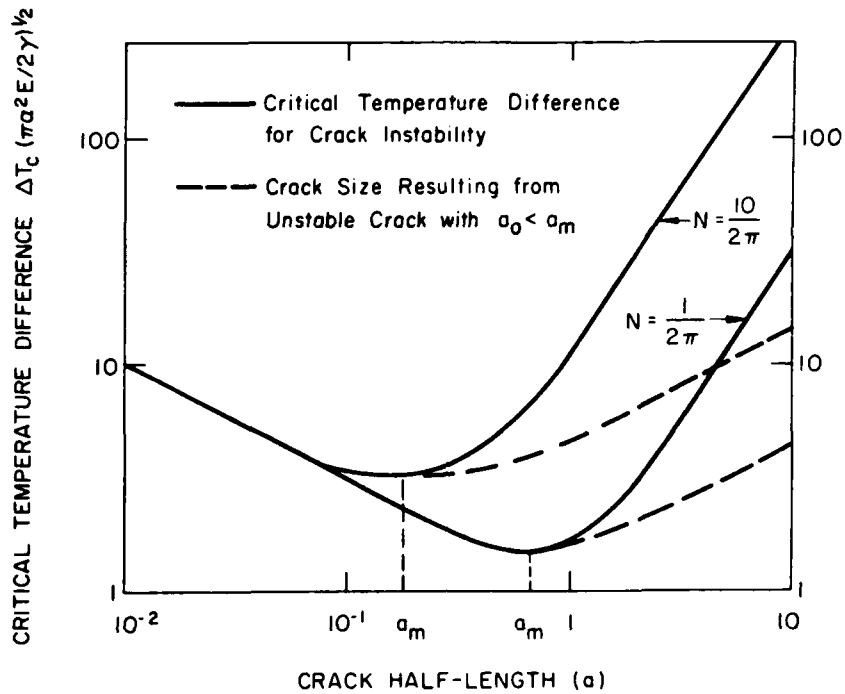
Fig. 2.   Crack stability and propagation behavior in
uniaxially constrained flat plate with parallel
non-interacting cracks, cooled through a
temperature difference ΔT (after Hasselman [34]).

Ichikawa [36]. Figure 3 shows the dependence of ΔT_c on the ratio of crack size (a) to crack spacing (d) as calculated by Singh et al. for a range of values of the ratio of row-to-row spacing (b) to crack size (d). At low values of a/d and high values of b/d, ΔT depends on crack length in a manner analogous to dependence shown in Fig. 2. As a/d → 0.5, ΔT decreases to zero due to crack coalescence.

GENERAL COMMENTS ON FIGURES-OF-MERIT

Presented above were a total of twenty-four cases for the thermal stress failure of brittle ceramics for non-redundant modes of heat transfer and failure criteria. Undoubtedly, in the near or far future other cases will be recognized and additional figures-of-merit will be derived. Regardless of the total number, it is clear that the solution of the problem of the high susceptibility of brittle structural ceramics to thermal stress failure is complex indeed. For any specific application, the choice of the material with optimum thermal stress resistance must be preceded by a thorough analysis of the mechanism(s) of heat transfer, the resulting magnitudes and distribution of the thermal stresses as well as the most probable mode of failure, all in light of the basic performance requirements of the component or structure in question. Because such an analysis involves the disciplines of heat transfer and mechanics as well as materials engineering, the problem of thermal stress fracture is most efficiently tackled by a multi-disciplinary approach.
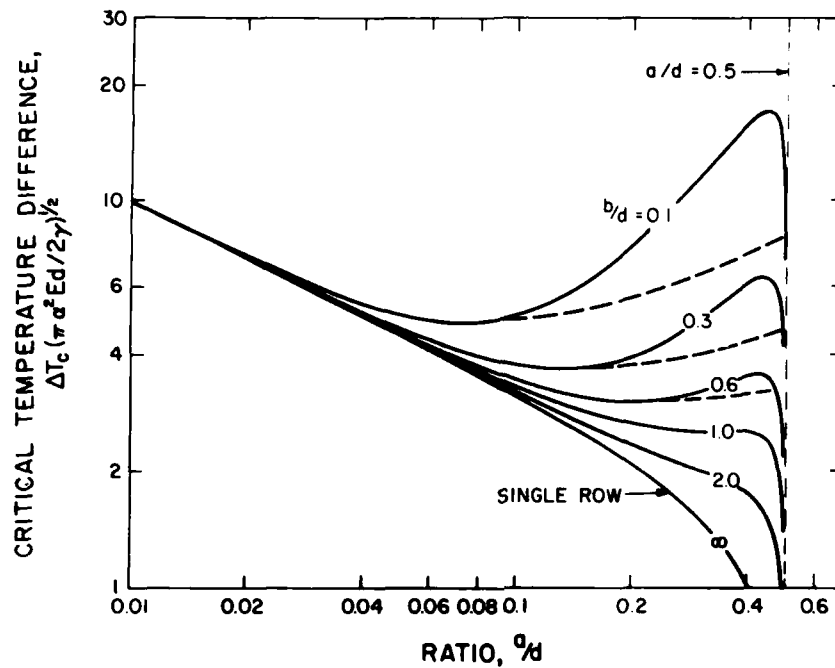
Fig. 3.   Effect of crack-interaction on critical
temperature difference of flat plate with
rows of co-linear cracks of size a, with
inter-crack spacing d and row-to-row
spacing b (after Singh, et al. [35]).

Fortunately, from the point of view of the materials technologist, the material properties which affect thermal stress fracture, at least for the twenty-four cases presented above, are clearly identified and are uncoupled from those variables which affect the transfer of heat to the component or structure. Even then, approximately a dozen and a half material properties or parameters enter the multitude of figures-of-merit. A complete characterization of any specific material for the purpose of predicting its thermal fracture behavior is a task of considerable magnitude. Such a task becomes even larger when it is recognized that most, if not all, mechanical, thermal or optical properties or parameters which make up the figures-of-merit, are a function of temperature, wavelength, environmental conditions, microstructure, composition or impurity level, loading conditions and many other variables. Nominal property values obtained from engineering handbooks at best are useful for first approximations only.

In this respect, the failure stress of brittle materials probably represents the property subject to the largest degree of uncertainty. A detailed review of the failure phenomena of brittle materials is beyond the scope of this study. In general, extensive experimental data have shown that the failure stress of such materials can be a function of the stress state (i.e., uniaxial vs. multi-axial), the stress distribution as well as the stressed volume (i.e., statistical aspects), loading rate, temperature, past mechanical or thermal history, environmental

(stress-corrosion) effects and numerous other variables. Adding to these effects is the fact that failure of brittle materials originates from structural defects introduced during processing or subsequent mechanical handling. Such defects usually are too small to be adequately characterized by non-destructive techniques currently available for the detection of flaw in metallic components. Because of the uncertainty in the magnitude of the failure stress coupled with the quantitative uncertainties of many modes of heat transfer such as those encountered in transient convection and radiation, calculation of the anticipated thermal fracture behavior of brittle structural ceramics, with the exception of perhaps the most simple case, must be regarded as order-of-magnitude estimates only.

Nevertheless, the equations and associated figures-of-merit presented above provide valuable guidelines for the design of components and selection of appropriate materials. Minimizing the component size or thickness in many instances reduces the magnitude of thermal stress, to result in a corresponding increase in the severity of the heat flux (or other criteria) to which the component can be subjected. Failure due to thermoelastic instability, which can be reduced by improving component thickness, probably represents the only exception to the above rule.

The optimum combination of material properties which yields high resistance to the initiation of thermal stress failure depends on the role of these properties in maximizing the figure-

of-merit for a specific thermal environment, performance criter-
ion (ΔT_c, q_{max}, etc.) and failure mode. Low values of the coef-
ficient of thermal expansion, Young's modulus and Poisson's ratio
are always preferred, in combination with as high a failure stress
as possible. Whenever appropriate, the value of thermal con-
ductivity and thermal diffusivity should be as high as possible.
Regardless of which material property is considered, no incom-
patibility exists in its role for the figures-of-merit presented
above for the resistance to the initiation of thermal fracture.

Such an incompatibility, however, can be found to exist in the
figures-of-merit related to crack stability and propagation. High
crack stability, in general, requires a low value of the coefficient
of thermal expansion and Young's modulus, combined with high values
of the fracture energy. These latter requirements of course are
not unexpected as all figures-of-merit involving the tensile fracture
stress can be converted into their corresponding fracture-mechanical
analogue, by means of the relation between fracture strength, Young's
modulus and fracture energy, appropriate for a given crack geometry,
if known.

In contrast, examination of the figure-of-merit appropriate
to unstable crack propagation (eq. 24c) shows that rapid crack
arrest (i.e., small values of final crack length, ℓ_f) requires a
low value of original tensile fracture stress and a high value of

Young's modulus of elasticity. This latter result derived in terms of fracture-mechanical principles is intuitively understandable, if it is recognized that the elastic energy at fracture is proportional to the ratio of the square of the fracture stress to Young's modulus. Low and high values of these two latter quantities will lead to low values of elastic energy at fracture and corresponding rapid crack arrest.

The above incompatibility in the role of the fracture stress and Young's modulus in the resistance to the initiation of thermal fracture on one hand and rapid crack arrest following unstable crack propagation on the other hand, presents a dilemma to the materials technologist in the development and selection of the optimum ceramic.

Materials selection based on maximizing the resistance to the initiation of fracture by increasing the fracture stress will also lead to an increasing extent of crack propagation for thermal conditions of such severity that failure cannot be avoided. If this latter occasion arises as is frequently the case in practice, material selection should be based on reducing the extent of crack propagation, which can be achieved by selection of materials with moderate to low strength. This will result in an improvement of thermal shock resistance in terms of retained physical characteristics and geometry following thermal stress fracture. However, this approach will reduce the total load-bearing ability, prior to or following the initiation of thermal stress fracture, required to fulfill the basic function of the component

for any specific application. For this reason, material selection based on crack arrest appears most appropriate for materials subjected to minimal mechanical load during service. This, in fact, is the case for refractory liners *for high-temperature* process vessels. For these types of materials without exception the criterion for high thermal shock resistance is based on rapid crack arrest as determined by experimental tests which measure the strength loss following the thermal fracture or related change in other physical characteristics.

Again, the above discussion indicates the need of a thorough analysis of the thermal environment, magnitude of stress, failure mode and extent of crack propagation before a judicious choice of the most suitable ceramic for any specific application can be made. For this purpose, especially, the qualitative and quantitative aspects of crack propagation under conditions of thermal stress need to be developed further in considerably greater detail.

EXPERIMENTAL

Initiation of Thermal Stress Fracture

The experimental measurement of the resistance of structural ceramics to thermal stress fracture depends on the information desired. In view of the qualitative and quantitative uncertainties in the nature of heat transfer and associated thermal stresses, in practice the resistance of thermal stress fracture of candidate materials is measured under conditions of heat

transfer which duplicate the actual service conditions as closely as possible. In this manner, the critical temperature difference (ΔT_c) required for failure in a single quench, the number of cycles required for failure in thermal fatigue, or other criteria of thermal stress resistance appropriate for a specific component subjected to specific service conditions can be measured. In industrial practice, a large number of such tests were developed. For practical purposes, such tests are entirely adequate as they generate information essential for the purpose of engineering design, performance prediction and failure analysis. However, since no attempts are made to analyze the data obtained by such tests in terms of thermo-elastic and failure theories, the results obtained must be regarded as empirical only and to be appropriate only in the specific conditions of such tests. As a result, great care needs to be taken in any attempt to extrapolate the result in other thermal conditions involving different mechanisms of heat transfer, geometry, failure mechanisms and other relevant criteria.

Studies carried out for the purpose of comparing predicted thermal fracture behavior with experimental data have met with varying degrees of success. Coble and Kingery [37] obtained reasonable agreement between calculated and experimental data for the critical temperature difference across the wall thickness of hollow concentric circular cylinders made of porous aluminum oxide subjected to steady-state heat flow.

Glenny and Royston [38] as well as Hasselman [39] found fair agreement between predicted and measured values for the critical temperature difference required to initiate fracture in circular rods of polycrystalline aluminum oxide subjected to a single quench from higher temperature into a water bath. Similar agreement between theory and experiment was found for spherical shapes of polycrystalline aluminum oxide quenched into molten salt as a quenching medium [40]. It should be pointed out, however, that the accuracy of predictions of results for quenching experiments is handicapped by the considerable uncertainty in the value of the heat transfer coefficient for heated surfaces in fluids under transient conditions. In particular, the heat transfer coefficient for a water bath is strongly affected by the highly temperature dependent effects of nucleate boiling and film formation as indicated by the studies of Farber and Scorah [41], Manson and Smith [15] and Singh, Tree and Hasselman [42].

For conditions of radiative heat transfer, Hasselman [17] found excellent agreement between calculated and measured values of the black-body temperature required to initiate thermal stress fracture in spheres of polycrystalline aluminum oxide, initially at room temperature and suddenly inserted into a furnace chamber at thermal equilibrium at temperatures at which radiation represents the primary mechanism of heat transfer.

For ceramic plates subjected to forced convective heat transfer over a central spot, Faber, Huang and Evans [43] obtained excellent agreement between calculated and predicted
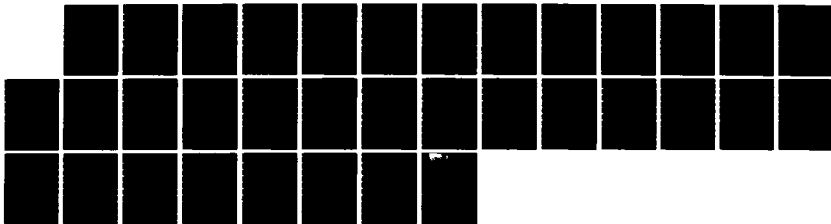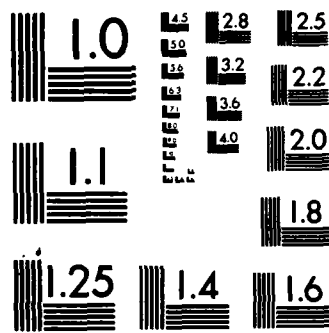
MICROCOPY RESOLUTION TEST CHART

NATIONAL BUREAU OF STANDARDS-1963-A

values of the critical temperature difference required to initiate failure at a given rate of gas flow. The good agreement obtained was facilitated by the calibration of the heat transfer coefficient by use of a ceramic with accurately known failure stresses. These latter values were established by indenting the plates by a diamond hardness indentation followed by an independent strength test. By this method the statistical aspect of the brittle fracture is removed. This overall approach must be considered unique in that the magnitude of thermal stress is established from the fracture process itself. The magnitude of heat transfer coefficient obtained from these data can then be used to calculate the stresses in other ceramic plates to be tested.

The prediction of thermal fatigue behavior of brittle ceramics has met with a varying degree of success. Figure 4 compares the observed and predicted number of cycles to failure of circular rods of a soda-lime-silica glass quenched into water measured by Hasselman, et al., [44]. However, it should be noted that the predicted thermal fatigue-life shown in Fig. 4 required the use of the Weibull theory in order to take into account that the failure probability under conditions of the multi-axial thermal stress field differs from the corresponding value under conditions of the uniaxial strength test. These differences in failure probabilities lead to the effect that the mean fracture stress under conditions of the thermal quench is far lower than the tensile fracture stress under conditions of uniaxial loading. It should be recognized that the formulation of the Weibull theory must be consid-

ered empirical. For this reason, the reasonable agreement shown in Fig. 4 to some extent may well be fortuitous. It should also be noted that even slight uncertainties in the kinetics of sub-critical crack growth can introduce large relative errors in predicted thermal fatigue-life. Nevertheless, the agreement indicated by the observed and predicted results shown in Fig. 4 offers encouragement towards future work in this area.

The thermal fatigue behavior of polycrystalline hot-pressed silicon nitride [45] showed good agreement between predicted and observed values for ranges of crack sizes expected to occur in this material. Nevertheless, thermal fatigue-life was found to depend critically on the assumption of the value of crack size in the original material prior to thermal fatigue. Non-destructive tests for the accurate measurement of flaw size of the order of 50-100 μm have not been developed at this stage of technical development. For this reason, the prediction of the thermal fatigue behavior of structural ceramics such as silicon nitride must be regarded as still relatively uncertain.

Observations on the Nature of Crack Propagation During
Thermal Stress Fracture

In view of its importance to engineering practice, crack propagation following the onset of thermal stress fracture has received quite a bit of attention. Literally explosive fracture of aluminum oxide and zirconium carbide subjected to high radia-tive heat fluxes was observed by Crandall and Ging [46] and Has-selman, Becher and Mazdiyasni [1], respectively. In these stu-
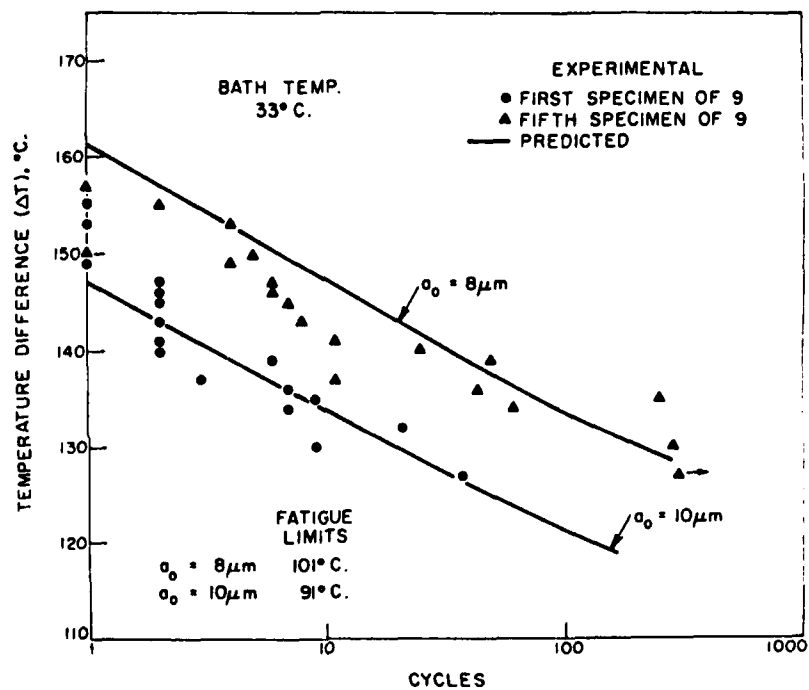
Fig. 4. Predicted and experimental cycles-to-failure of soda-lime-silica glass rods with initial flaw depth of 8.6 μm subjected to thermal fatigue by quenching into water bath at 33°C (after Hasselman et al. [44]).

dies, the samples were fractured in a number of separate fragments. Clearly, this fracture mode is highly undesirable as the crack sizes exceeded the dimensions of the materials being tested. This mode of failure is quite commonly encountered in practice especially for components of relatively large size.

Under other conditions of thermal stress fracture such as a quench into water or other appropriate fluids, the cracks formed will arrest within the material. Such cracks, because of little or no permanent crack-opening-displacement, frequently are not easily detected unless by highly specialized laboratory techniques such as electron-optical method. Nevertheless, such cracks can have a significant effect on load-bearing characteristics. For this reason and for convenience, experimental studies of the nature of crack propagation have concentrated on measurements of load-bearing characteristics, specifically tensile strength as a function of severity of the conditions of the thermal shock test.

The crack stability and propagation behavior shown in Figure 2, derived for a simple mechanical model with non-interacting cracks, should be qualitatively valid also for other stress conditions involving tensile failure. As can be inferred from Fig. 2, Fig. 5 depicts schematically the expected relative dependence of crack size and corresponding tensile strength for unstable and stable crack propagation as a function of severity of thermal shock, expressed in such terms as ΔT in a quenching experiment, rate of heat flow or other appropriate measure. For unstable crack propagation, crack size and strength exhibit a discontinu-

ous increase and decrease, respectively. The crack size which results at ΔT_c is sub-critical and will not change in size until ΔT reaches the value $\Delta T'$. For $\Delta T > \Delta T'$, the crack will propagate in a stable manner.

In contrast, for stable crack propagation, for $\Delta T > \Delta T_c$, crack and strength will increase and decrease, respectively in a monotonic manner as shown in Figs. 5c and 5d.

The general strength behavior for unstable crack propagation shown in Fig. 5b was verified experimentally by a number of investigators for a variety of structural ceramics such as aluminum oxide, silicon nitride, berylium oxide, silicon carbide, boron carbide, zinc oxide and soda-lime silica glass [48-55].

Figure 6 shows typical data for an industrial grade polycrystalline aluminum oxide subjected to a quench into a water bath at room temperature followed by a strength test. The instantaneous loss in strength at ΔT_c as well as the region of sub-criticality of the cracks for $\Delta T_c \leq \Delta T \leq \Delta T_c'$ as shown in Fig. 5b is clearly evident.

In the analysis of unstable crack propagation it was predicted that the strength retained following the initiation of thermal stress fracture was an inverse function of the strength prior to fracture. In this respect, it is of interest to compare the experimental data shown in Fig. 7 for another industrial alumina obtained under identical quenching conditions as the data shown in Fig. 6.
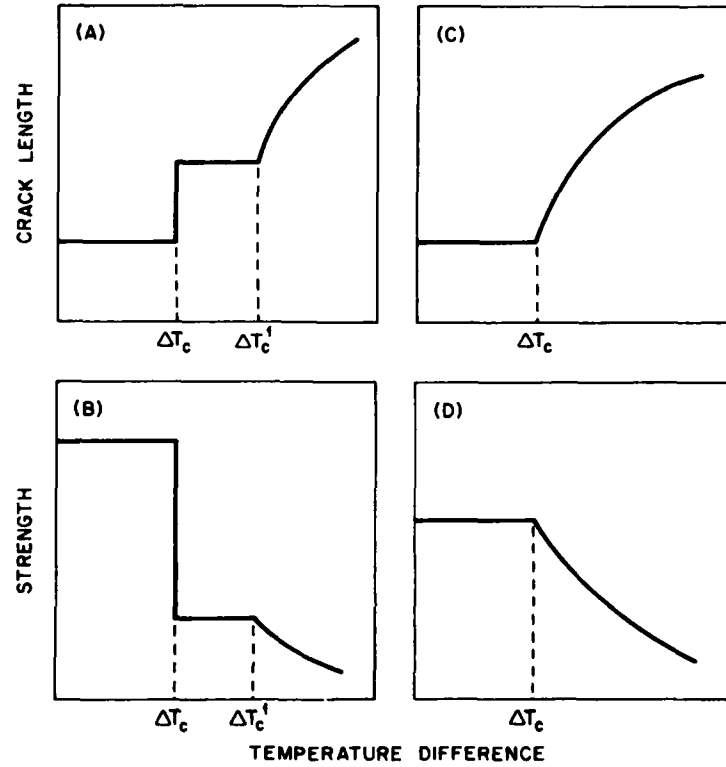
Fig. 5. Schematic representation of the crack length and corresponding strength behavior as a function of severity of thermal shock for unstable (A,B) and stable (C,D) crack propagation (after ref. [47]).
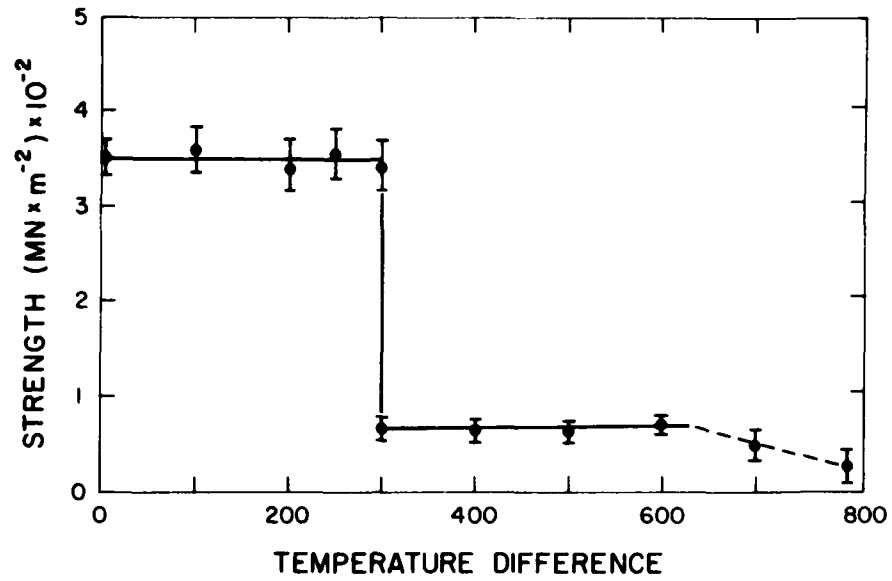
Fig. 6. Tensile strength of an industrial poly-
crystalline aluminum oxide following a
quench from higher temperature into a
water bath as a function of quenching
temperature difference (after Hasselman,
1970) (For further details see ref. [39]).
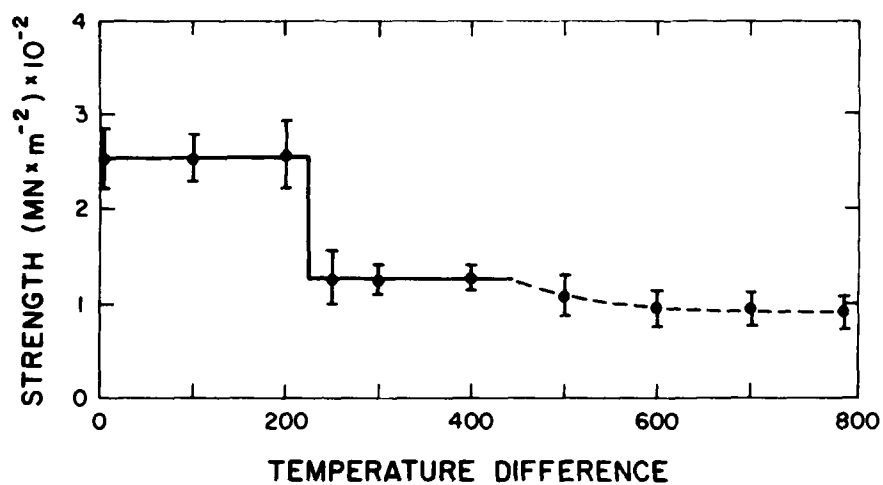
Fig. 7. Tensile strength of a lower grade polycrystalline aluminum oxide subjected to water quench, showing a much lower relative strength loss at ΔT_C than for the alumina shown in Fig. 6 (For further details see ref. [39]).

A comparison of the data shown in Figs. 6 and 7 shows that the alumina of Fig. 6 has a higher initial strength in the untested condition (i.e. $\Delta T = 0$) than the alumina of Fig. 7. In view of the role of strength, it is expected that a higher quenching temperature difference is required to initiate failure in the initially stronger alumina than in the weaker alumina. This conclusion is confirmed by the experimental data for the quenching temperature difference required to initiate failure which is about 300°C for the stronger alumina and around 225°C for the weaker alumina.

From the role of strength in the extent of crack propagation, as analyzed earlier, it is predicted that the strength retained following the initiation of thermal failure is an inverse function of the original strength. The validity of this conclusion is easily confirmed by the strength for $\Delta T > \Delta T_c$ given in Figs. 6 and 7. In general, these data are illustrative of the diametrically opposite roles of strength in the resistance of the initiation of thermal stress fracture and the extent of crack propagation and resulting degree of damage following the onset of crack propagation. Considering the two aluminas of Figs. 6 and 7, clearly for thermal conditions involving thermal stresses of low magnitude and failure probability, the aluminum oxide of Fig. 6 is the preferred candidate in view of its superior load-bearing characteristics possibly required for its intended purpose. On the other hand, for magnitudes of thermal stresses for which failure is initiated in both aluminas, the alumina of Fig. 7 is pre-

ferred in view of its superior strength behavior following the onset of thermal stress failure.

Figure 8 shows the strength behavior typical of stable crack propagation as found by Larson et al. [47] for a high-alumina refractory material subjected to a water-quench. Note that original strength ($\Delta T = 0$) of the material is very low indeed compared to strengths commonly found in other general structural materials. This low strength value, in terms of the simple analysis presented earlier, assures that the size of failure-initiating cracks is sufficiently large that the unstable mode of crack propagation is suppressed and that crack propagation will occur only in the stable mode. This latter mode of crack propagation is preferred because at a given value of ΔT, as easily ascertained from Fig. 1, the extent of stable crack propagation is less than for unstable crack propagation.

Critical to note, again as easily ascertained from Fig. 2, is that whether a crack will propagate in a stable or unstable manner depends on the total number of cracks which participate simultaneously in the fracture process. This implies that the mode of crack propagation and associated strength loss for any given material will depend on the nature of the thermal shock environment. Indeed, Larson et al [56] found that samples of a high-alumina refractory when subjected to a water quench failed by stable crack propagation, whereas samples of the same material when subjected to thermal shock by radiation heating failed in unstable mode. These differences in fracture mode can be traced
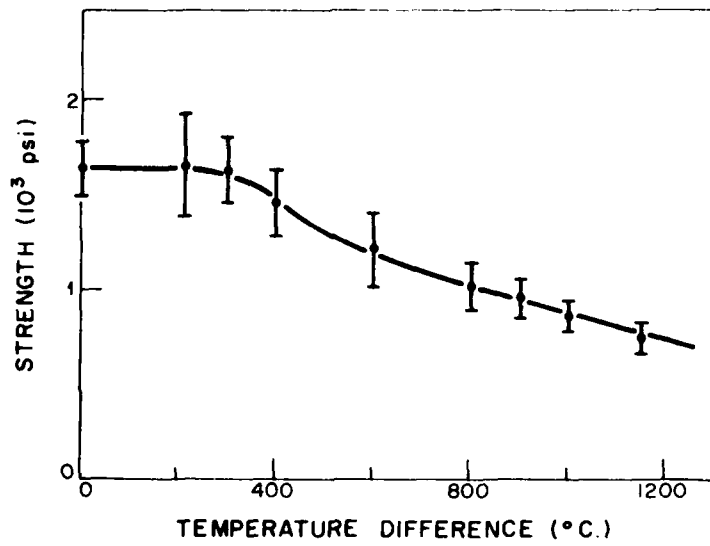
Fig. 8. Strength loss typical for stable crack propagation in high-alumina refractory subjected to quench into water bath (after ref. [47]).

directly to differences in crack density. During the water quench tensile failure is nucleated at numerous surface sites, because the total surface is subjected to a high value of tensile stress. In contrast, during radiation heating, the maximum tensile stress is found along a single line or plane so that fracture will originate at a limited number of sites only. Again, prior knowledge of the mode of heat transfer must be established before a candidate material can be selected on the basis of the nature of crack propagation.

Figures 6 and 7 clearly indicate evidence for unstable crack propagation. It is critical to point out that such strength loss behavior, as found by Ziegler and Hasselman [60], can be masked by excessive data scatter to exhibit an apparent stable failure mode as shown in Figs. 5 and 8.

The dependence of ΔT on crack length as shown in Fig. 2 also predicts that at the transition from unstable to stable crack propagation (at $\ell_o = \ell_m$), ΔT_c should be independent of crack length. This conclusion was confirmed by Gupta [48] for a number of polycrystalline aluminum oxides with a range of strength. For all these sets of data, ΔT_c was found to be independent of strength, with the high strength samples exhibiting unstable crack propagation and the low strength samples failing in a stable mode.

Finally, Fig. 2 suggests that materials with very high density of micro-cracks should exhibit exceptional thermal shock resistance. Indeed, this prediction is verified by the dramatic

results of Rossi [57] for a polycrystalline magnesium oxide in which micro-cracking was induced by a dilute dispersed phase of spherical particles of tungsten. In the resulting composite, the micro-cracking resulted from the large mismatch in the coefficients of thermal expansion of the magnesium oxide matrix and tungsten dispersed phase. It may be added that micro-cracking can cause an appreciable reduction in thermal conductivity [58]. For this reason, micro-cracked materials should prove to be particularly suited to design situations having the simultaneous requirement of high thermal shock resistance in combination with high thermal insulating ability [59].

FINAL COMMENTS

It appears reasonable to conclude that the principles which underlie thermal stress fracture have been developed to a considerably greater degree than the predictions of such fracture, which in practice are handicapped by uncertainties in the qualitative and quantitative aspects of heat transfer as well as uncertainties in the relevant material properties. The high degree of brittleness of ceramic materials exacerbates the problem even further as the safety features of non-linear deformation found for many metals and polymers is entirely absent. Such properties as the coefficient of thermal expansion, Young's modulus, Poisson's ratio, thermal conductivity and optical properties which are governed by inter-atomic effects are under control of the material specialist to a very limited degree only. For this reason, improvements in the resistance of brittle ceramics to frac-

ture must rely primarily on improvements of strength and fracture toughness (energy). Surface-compression-strengthening and the formation of materials with thermal conductivity gradients may also be used to advantage [61-65]. Alternatively, for structural ceramics available at present, design modifications may be required in order to reduce the magnitude of thermal stress to acceptable levels. Further understanding of the nature of crack propagation in steady-state or transient thermal stress field can be enhanced by additional theoretical work. This latter area is judged to be of particular practical importance as it should enhance the reliability of design of components or structures made from brittle ceramics subject to thermal stress failure.

Acknowledgment

REFERENCES

1. D. P. H. Hasselman, P. F. Becher and K. S. Mazdiyasni, Analysis of the Resistance of High E- Low E Brittle Composites to Failure by Thermal Shock, Materials Technology and Testing, Vol. 11, pp. 82-92, 1980.

2. David Burgreen, Elements of Thermal Stress Analysis, pp. 462, C. P. Press, New York, 1971.

3. J. D. Eshelby; pp. 89-139 in Progress in Solid Mechanics, Vol. II, eds. I. N. Sneddon and R. Hill, North-Holland Publishing Company, Amsterdam, 1961.

4. J. Selsing, Internal Stresses in Ceramics, J. Amer. Ceram. Soc., Vol. 44, No. 8, pp. 419, 1961.

5. S. Timoshenko and J. N. Goodier, Theory of Elasticity, McGraw-Hill Book Company, New York, 1951.

6. C. H. Kent, Thermal Stresses in Thin-Walled Cylinders, Trans. ASME, Vol. 53, pp. 167-80, 1931.

7. Thermal Stress Techniques in the Nuclear Industry, eds. Z. Zudans, T. C. Yen and W. H. Steigelmann, American Elsevier Publishing Company, New York, 1965.

8. A. F. Florence and J. N. Goodier, Thermal Stress at Spherical Cavities and Circular Holes in Uniform Heat Flow, Trans. ASME, J. Appl. Mech., Vol. 81, Ser. E, pp. 293-94, 1959.

9.   T. R. Tauchert, Thermal Stresses at Spherical Inclusions in
     Uniform Heat Flow, J. Compos. Mater., Vol. 2, No. 4, pp.
     478-86, 1968.

10. Ya. B. Fridman in Thermal Stability of Plates and Shells,
     ed. Ya. B. Fridman, Consultants Bureau, New York, 1964.

11. G. Buergermeister and H. Steup, Stability Theory (Stabili-
     taets Theorie), Akademie Verlaq, Berlin, Federal Republic
     of Germany, 1957.

12. B. A. Boley and J. H. Weiner, Theory of Thermal Stresses,
     John Wiley and Sons, Inc., New York, 1960.

13. D.P.H. Hasselman, Role of Physical Properties in Post-Ther-
     mal Buckling Resistance of Brittle Ceramics, J. Amer. Ceram.
     Soc., Vol. 61, No. 3-4, pp. 178, 1978.

14. J. C. Jaeger, On Thermal Stresses in Circular Cylinders,
     Phil. Mag., Vol. 36, No. 7, pp. 419-28, 1945.

15. S. S. Manson and R. W. Smith, Quantitative Evaluation of
     Thermal-Shock Resistance, Trans. ASME, Vol. 78, pp. 533-44,
     1956.

16. W. R. Buessem, Resistance of Ceramic Bodies to Temperature
     Fluctuations, Sprechsaal Keram. Glas Email Silikate, Vol.
     93, No. 6, pp. 137-41, 1960.

17. D.P.H. Hasselman, Thermal Shock by Radiation Heating, J. Amer. Ceram. Soc., Vol. 46, pp. 229-34, 1963.

18. D.P.H. Hasselman, Theory of Thermal Shock Resistance of Semi-Transparent Ceramics Under Radiation Heating, J. Amer. Ceram. Soc., Vol. 49, No. 2, pp. 103-104, 1966.

19. D.P.H. Hasselman, J. R. Thomas, Jr., M. P. Kamat and K. Satyamurthy, Thermal Stress Analysis of Partially Absorbing Brittle Ceramics Subjected to Symmetric Radiation Heating, J. Amer. Ceram. Soc., Vol. 63, No. 1-2, pp. 21-25, 1980.

20. J. R. Thomas, Jr., J. P. Singh and D.P.H. Hasselman, Analysis of Thermal Stress Resistance of Partially Absorbing Ceramic Plate Subjected to Asymmetric Radiation, I: Convective Cooling at Rear Surface, J. Amer. Ceram. Soc., Vol. 64, No. 3, pp. 163-169, 1981.

21. J. P. Singh, K. Satyamurthy, J. R. Thomas, Jr., and D.P.H. Hasselman, Analysis of Thermal Stress Resistance of Partially Absorbing Ceramic Plate Subjected to Asymmetric Radiation, II: Convective Cooling at Front Surface, J. Amer. Ceram. Soc., Vol. 64, No. 3, pp. 169-73, 1981.

22. G. Grüenburg, Über den in einer isotropen Kugel durch ungleichformige Erwarmung erregten Spannungszustand, Z. Physik, Vol. 35, pp. 548-555, 1925.

23. H. Poritsky and F. A. Fend, Relief of Thermal Stresses Through Creep, Trans. ASME, J. Appl. Mech., Vol. 25, No. 4, pp. 589-97, 1958.

24. D.P.H. Hasselman, Approximate Theory of Thermal Stress Resistance of Brittle Ceramics Involving Creep, J. Amer. Ceram. Soc., Vol. 50, No. 9, pp. 454-57, 1967.

25. D.P.H. Hasselman and W. Zdaniewski, Thermal Stress Resistance Parameters for Brittle Materials Subjected to Thermal Stress Fatigue, J. Amer. Ceram. Soc., Vol. 61, No. 7-8, pp. 375, 1978.

26. A. G. Evans, A Method of Evaluating the Time-Dependent Failure Characteristics of Brittle Materials and Its Application to Polycrystalline Alumina, J. Mat. Sc., Vol. 7, No. 10, pp. 1137-46, 1972.

27. D. Stahn, Thermal Stresses in Large Glass Plates, Glastechnische Berichte, Vol. 50, No. 7, pp. 149-58, 1977.

28. D. Stahn and F. Kerkhof, Danger of Thermal Stress Fracture of Glass Plates, Glastechnische Berichte, Vol. 50, No. 6, pp. 121-28, 1977.

29. M. Stern, The Numerical Calculation of Thermally Induced Stress Intensity Factors, J. Elasticity, Vol. 9, No. 1, pp. 91-95, 1979.

30. A. F. Emery, G. E. Walker, Jr., and J. A. Williams, A Greens Function for the Stress Intensity Factors of Edge Cracks and Its Application to Thermal Stresses, Trans. ASME, J. Basic Eng., Vol. 91, No. 4, Ser. D, pp. 618-24, 1969.

31. A. F. Emery, J. A. Williams and J. Avery, Thermal Stress Concentration Caused by Structural Discontinuities, Experimental Mechanics, Vol. 9, No. 12, pp. 558-64, 1969.

32. J. P. Singh, K. Niihara and D.P.H. Hasselman, Analysis of Thermal Fatigue Behavior of Brittle Structural Materials, J. Mat. Sc., Vol. 16, pp. 2789-97, 1981.

33. J. L. Nowinski, Theory of Thermoelasticity with Applications, p. 546, Sijthoff and Noordhoff International Publishers, Alphen aan den Rijn (Netherlands) 1978.

34. D.P.H. Hasselman, Thermal Stress Crack Stability and Propagation in Severe Thermal Environments, pp. 89-103 in Materials Science Research, Vol. 5, W. W. Kriegel and H. Palmour III, Plenum Press, N.Y., 1971.

35. J. P. Singh, C. Shih and D.P.H. Hasselman, Analysis of Role of Crack Interaction on Nature of Strength-Loss of Brittle Ceramics Subjected to Thermal Shock, Comm. Amer. Ceram. Soc., Vol. 64, No. 8, pp. 106-109, 1981.

36. T. Yokobori and M. Ichikawa, Elastic Solid with Infinite Row of Colinear Cracks and the Fracture Criterion, J. Phys. Soc. Japan, Vol. 19, pp. 2341-42, 1964.

37. R. L. Coble and W. D. Kingery, Effect of Porosity on Thermal Stress Fracture, J. Amer. Ceram. Soc., Vol. 38, No. 1, pp. 33-37, 1955.

38. E. Glenny and M. G. Royston, Transient Thermal Stresses Promoted by the Rapid Heating and Cooling of Brittle Circular Cylinders, Trans. Brit. Ceram. Soc., Vol. 57, No. 10, pp. 645-77, 1958.

39. D.P.H. Hasselman, Strength Behavior of Polycrystalline Alumina Subjected to Thermal Shock, J. Amer. Ceram. Soc., Vol. 53, No. 9, pp. 490-95, 1970.

40. D.P.H. Hasselman and W. B. Crandall, Thermal Shock Analysis of Spherical Shapes, II, J. Amer. Ceram. Soc., Vol. 46, pp. 434-37, 1963.

41. E. A. Farber and R. L. Scorah, Heat Transfer to Water Boiling Under Pressure, Trans. ASME, Vol. 70, pp. 369-384, 1948.

42. J. P. Singh, Y. Tree and D.P.H. Hasselman, Effect of Bath and Specimen Temperature on the Thermal Stress Resistance of Brittle Ceramics Subjected to Thermal Quenching, J. Mat. Sc., Vol. 16, pp. 2109-2118, 1981.

43. K. T. Faber, M. D. Huang and A. G. Evans, Quantitative Studies of Thermal Shock in Ceramics Based on a Novel Test Technique, J. Amer. Ceram. Soc., Vol. 64, No. 5, pp. 296-301, 1981.

44. D.P.H. Hasselman, R. Badaliance, K. R. McKinney and C. H. Kim, Failure Prediction of the Thermal Fatigue Resistance of a Glass, J. Mat. Sc., Vol. 11, pp. 458-64, 1976.

45. D.P.H. Hasselman, E. P. Chen, C. L. Ammann, J. E. Doherty and C. C. Nessler, Failure Prediction of Thermal Fatigue of Silicon Nitride, J. Amer. Ceram. Soc., Vol. 58, No. 11-12, pp. 513-16, 1975.

46. W. B. Crandall and J. Ging, Thermal Shock Analysis of Spherical Shapes, J. Amer. Ceram. Soc., Vol. 38, No. 1, pp. 44-54, 1955.

47. D. R. Larson, J. A. Coppola, D.P.H. Hasselman and R. C. Bradt, Fracture Toughness and Spalling Behavior of High-Al_2O_3 Refractories, J. Amer. Ceram. Soc., Vol. 57, No. 10, pp. 417-21, 1974.

48. T. K. Gupta, Strength Degradation and Crack Propagation in Thermally Shocked Al_2O_3, J. Amer. Ceram. Soc., Vol. 55, No. 5, pp. 249-53, 1972.

49. K. Anzai and H. Hashimoto, Thermal Shock Resistance of Silicon Nitride, J. Mat. Sc., Vol. 12, pp. 2351-53, 1977.

50. D. A. Krohn, D. R. Larson and D.P.H. Hasselman, Comparison of Thermal Stress Resistance of Polycrystalline Al_2O_3 and BeO, J. Amer. Ceram. Soc., Vol. 56, No. 9, pp. 490-92, 1973.

51. J. A. Coppola and R. C. Bradt, Thermal-Shock Damage in SiC, J. Amer. Ceram. Soc., Vol. 56, No. 4, pp. 214-17, 1973.

52. C. C. Seaton and S. K. Dutta, Effect of Grain Size on Crack Propagation in Thermally Shocked B_4C, J. Amer. Ceram. Soc., Vol. 57, No. 5, pp. 228-29, 1975.

53. T. K. Gupta, Strength Behavior of Thermally Shocked ZnO, J. Amer. Ceram. Soc., Vol. 55, No. 8, p. 429, 1972.

54. D. A. Krohn and D.P.H. Hasselman, Effect of Abrasion on Strength and Thermal Stress Resistance of a Glass, J. Amer. Ceram. Soc., Vol. 56, No. 6, pp. 337-38, 1973.

55. N. Claussen and D.P.H. Hasselman, Improvement of Thermal Shock Resistance of Brittle Structural Ceramics by a Dispersed Phase of Zirconia, pp. 381-96 in Thermal Stresses in Severe Environments, D.P.H. Hasselman and R. A. Heller, Plenum Press, N.Y., 1980.

56. D. R. Larson and D.P.H. Hasselman, Comparative Spalling Behavior of High-Alumina Refractories Subjected to Sudden Heating and Cooling, Trans. and J. Brit. Ceram. Soc., Vol. 74, No. 2, pp. 59-65, 1975.

57. R. C. Rossi, Thermal-Shock-Resistant Ceramic Composites, Ceram. Bull., Vol. 48, No. 7, pp. 736-37, 1969.

58. D.P.H. Hasselman, Effect of Cracks on Thermal Conductivity, J. Comp. Mat., Vol. 12, pp. 403-07, 1978.

59. D.P.H. Hasselman and J. P. Singh, Analysis of the Thermal Stress Resistance of Micro-Cracked Brittle Ceramics, Ceram. Bull., Vol. 58, No. 9, pp. 856-60, 1979.

60. G. Ziegler and D.P.H. Hasselman, Effect of Data Scatter on Apparent Thermal Stress Failure Mode of Brittle Ceramics, Ceramurgia International, Vol. 5, No. 3, pp. 126-28, 1979.

61. H. P. Kirchner and R. M. Gruver, The Elevated Temperature Flexural Strength and Impact Resistance of Alumina Ceramics Strengthened by Quenching, Mat. Sc. Engr., Vol. 13, pp. 63-69, 1974.

62. H. P. Kirchner, R. E. Walker and D. R. Platts, Strengthening Alumina by Quenching in Various Media, J. Appl. Phys., Vol. 42, No. 10, pp. 3685-92, 1971.

63. H. P. Kirchner, R. M. Gruver and R. E. Walker, Strengthening Sapphire by Compressive Surface Layers, J. Appl. Phys., Vol. 40, No. 9, pp. 3445-52, 1969.

64. D.P.H. Hasselman and G. E. Youngblood, Enhanced Thermal Stress Resistance of Structural Ceramics with Thermal Conductivity Gradient, J. Amer. Ceram. Soc., Vol. 61, No. 1-2, pp. 49-52, 1978.

65. K. Satyamurthy, J. P. Singh, D. P. H. Hasselman and M. P. Kamat, Effect of Spatially Varying Thermal Conductivity on the Magnitude of Thermal Stress in Brittle Ceramics Subjected to Convective Heating, J. Amer. Ceram. Soc., Vol. 63, No. 7-8, pp. 363-67, 1980.

BASIC DISTRIBUTION LIST

Technical and Summary Reports

Organization	No. of Copies	Organization	No. of Copies
Defense Documentation Center Cameron Station Alexandria, Virginia 22314	(12)	Naval Construction Batallion Civil Engineering Laboratory Port Hueneme, California 93043 Attn: Materials Division	(1)
Office of Naval Research Department of the Navy		Naval Electronics Laboratory Center San Diego, California 92152	
Attn: Code 471 Code 102 Code 470	(1) (1) (1)	Attn: Electron Materials Science Division	(1)
Commanding Officer Office of Naval Research Branch Office 495 Summer Street Boston, Massachusetts 02210	(1)	Naval Missile Center Materials Consultant Code 3312-1 Point Mugu, California 93041	(1)
Commanding Officer Office of Naval Research Branch Office 536 South Clark Street Chicago, Illinois 60605	(1)	Commanding Officer Naval Surface Weapons Center White Oak Laboratory Silver Spring, Maryland 20910 Attn: Library	(1)
Office of Naval Research San Francisco Area Office One Hallidie Plaza, Suite 601 San Francisco, California 94102	(1)	David W. Taylor Naval Ship R&D Center Materials Department Annapolis, Maryland 21402	(1)
Naval Research Laboratory Washington, D.C. 20390		Naval Undersea Center San Diego, California 92132 Attn: Library	(1)
Attn: Code 6000 Code 6100 Code 6300 Code 6400 Code 2627	(1) (1) (1) (1) (1)	Naval Underwater System Center Newport, Rhode Island 02840 Attn: Library	(1)
		Naval Weapons Center China Lake, California 93555 Attn: Library	(1)
Naval Air Development Center Code 302 Warminster, Pennsylvania 18974 Attn: Mr. F. S. Williams	(1)	Naval Postgraduate School Monterey, California 93940 Attn: Mechanical Engineering Dept.	(1)
Naval Air Propulsion Test Center Trenton, New Jersey 08628 Attn: Library	(1)	Naval Air Systems Command Washington, D.C. 20360 Attn: Code 52031 Code 52032	 (1) (1)

Organization	No. of Copies	Organization	No. of Copies
Naval Sea System Command Washington, D. C. 20362 Attn: Code 035	(1)	NASA Headquarters Washington, D. C. 20546 Attn: Code RRM	(1)
Naval Facilities Engineering Command Alexandria, Virginia 22331	(1)	NASA Lewis Research Center 21000 Brookpark Road Cleveland, Ohio 44135 Attn: Library	(1)
Scientific Advisor Commandant of the Marine Corps Washington, D.C. 20380 Attn: Code AX	(1)	National Bureau of Standards Washington, D.C. 20234 Attn: Metallurgy Division Inorganic Materials Division	(1) (1)
Naval Ship Engineering Center Department of the Navy Washington, D.C. 20360 Attn: Code 6101	(1)	Defense Metals and Ceramics Information Center Battelle Memorial Institute 505 King Avenue Columbus, Ohio 43201	(1)
Army Research Office P.O. Box 12211 Triangle Park, N.C. 27709 Attn: Metallurgy & Ceramics Program	(1)	Office of Naval Research, Branch Office 1030 East Green Street Pasadena, CA. 91106	(1)
Army Materials and Mechanics Research Center Watertown, Massachusetts 02172 Attn: Research Programs Office	(1)	Metals and Ceramics Division Oak Ridge National Laboratory P.O. Box X Oak Ridge, Tennessee 37380	(1)
Air Force Office of Scientific Research Bldg. 410 Bolling Air Force Base Washington, D.C. 20332 Attn: Chemical Science Directorate Electronics and Solid State Science Directorate	(1) (1)	Los Alamos Scientific Laboratory P.O. Box 1663 Los Alamos, New Mexico 87544 Attn. Report Librarian Argonne National Laboratory Metallurgy Division P.O. Box 229 Lemont, Illinois 60439	(1) (1)
Air Force Materials Lab (LA) Wright-Patterson AFB Dayton, Ohio 45433	(1)	Brookhaven National Laboratory Technical Information Division Upton, Long Island New York 11973 Attn: Research Library	(1)
Library, Bldg 50, Rm 134 Lawrence Radiation Laboratory Berkeley, CA 94720	(1)		

Organization	No. of Copies
Director Applied Physics Laboratory University of Washington 1013 Northeast Fortieth Street Seattle, Washington 98105	(1)

SUPPLEMENTARY DISTRIBUTION LIST

Advanced Research Project Agency
Materials Science Director
1400 Wilson Boulevard
Arlington, VA 22209

Mr. George Boyer
Sensor Systems Program
Office of Naval Research
Code 222
Arlington, VA 22217

Professor R. Bradt
Dept. of Mining, Metallurgical and
  Ceramic Engineering
College of Engineering, FB-10
University of Washington
Seattle, Wash. 98195

Professor L. E. Cross
The Pennsylvania State University
Materials Research Laboratory
University Park, PA 16802

Dr. A. G. Evans
Department Materials Science
  and Engineering
Hearst Mining Building
University of California
Berkeley, CA 94720

Dr. Gene Haertling
Motorola Corporation
3434 Vassar, NE
Albuquerque, NM 87107

Dr. L. L. Hench
Department of Metallurgy
University of Florida
Gainesville, FL 32603

Dr. A. A. Heuer
Professor of Ceramics
Case Western Reserve University
University Circle
Cleveland, OH 44106

Dr. D. J. Rowcliffe
Stanford Research Institute
333 Ravenswood Avenue
Menlo Park, CA 94025

Dr. R. N. Katz
Army Materials and Mechanics
  Research Center
Watertown, MA 02172

Dr. H. Kirchner
Ceramic Finishing Company
P.O. Box 498
State College, PA 16801

Dr. B. G. Koepke
Honeywell, Inc.
Corporate Research Center
10701 Lyndale Avenue South
Bloomington, MN 55420

Mr. Frank Koubek
Naval Surface Weapons Center
White Oak Laboratory
Silver Spring, MD 20910

Dr. J. Lankford
Southwest Research Institute
8500 Culebra Road
San Antonio, TX 78284

Professor P. B. Macedo
The Catholic University of America
Washington, DC 20017

Dr. N. Perrone
Code 474
Office of Naval Research
800 N. Quincy Street
Arlington, VA 22217

Dr. R. Rice
Naval Research Laboratory
Code 6360
Washington, DC 20375

Mr. R. T. Swann
Md-Materials Research Branch
Mail Stop 396
NASA Langley Research Center
Hampton, VA 23665

Dr. K. H. Holko, Manager
Materials Applications
General Atomic Company
P.O. Box 81608
San Diego, CA 92138

Dr. W. Bakker
EPRI
3412 Hillview Avenue
P.O. Box 10412
Palo Alto, CA 94303

Dr. P. A. Miles, Research
Raytheon Company
28 Seyon Street
Waltham, MA 02154

Dr. J. Ritter
University of Massachusetts
Dept. of Mech. Engr.
Amherst, MA 01002

Professor T. J. Rocket
University of Rhode Island
Kingston, RI 02881

Dr. G. E. Youngblood
Montana College of Mineral Technology
Butte, MT 59701

Dr. E. G. Kobetich
Experimental Station, Bldg. 302
E. I. DuPont Company
Wilmington, DE 19898

Dr. M. A. Adams
Jet Propulsion Laboratory
California Institute of Technology
4800 Oak Grove Drive
Pasadena, CA 91103

Dr. Clifford Astill
Solid Mechanics Program
National Science Foundation
Washington, DC 20550

Dr. R. J. Gottschall
U. S. Dept. of Energy
Div. of Materials Science
Mail Stop J309
Washington, DC 20545

Prof. R. Roy
Pennsylvania State University
Materials Research Laboratory
University Park, PA 16802

Dr. M. P. Borom
Research and Development
General Electric Company
Box 8
Schenectady, NY 12301

Hague International
3 Adams Street
South Portland, ME 04106

Mr. J. D. Walton
Engineering Exp. Station
Georgia Institute of Technology
Atlanta, GA 30332

Dr. W. F. Adler
Effects Technology, Inc.
5383 Hollister Avenue
P.O. Box 30400
Santa Barbara, CA 92105

Dr. L. R. Hettche
Metallurgy Division
Naval Research Laboratory
Washington, D. C. 20375

Mr. W. B. Harrison
Honeywell Ceramics Center
1885 Douglas Drive
Golden Valley, MN 55422

Dr. J. Rosolowski
General Electric Company
Research and Development Center
P. O. Box 8
Schenectady, NY   02301

Dr. J. H. Simmons
Catholic University of America
Washington, DC   20064

Dr. P. L. Smith
Naval Research Laboratory
Code 6361
Washington, DC   20375

Dr. R. W. Timme
Naval Research Laboratory
Code 8275
Underwater Sound Reference Division
P. O. Box 8337
Orlando, FL   32806

Dr. Charles C. Walker
Naval Sea Systems Command
National Center #3
2531 Jefferson Davis Highway
Arlington, VA   20390

Dr. Paul D. Wilcox
Sandia Laboratories
Division 2521
Albuquerque, NM   87115

Dr. Murray Gillen
Australian Embassy
Washington, DC   33801

Mr. J. D. Sibold
Coor Porcelain Company
17750 W. 32nd Avenue
Golden, CO   80401

Dr. S. M. Wiederhorn
Physical Properties Section
Bldg. 223, Rm. A355
National Bureau of Standards
Washington, DC   20234

Dr. P. F. Becher
Metals and Ceramics Division
Oak Ridge National Laboratories
Box X , Oak Ridge, TN   37830

Dr. R. Jaffee
Electric Power Research Institute
3412 Hillview Avenue
P. O. Box 10412
Palo Alto, CA   94303

Dr. B. A. Wilcox
Metallurgy and Materials Division
National Science Foundation
Washington, DC   20550

Dr. H. E. Bennett
Naval Surface Weapons Center
Research Department Code 601
China Lake, CA   93555

Dr. R. J. Charles
General Electric Company
Research and Development Center
Schenectady, NY   12301

Dr. A. R. C. Westwood
Martin-Marietta Laboratories
1450 South Rolling Road
Baltimore, MD   21227

Dr. N. S. Corney
Ministry of Defense
(Procurement Executive)
The Adelphi
John Adam Street
London WC2N 6BB
UNITED KINGDOM

Dr. D. E. Niesz
Battelle Memorial Institute
505 King Avenue
Columbus, OH   43201

Dr. R. E. Engdahl
Deposits and Composites, Inc.
318 Victory Drive
Herndon, VA   22070

Professor W. D. Kingery
Ceramics Div. Rm. 13-4090
MIT
77 Mass. Avenue
Cambridge, MA   02139

Dr. J. J. Petrovic
Los Alamos National Lab
MST-5
Los Alamos, NM 87545

Dr. W. H. Rhodes
GTE Laboratories Inc.
40 Sylvan Rd.
Waltham, MA 02154

Dr. D. C. Larson
IIT Research Inst.
10 W. 35th Street
Chicago, IL 60616

Dr. B. Butler, Chief
Materials Branch
Solar Energy Research Institute
1536 Cole Blvd.
Golden, CO 80501

Dr. S. Greenberg
Materials Science Division
Argonne National Laboratory
Argonne, IL 60439

Dr. F. E. Kennedy
Thayer School of Engineering
Dartmouth School of Engineering
Hanover, NH 03755

Dr. R. J. Bratton
R&D Center
Westinghouse Electric Corp.
Pittsburgh, PA 15235

Mr. B. North
Kennametal Inc.
1011 Old Salem Rd.
P. O. Box 639
Greensburg, VA 15601

Dr. D. J. Godfrey
Admiralty Materials Laboratory
Ministry of Defense
(Procurement Executive)
Holton Heath
Poole, Dorset
BH 16 6 JU
UNITED KINGDOM

Dr. Wm. Kessler
AFML
Wright-Patterson Air Force Base
OH 45433

Dr. S. F. Galasso
United Aircraft Research Laboratories
East Hartford, CN 06108

Dr. M. Srinivasan
The Carborundum Comp.
P. O. Box 1054
Niagara Falls, NY 14302

Dr. W. D. Tuohig
Bendix Research Laboratories
Southfield, MI 48076

Dr. Robert Ruh
AFML/LLM
Wright-Patterson AFB
OH 45433

Mr. J. Schuldies
Airesearch Manufacturing Company
P. O. Box 5217
Phoenix, AZ 85010

Dr. S. Musikant
General Electric Company
3198 Chestnut Street
Philadelphia, PA 19101

Dr. D. W. Richerson Comp. Code 503-44
Garrett Corp.
111 S. 34th Str., Box 5217
Phoenix, AZ 85034

Dr. R. Baumgartner
PPG Industries
P. O. Box 31
Barberton OH 44203

Globe-Union, Inc.
5757 North Green Bay Avenue
Milwaukee, WI 53201
Attn: G. Goodman

Mr. J. F. McDowell
Sullivan Park
Corning Glass Works
Corning, NY 14830

Dr. E. K. Beauchamp, Div. 5846
Sandia Laboratories
Albuquerque, NM 87185

Dr. J. A. Rubin
Kyocera International, Inc.
8611 Balboa Avenue
San Diego, CA 92123

Dr. W. V. Kotlensky
Materials Technology Department
TRW, Inc.
One Space Park
Redondo Beach, CA 90278

Dr. N. N. Ault
NORTON Comp.
One New Bond Street
Worcester, MA 01606

Dr. Hayne Palmour III
Engineering Research Division
N. C. State University
P.O. Box 5995
Raleigh, NC 27650

Dr. D. Ulrich
AFOSR, Code NC
Chemical Sciences Div.
1400 Wilson Blvd.
Arlington, VA 22209

Dr. C. A. Anderson
Research and Development Center
Westinghouse Electric Corporation
1310 Beulah Road
Pittsburg, PA 15235

Dr. D. R. Petrak
Lynchburg Research Center
Babcock and Wilcox Co.
Box 1260
Lynchburg, VA 24505

Dr. S. C. Dixon
SDD-Thermal Structure Branch
Mail Stop 395
NASA Langley Research Center
Hampton, VA 23665

Dr. F. W. Clinard, Jr.
Los Alamos Scientific Laboratory
MS 546
P.O. Box 1663
Los Alamos, NM 87544

Dr. D. DeCoursin
Fluidyne Eng.
5900 Olson Memorial Hwy.
Minneapolis, MN 55422

Dr. F. F. Lange
Rockwell International
P.O. Box 1085
1049 Camino Dos Rios
Thousand Oaks, CA 91360

Dr. T. Vasilos
AVCO Corporation
Research and Advanced Development
  Division
201 Lowell Street
Wilmington, MA 01887

Dr. R. E. Rondeau
AFML-LDJ
Wright-Patterson AFB
OH 45433

Dr. S. Dutta
NASA-Lewis Research Center
Mail Stop 49-3
21000 Brookpark Road
Cleveland, OH 44135

Mr. B. Probst
NASA-Lewis Research Center
21000 Brookpark Road
Cleveland, OH 44135

Dr. S. W. Freiman
Deformation and Fracture Group
Physical Properties Section, Bldg. 223
National Bureau of Standards
Washington, DC 20234

Mr. W. Trombley
Garrett Corporation
1625 I Street NW
Suite 515
Washington, DC 20006

Dr. P. Heitman
Detroit-Diesel Allison
Mail Stop W5
P. O. Box 894
Indianapolis, IN 46206

Mr. Charles P. Blankenship
Chief, Materials Division
Mail Stop 188M
NASA-Langley Research Center
Hampton, VA 23665

Dr. R. J. Palicka
CERADYNE, Inc.
3030 South Red Hill Avenue
Santa Ana, CA 92705

Dr. W. R. Prindle
Research and Development
Corning Glass Works
Corning, NY 14830

Dr. K. H. Styhr
AiResearch Casting Co.
2525 W. 190th St.
Torrance, CA 90509

Dr. Donald M. Curry, ES32
Thermal Technology Br.
National Aeronautics and
Space Administration
Lyndon B. Johnson Space Center
Houston, TX 77058

Dr. F. L. Kennard III
A. C. Spark Plug Division
General Motors Corp.
1300 N. Dort Hwy.
Flint, MI 48556

Dr. M. E. Gulden
INESCO
11077 N. Torrey Pines Rd.
La Jolla, CA 92037

Dr. J. J. Brennan
United Technologies Research Center
East Hartford, CT 06108

Dr. C. O. Hulse
United Technollgies Research Center
East Hartford, CT 06108

Dr. S. Rangaswamy
METCO, Inc.
1101 Prospect Avenue
Westbury, NY 11590

Dr. E. M. Anderson
Research and Engineering
Exxon Corporation
P. O. Box 101
Florham Park, NJ 07923

Dr. Fred Schmidt
E. I. DuPont
Engineering Dept. E-304
Experimental Station
Wilmington, DE 19898

END

FILMED

5-84

DTI